FZR-443

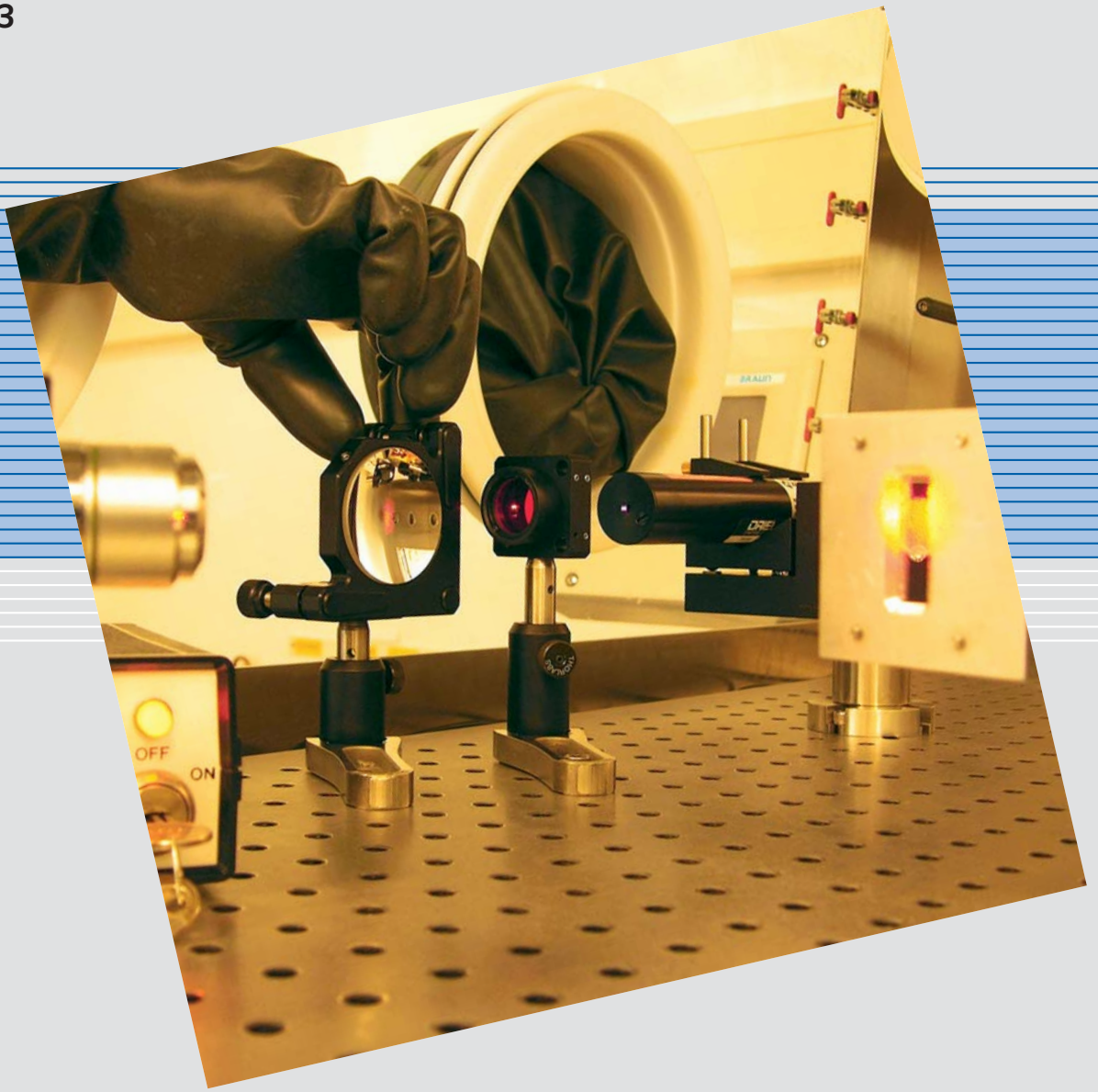

Wissenschaftlich-Technische Berichte
FZR-443 2006 · ISSN 1437-322X

Annual Report 2005

Institute of Radiochemistry

Forschungszentrum
Rossendorf

Wissenschaftlich-Technische Berichte
FZR-443
2006

Annual Report 2005

Institute of Radiochemistry

Editor: **Prof. Dr. G. Bernhard**

Editorial staff: **Dr. H. Foerstendorf**
Dr. J. Mibus
Dr. A. Richter
Dr. K.-U. Ulrich

Forschungszentrum
Rossendorf

Contact:

Forschungszentrum Rossendorf
Institute of Radiochemistry

Postal Address	***Address for visitors***
P.O. Box 51 01 19	Bautzner Landstraße (SW) 128
D-01314 Dresden	D-01328 Dresden
Germany	Germany

Phone: ++49 (0) 351 260 3210
Fax: ++49 (0) 351 260 3553
http://www.fz-rossendorf.de/FWR
e-mail: contact.radiochemistry@fz-rossendorf.de

Cover picture:

Setup of an optical experiment in the glove box at the free electron laser facility – FELBE.

Preface

The Institute of Radiochemistry (IRC), one of the six institutes of the Forschungszentrum Rossendorf (FZR), performs application-oriented research in the fields of radiochemistry and radioecology. Motivation and background of our research are environmental processes relevant for the installation of nuclear waste repositories, for remediation of uranium mining and milling sites, and for radioactive contaminations caused by nuclear accidents and fallout. Due to their high radiotoxicity and long half-life the actinides are of special interest. Hence our research focuses on the chemical behavior of actinides at the molecular level in order to predict the relevant macroscopic processes in the environment.
Within this framework, special emphasis is on the interface between geological and biological systems.

In the last year our research topics were as follows:

- Aquatic chemistry of actinides
- Actinides in bio-systems
- Interaction of actinides with solid phases
- Reactive transport of actinides

About 60 scientists, technicians and PhD students are employed in the Institute of Radiochemistry.
We have achieved a wide range of new scientific results in the past year, which are presented in this Annual Report. Among them only a few can be highlighted here in this preface. For the first time it was possible to determine uranium speciation *in situ* in drinking and mineral waters *e.g.* by a dedicated fluorescence spectrometer at lowest µg/L concentrations. This methodical progress is an important prerequisite to study the uranium toxicity and its dependence on chemical speciation.
We were very successful in the determination of formation pathways and structure of various actinide complexes, *e.g.*, the surface complexes of uranium (VI) onto mica and iron hydroxides over a wide range of pH and carbonate concentration. These results contribute to a better understanding of actinide speciation in geo- and bio-systems, especially with respect to the chemical processes on the interfaces.
Studies to the interaction of uranium with biofilms, green algae and bacteria coming from extreme habitats extended our research on the field of bio-systems.
Major progress in the structural analysis of multiple uranium species has been achieved by applying Monte Carlo simulations and iterative transformation factor analysis to EXAFS spectroscopy.
Furthermore, our new radiochemical experimental station at the Free Electron Laser of the Rossendorf accelerator ELBE is now in full operation. We have started first experiments on the uranium and neptunium complexation on selected mineral surfaces.

A team of scientists of our institute (G. Geipel, S. Amayri, G. Bernhard) was awarded the "Kurt-Schwabe-Preis 2005" of the Saxon Academy of Sciences for their contributions to the environmental chemistry of uranium.

I would like to thank our German and international visitors for their interest in our research and for their contributions to our scientific seminars. I would also like to thank our scientific collaborators and the visiting scientists for coming to Rossendorf/Dresden in 2005 to share their knowledge and experience with us. This is an important asset for our institute and I would like to encourage collaborations and visits. Special thanks are due to the Executive Board of the Forschungszentrum Rossendorf, the Ministry of Science and Arts of the State Saxony, the Federal Ministry of Education and Research, the Federal Ministry of Economics and Technology, the Deutsche Forschungsgemeinschaft, the European Commission, and other organizations for their support.

Prof. Dr. G. Bernhard

Content

Scientific contributions

Part 1: Aquatic chemistry of actinides

Part 2: Actinides in bio-systems

Part 3: Interaction of actinides with solid phases

Part 1:

Aquatic chemistry of actinides

Study of the interaction of calcium with $UO_2PO_4^-$ at pH 7.5

G. Geipel

The ionic complex $UO_2PO_4^-$ is the main species formed at pH 7.5 in uranylphosphate solutions. The interaction of this species with alkaline earth elements was studied by TRLFS.

In analogy to the formation of the alkaline earth uranyl carbonates it is assumed that also the uranyl phosphates can form ternary complexes. At pH 7.5 the formation of species with the common formula $Me(UO_2PO_4)_x^{(2-x)+}$ is expected ($Me^{2+} = Mg^{2+}$; Ca^{2+}; Sr^{2+} and Ba^{2+}).

EXPERIMENTAL. Solutions of $5.0 \cdot 10^{-6}$ M UO_2^{2+} and $1.0 \cdot 10^{-2}$ M PO_4^{3-} with increasing concentrations of alkaline earth elements ($0 \ldots 2.0 \cdot 10^{-3}$ M) were prepared at room temperature. The pH was adjusted to pH 7.5 and the ionic strength of the solutions was 0.1 M. In a second series with addition of Ca^{2+} also a phosphate concentration of $5.0 \cdot 10^{-3}$ M was applied. The fluorescence of the solution species was measured by time-resolved laser-induced fluorescence spectroscopy. The principal scheme is described in [1,2].

RESULTS. At pH 7.5 the fluorescence spectra show an increase of the fluorescence intensity with increasing alkaline earth concentration. Measuring the fluorescence immediately after the sample preparation no shift in the main emission bands is observed. The fluorescence spectroscopic properties are given in Table 1. A series of fluorescence spectra is shown in Fig. 1. Evidence on the formation of one additional dissolved species was derived from factor analysis of the fluorescence spectra.

In the series with Ca^{2+} as a second metal ion in solution an aging process was observed at higher Ca concentrations. This process was clearly detectable by a shift in the fluorescence emission bands. However, the fluorescence decay times did not change significantly. This result can be interpreted by the formation of a second species, of which the one acts as a precursor.

In agreement with results derived for the formation of the $MgUO_2(CO_3)_3^{2-}$ species [3] the first formed species is therefore assigned to be a $Me(UO_2PO_4)^+$ species.

According to the reaction

$$Me^{2+} + UO_2^{2+} + PO_4^{3-} \leftrightarrow Me(UO_2PO_4)^+ \quad (1)$$

the stability constants were derived. The results are summarized in Table 2.

Studies on the second species formed during the aging process are necessary in order to assign the complete set of stability constants. However, it is expected that species of the common formula $Me(UO_2PO_4)_{2(aq)}$ show extremely low solubilities.

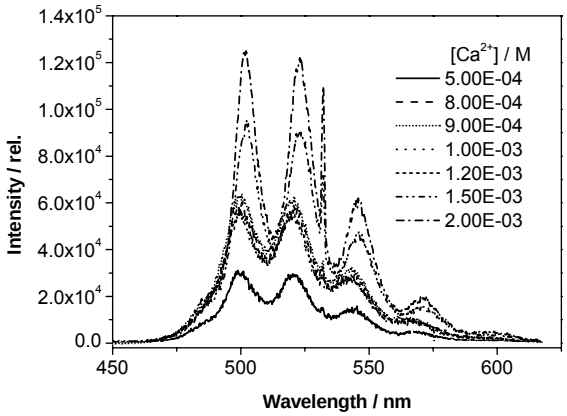

Fig. 1: Fluorescence spectra in the system $Ca^{2+} - UO_2^{2+} - PO_4^{3-}$ as a function of the Ca^{2+} concentration.

Tab. 1: Fluorescence spectroscopic properties of the $Me(UO_2PO_4)^+$ complexes.

Metal ion	Emission wavelength [nm]	Fluorescence decay time [µs]
Mg^{2+}	484.5; 500.1; 521.0; 543.6; 565.7; 598.5	3.56 ± 0.13 0.91 ± 0.02
Ca^{2+}	488.1; 501.9; 522.7; 544.4; 564.5; 572.7	2.7 ± 0.2 24.9 ± 1.0
Sr^{2+}	487.1; 502.2; 522.8; 544.3; 566.5	7.5 ± 0.4
Ba^{2+}	483.8; 503.8; 527.8; 547.6; 565.4; 588.4	4.2 ± 0.3 0.51 ± 0.07

Tab. 2: Stability constants of the $Me(UO_2PO_4)^+$ complexes.

Metal ion	$\log \beta^0_{111}$
Mg^{2+}	16.9 ± 0.2
Ca^{2+}	16.6 ± 0.2
Sr^{2+}	17.4 ± 0.4
Ba^{2+}	16.9 ± 0.4

REFERENCES

[1] Geipel, G. *et al.* (1996) *Radiochim. Acta* **75**, 199-204.
[2] Geipel, G. (2005) *Handbook of Elemental Speciation*, p. 509-563, Wiley & Sons Ltd., London.
[3] Amayri, S. (2003) *Thesis*, Dresden University of Technology.

Uranium complexation with phosphorylcholine studied by TRLFS

A. Koban, G. Geipel, G. Bernhard

In the aqueous uranyl phosphorylcholine system a 1:1 complex could be identified at low pH range. An increase of the fluorescence intensity, connected with a red shift of the fluorescence maxima, was observed. The formation constant was calculated.

Several investigations of bio-systems like microorganisms and plants with various analytical and spectroscopic methods show that the phosphate group seems to be quite effective for uranium binding [1, 2]. On the way of incorporation of actinides up to elimination or deposition, membranes play an important role. Phospholipids are beside proteins the basis of membranes. The reactive hydrophilic ends of phospholipids consist in several phosphate esters like phosphorylcholine.

EXPERIMENTAL. The TRLFS experiments were carried out at a total uranyl concentration of 10^{-5} M as a function of the phosphorylcholine (PC) concentration (10^{-5} M to $2 \cdot 10^{-3}$ M) at pH = 4 or as a function of pH (2 to 4) at fixed ligand concentration ($5 \cdot 10^{-4}$ M). The ionic strength was adjusted to 0.1 M ($NaClO_4$). The spectra were recorded at 22 °C using a pulsed Nd:YAG laser system. The excitation wavelength of the uranyl fluorescence was 266 nm with a pulse energy of 0.2 - 0.5 mJ.

RESULTS. Fig. 1 shows the fluorescence spectra of uranium(VI) as a function of the total phosphorylcholine concentration. With increasing ligand concentration we notice a strong increase in fluorescence intensity, connected with a red-shift of about 8 nm compared to the uranyl ion.

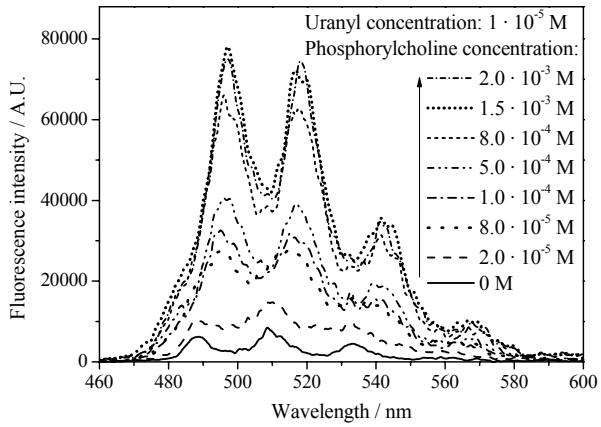

Fig. 1: Fluorescence spectra of uranium(VI) as a function of the ligand concentration at pH = 4.

The TRLFS spectra show di-exponential decays indicating a mixture of two species. The intensity of the shorter lifetime (610 ± 110 ns) increases with increasing ligand concentration and can be assigned to a uranyl phosphorylcholine complex. The longer lifetime (6 ± 2 µs) with a low but constant intensity can be attributed to uranyl hydroxide.

To validate the stoichiometry of the complex a graphical analysis of the logarithmic mass action law was performed (see Fig. 2). The concentrations of the free uranyl ion and the complex species were determined from the measured fluorescence spectra using conventional peak deconvolution. The slope of 1.09 suggests a metal-to-ligand ratio of 1:1. The intersection corresponds to the formation constant log k* of this complex.

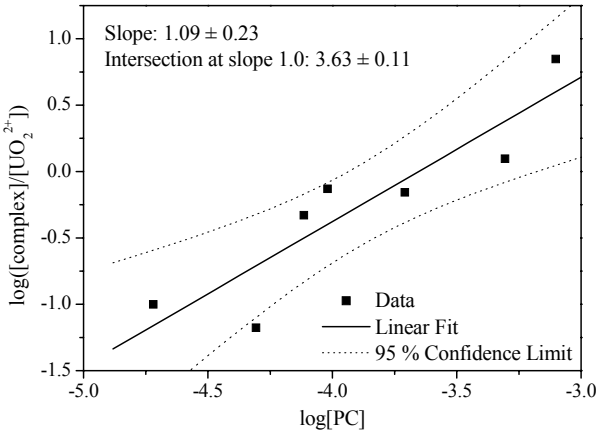

Fig 2: Slope analysis of the complex formation at pH = 4.

The graphical analysis of the mass action law as a function of pH shows the number of protons involved in the complex formation (see Fig. 3). The slope of 1.14 indicates that 1 proton is involved in the complex formation.

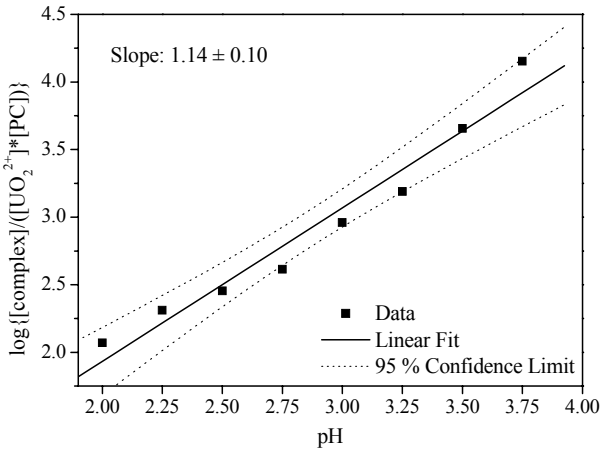

Fig 3: Slope analysis of the complex formation at constant ligand concentration as a function of pH.

The complex formation reaction can be written as:

$$UO_2^{2+} + {}^{+}(CH_3)_3N(CH_2)_2PO_3H^{-} \leftrightarrow UO_2[(CH_3)_3N(CH_2)_2PO_3]^{+} + H^{+} \quad \log k^*$$

Considering the protonation constant of phosphorylcholine [3], the complex stability constant of the 1:1 complex could be determined to be $\log \beta_{110} = 5.39 \pm 0.11$.

The spectra of the uranyl phosphorylcholine complex can be isolated from the composite spectra using conventional peak deconvolution. The peak maxima are located at 482, 497, 518, 541, and 567 nm.

REFERENCES

[1] Günther, A. *et al.* (2003) *Radiochim. Acta* **91**, 319-328.
[2] Merroun, M. *et al.* (2003) *Biometals* **16**, 331-339.
[3] Robitaille, P.-M.L. *et al.* (1991) *J. Magn. Reson.* **92**, 73-84.

The influence of Cl on the U-O_{eq} bond distance in U(VI) aquo chloro complexes

C. Hennig, A. Rossberg, A.C. Scheinost, J. Tutschku, G. Bernhard

The influence of Cl on the U-O_{eq} bond distance in high concentrated aqueous chloride solution has been studied by U L_{III}-edge EXAFS.

The coordination of U(VI) in high concentrated aqueous chloride solution has been studied by U L_{III}-edge EXAFS [1,2]. We observed the complexes $UO_2(H_2O)_4Cl^+$, $UO_2(H_2O)_3Cl_2^0$ and $UO_2(H_2O)_2Cl_3^-$ with U–Cl distances of 2.71 ± 0.02 Å. Conventional shell-fitting EXAFS analysis indicates that the U-O bond lengths increases from 2.41 Å to 2.51 Å with increasing [Cl^-]. This elongation was described for the first time by Allen et al. [3] and was interpreted as a chemical effect due to the presence of chloride ions. We could also verify this bond elongation by shell-fitting.

However, Wasserman *et al.* [4] showed that the standard EXAFS analysis of U(VI) aquo chloro complexes has some inherent limitations which can be overcome by model-independent statistical methods. Hence, the experimental spectra were analyzed with factor analysis. Three main factors representing the O_{eq} atoms at 2.41 Å and at 2.51 Å as well as the Cl shell were expected. The experimental spectra are decomposed by factor analysis in a set of abstract spectra (without direct physical meaning). Fig. 1 shows the decomposition results. The first two abstract spectra have large amplitudes and generate the main features in the Fourier transform. The amplitude of the third abstract spectrum does not raise above the experimental noise level. Hence all meaningful spectral features are reproduced by only two factors.

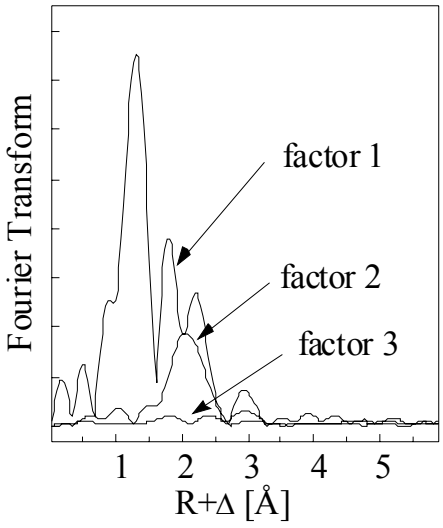

Fig. 1: Fourier transformation of the first three isolated abstract spectra of the experimental U(VI)/Cl series.

If a second O_{eq} shell with a longer distance of 2.51 Å existed in part of the spectra, one would expect that a third factor is required to reproduce the spectra, and that the Fourier transform of this factor shows a peak in between those arising from O_{eq} and Cl atoms, *i.e.* at approximately 2 Å (uncorrected for phase shift). The absence of such a third factor suggests that an additional U-O_{eq} bond length of 2.51 Å does not exist.

In order to verify that factor analysis would be sensitive enough to detect the possibly weak contribution of a second O_{eq} shell, we generated a set of model EXAFS spectra based on our first shell fitting results, *i.e.* including the U-O_{eq} distance of 2.51 Å. To make the calculated spectra comparable to experimental spectra, artificial noise was added. This set of calculated model spectra was then decomposed with factor analysis in a set of abstract spectra, the same way as it was done before with the experimental spectra. The Fourier transform of the third abstract spectrum clearly reveals the expected peak due to the additional, longer U-O_{eq} distance (Fig. 2). This means that such an elongated U-O_{eq} distance would be detectable by factor analysis. Therefore, this sensitivity test clearly demonstrates that such an elongated U-O_{eq} distance does not exist. The most likely explanation for its appearance in shell fitting attempts is that the strongly overlapping frequencies cannot be properly resolved, hence that it is a mere fitting artifact.

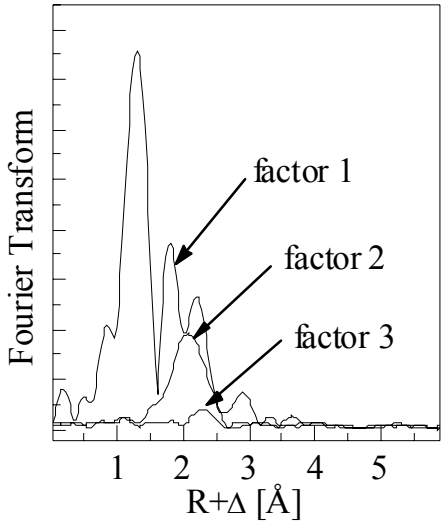

Fig. 2: Fourier transformation of the first three isolated abstract spectra of the simulated U(VI)/Cl series. The model EXAFS spectra were created using the fit parameters of the experimental series, *i.e.* including an additional elongated U-O_{eq} distance.

Decomposition of the spectra by factor analysis clearly demonstrated that the bond lengths remain invariant within ± 0.02 Å. The elongation observed with shell fitting is hence a fit artifact. Consequently, the influence of Cl on the U-O bond length seems to be weak.

REFERENCES

[1] Hennig, C. *et al.* (2004) *Report FZR-419*, p. 9.
[2] Hennig, C. *et al.* (2005) *Inorg. Chem.* **44**, 6655-6661.
[3] Allen, P.G. *et al.*(1997) *Inorg. Chem.* **36**, 4676-4683.
[4] Wasserman, S.R. *et al.* (1999) *J. Synchrotron Rad.* **6**, 284-286.

Complex formation of curium with L-threonine studied by TRLFS

H. Moll, G. Bernhard

Three complexes were identified by their individual fluorescence emission spectra and fluorescence lifetimes. The following formation constants were determined: log β_{101} = 6.72 ± 0.07, log β_{102} = 10.22 ± 0.09, and log $\beta_{1\text{-}22}$ = -(7.22 ± 0.19).

Amino acids are important biomolecules because they constitute essential chemical substances in the life cycle. These substances can have several functional groups in the fundamental chain and in side chains, *e.g.*, carboxyl, amino, hydroxyl, sulfuryl and phosphate groups. All these functionalities are potential binding sites for heavy metals. Therefore the investigation of the complexation of actinides with such biomolecules is challenging. At present the knowledge of the complexation behavior of Cm(III) with amino acids is very limited.

EXPERIMENTAL. The stock solutions of threonine (Carl Roth GmbH, Karlsruhe) were prepared freshly for each run. The experiments were performed under N_2 atmosphere at 25 °C. As a background electrolyte 0.5 M NaCl was used. The [Cm(III)] was fixed to $3 \cdot 10^{-7}$ M. The pH was varied between 3 and 9.4. [Thr] was varied from 0.001 to 0.25 M. TRLFS spectra were recorded using a flash lamp pumped Ti:sapphire laser (Elight, Titania). Details on the experimental set-up are summarized in [1].

RESULTS. At pH 3.6 a complex formation between Cm(III) and threonine was detected at ligand concentrations above 0.02 M (see Fig. 1A). The emission maximum close to 600 nm shows the formation of a first species. At large [Thr] ≥ 0.1 M, the shoulder at 603.8 nm indicates the occurrence of a second complex.

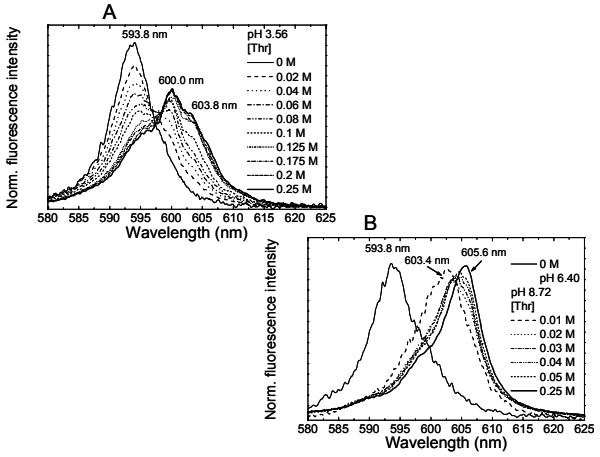

Fig. 1: TRLFS spectra in the threonine system; A) at pH 3.6 and B) at pH 8.7 and varying [Thr]. The spectra are scaled to the same peak area.

At pH values above 6 and [Thr] ≥ 0.05 M, the emission maxima around 606 nm points to the presence of a third complex (see Fig. 1B). This relatively large red shift, approx. 13.2 nm, compared to the emission band of Cm^{3+} indicates that most likely a chelate complex is formed. The spectral changes detected were used in the factor analysis program code SPECFIT as described in [2]. The single component spectra of the individual species are summarized in Fig. 2.

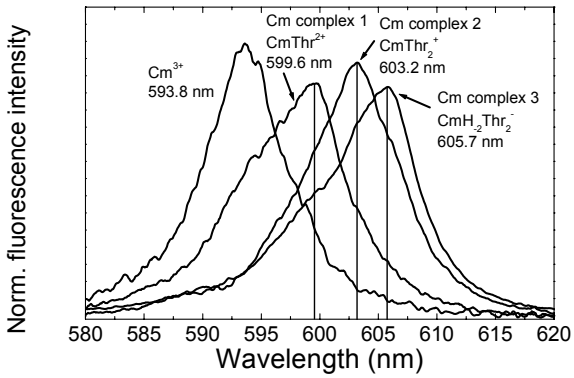

Fig. 2: TRLFS spectra of the single components in the Cm-threonine system as derived by peak deconvolution using SPECFIT. The spectra are scaled to the same peak area.

The dependencies found in the TRLFS data could be expressed by the following equilibria:

$$Cm^{3+} + Thr^{-} \leftrightarrow CmThr^{2+} \quad (1)$$

$$Cm^{3+} + 2Thr^{-} \leftrightarrow CmThr_2^{+} \quad (2)$$

$$Cm^{3+} + 2Thr^{2-} \leftrightarrow CmH_{-2}Thr_2^{-} + 2H^{+} \quad (3)$$

Formation constants for reactions (1) to (3) were calculated to be log $ß_{101}$ = 6.72 ± 0.07, log $ß_{102}$ = 10.22 ± 0.09 and log $ß_{1\text{-}22}$ = -(7.22 ± 0.19), respectively.

In test solutions with dominant amounts of the complexes $CmThr^{2+}$, $CmThr_2^{+}$ and $CmH_{-2}Thr_2^{-}$, increasing fluorescence lifetimes of 76 ± 4, 104 ± 5 and 180 ± 5 µs, respectively, were measured. The number of coordinated water molecules was calculated to be for a) $CmThr^{2+}$ 7.8, b) $CmThr_2^{+}$ 5.4, and c) $CmH_{-2}Thr_2^{-}$ 2.8 using the Kimura & Choppin equation [3]. This suggests for the 1:1 complex a monodentate coordination of the anion *via* one oxygen of the carboxylic group. In the 1:2 complex, the two anions are most likely coordinated *via* one oxygen of the carboxylic group and the nitrogen of the $–NH_2$ group in a "glycine-like" chelate ring as found for $CuThr_2$ in [4]. The large red shift of the emission band of the third species, 11.9 nm, compared to Cm^{3+} in combination with the increased lifetime, 180 µs, points to a formation of a 1:2 chelate complex. Most likely a five-membered chelate ring is formed in which the donors are the N (amino) and O (deprotonated -OH group) atoms. The $–COO^{-}$ groups come near to an axial position and interact also with the Cm ion. This chelate structure was first discussed for the corresponding copper complex [4].

ACKNOWLEDGEMENTS. This work was funded by the BMWi under contract number: 02E9985.

REFERENCES

[1] Stumpf, Th. *et al.* (2002) *J. Chem. Soc., Dalton Trans.* 3799-3804.
[2] Moll, H. *et al.* (2005) *Inorg. Chim. Acta* **358**, 2275-2282.
[3] Kimura, T. *et al.* (1994) *J. Alloys Comp.* **213/214**, 313-317.
[4] Grenouillet, P. *et al.* (1973) *Biochim. Biophys. Acta* **322**, 185-194.

Complex formation of curium with O-phospho-L-threonine studied by TRLFS

H. Moll, G. Bernhard

Two species, $M_pH_qL_r$, could be characterized by their individual fluorescence emission spectra and fluorescence lifetimes. The following formation constants were determined: log β_{121} = 18.03 ± 0.13 and log β_{111} = 14.17 ± 0.09.

A key reaction in the activation or deactivation of enzymes in biological systems is the reversible phosphorylation of proteins which is mainly observed on the hydroxyl group of the essential amino acids serine, threonine or tyrosine. To the knowledge of the authors, no results about the complex formation of phosphothreonine with trivalent actinides are published. In order to explain the interaction of actinides with *e.g.*, microbes on a molecular level, the investigation of complex formation equilibria with relevant model compounds is necessary.

EXPERIMENTAL. Phosphothreonine (PThr) (Sigma-Aldrich) stock solutions were prepared freshly for each run. The experiments were performed under N_2 atmosphere at 25 °C. As a background electrolyte 0.154 M NaCl was used. The [Cm(III)] was fixed to $3 \cdot 10^{-7}$ M. The pH was varied between 1.5 and 8.14. [PThr] was changed between $3 \cdot 10^{-6}$ and 0.025 M. TRLFS spectra were recorded using a flash lamp pumped Ti:sapphire laser (Elight, Titania). Details on the experimental set-up are summarized in [1].

RESULTS. In contrast to the threonine system [2], we obtained changes in the TRLFS spectra due to complex formation reactions already at a pH of 2.9 (Fig. 1A). One dominating species with an emission at 599 nm is formed at pH 2.9 and [PThr] ≥ $1 \cdot 10^{-4}$ M. By changing the pH to 6.5, an increased influence of a second species was detected (Fig. 1B). The main emission band is shifted to 602 nm.

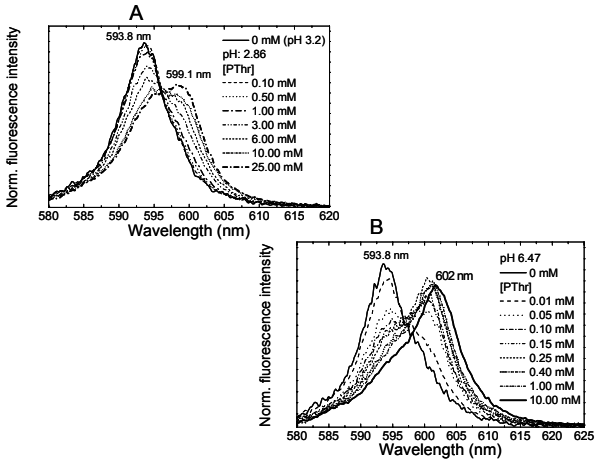

Fig. 1: TRLFS spectra measured in the phosphothreonine system; A) at pH 2.9 and B) at pH 6.5 and varying [PThr]. The spectra are scaled to the same peak area.

The influence of two Cm(III)-phosphothreonine species was also detected in the pH dependence of the fluorescence signal measured at a fixed [PThr] of $3 \cdot 10^{-4}$ M (data not shown). In contrast to threonine, interaction processes between Cm(III) and phosphothreonine species were also obtained at lower ligand concentrations, *e.g.* $3 \cdot 10^{-6}$ M in the pH range ≥ 5.5 (data not shown).
The spectral changes were again used in the factor analysis program code SPECFIT as described in [2, 3] to characterize the complex formation reactions in the phosphothreonine system. The single component spectra of the individual species are summarized in Fig. 2.

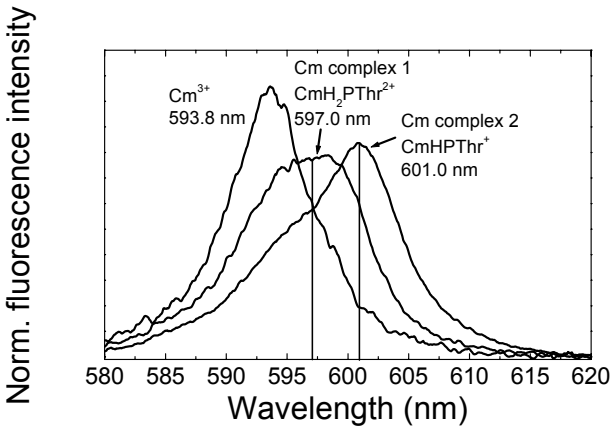

Fig. 2: TRLFS spectra of the single components in the phosphothreonine system as derived by peak deconvolution using SPECFIT. The spectra are scaled to the same peak area.

In all cases 1:1 species were detected. The dependencies observed in the TRLFS data (see Fig. 1) could be described by the following equilibria:

$$Cm^{3+} + 2H^+ + PThr^{3-} \leftrightarrow CmH_2PThr^{2+} \quad (1)$$
$$Cm^{3+} + H^+ + PThr^{3-} \leftrightarrow CmHPThr^{+} \quad (2)$$

Formation constants for reactions (1) and (2) were calculated to be log β_{121} = 18.03 ± 0.13 and log β_{111} = 14.17 ± 0.09, respectively.
In all samples a mono-exponential fluorescence decay behavior was obtained. In test solutions with dominant amounts of the complexes CmH_2PThr^{2+} and $CmHPThr^{+}$, fluorescence lifetimes of 77 ± 1 and 83 ± 1 µs, respectively, were measured. The number of coordinated water molecules was calculated to be for a) CmH_2PThr^{2+} 7.6 and b) $CmHPThr^{+}$ 7.0 by applying the Kimura & Choppin equation [4]. Eight remaining water molecules in the 1:2:1 complex suggest a monodentate coordination of the anion, H_2PThr^{-}, *via* one oxygen atom of the phosphate or the carboxylate group. In the 1:1:1 complex where seven remaining water molecules were detected, Cm^{3+} could be coordinated in a bidentate fashion to the two oxygens of the phosphate group. The formation of a seven-membered chelate ring as discussed in [5] for the copper MHL complex is also possible. Here Cm(III) binds to one oxygen from the phosphate and one oxygen from the carboxylic group.

ACKNOWLEDGEMENTS. This work was funded by the BMWi under contract number: 02E9985.

REFERENCES

[1] Stumpf, Th. *et al.* (2002) *J. Chem. Soc., Dalton Trans.* 3799-3804.
[2] Moll, H. *et al.* this report, p. 12.
[3] Moll, H. *et al.* (2005) *Inorg. Chim. Acta* **358**, 2275-2282.
[4] Kimura, T. *et al.* (1994) *J. Alloys Comp.* **213/214**, 313-317.
[5] Mohan, M. S. *et al.* (1978) *Inorg. Chem.* **17**, 2203-2207.

Spectroscopic study of the uranium(VI) complexation by humic acid under neutral pH conditions

S. Sachs, V. Brendler, G. Geipel

The complexation of U(VI) with humic acid (HA) was studied at pH 7. The complex stability constant for the formation of the ternary U(VI) mono hydroxo humate complex was determined using two independent laser-induced spectroscopic methods (log $\beta_{0.1M}$: 6.58 ± 0.24).

Reliable data on the interaction of uranium with humic acids (HA) are necessary to perform the safety analysis of future nuclear waste repositories and for remediation of uranium mining sites. However, only few studies exist on the interaction of U(VI) with HA under neutral pH conditions where ternary U(VI) humate complexes are formed, *e.g.*, [1]. We studied the U(VI)-HA complexation at pH 7 by conventional laser-induced fluorescence spectroscopy (TRLFS) and TRLFS with ultrafast pulses (fs-TRLFS).

EXPERIMENTAL. U(VI) humate solutions were prepared from purified Aldrich HA. The HA concentration was kept constant at 2 mg/L and the U(VI) concentration was varied between $1 \cdot 10^{-7}$ and $1 \cdot 10^{-5}$ mol/L. The studies were performed in 0.1 M $NaClO_4$ at pH 7.01 ± 0.02 under N_2 atmosphere. Reference samples without HA were prepared to characterize the fluorescence behavior of U(VI) hydroxo species present in solution.
The determination of the U(VI) speciation in solution was performed by TRLFS with a Nd-YAG laser (Spectron; repetition rate: 25.5 Hz, excitation wavelength: 266 nm, energy: ~500 µJ). Time-resolved fluorescence spectra were recorded between 446 and 618 nm with an intensified CCD camera (Roper-Scientific; delay times: 0.03 - 30.03 or 56.28 µs, gate time: 2 µs). The HA fluorescence as a function of the U(VI) concentration was measured with fs-TRLFS, using a Nd-YVO_4 laser coupled with an intensified CCD camera (Spectra Physics; excitation wavelength: 266 nm, energy: ~200 µJ) [2]. The spectra were measured in the wavelength range between 330 and 524 nm (delay times: 0 - 9 ns, gate time: 0.5 ns).

COMPLEXATION MODEL. The experimental data were evaluated based on the complexation reaction:

$$UO_2OH^+ + HA(I)^- \leftrightarrow UO_2(OH)HA(I) \qquad (1)$$

The stability constant is described by:

$$\beta = \frac{[UO_2(OH)HA(I)]}{[UO_2OH^+]_{free} \cdot [HA(I)]_{free}} \qquad (2)$$

The free HA concentration ($[HA(I)]_{free}$) was evaluated assuming that all proton exchanging functional groups of the HA are available for U(VI) complexation ($[HA(I)]_{tot}$ = 100 %). For TRLFS data analysis, $[HA(I)]_{free}$ was alternatively determined according to the charge neutralization model (CNM) using the loading capacity LC [3].

RESULTS. Fig. 1 shows TRLFS spectra of U(VI) at fixed HA and varying U(VI) concentration. The TRLFS spectra are dominated by $(UO_2)_3(OH)_5^+$ [4]. No other U(VI) species are relevant for spectra analysis at delay times >10 µs. The concentrations of non-complexed $(UO_2)_3(OH)_5^+$ in solution were derived from TRLFS spectra. From that, the concentrations of total non-HA-complexed U(VI) ($[U(VI)]_{non\text{-}HA}$) and UO_2OH^+ were calculated using EQ3/6 [5]. The concentrations of the complex and of the free, non-complexed HA were derived based on Eq. (3) and (4). Additionally, $[HA(I)]_{free}$ was evaluated according to the CNM.

$$[UO_2(OH)HA(I)] = [U(VI)]_{tot} - [U(VI)]_{non\text{-}HA} \qquad (3)$$

$$[HA(I)]_{free} = [HA(I)]_{tot} - [UO_2(OH)HA(I)] \qquad (4)$$

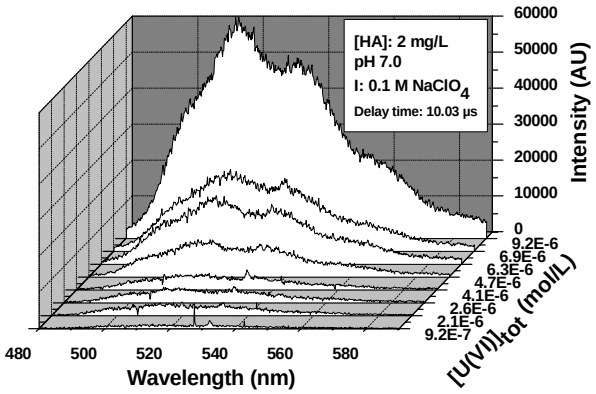

Fig. 1: TRLFS spectra of U(VI) humate solutions 10.03 µs after laser pulse excitation.

The non-complexed HA concentration was obtained from fs-TRLFS. Based on that, the concentrations of $UO_2(OH)HA(I)$ and of the total non-HA-complexed U(VI) were calculated with the relationships given in Eq. (3) and (4). From that, the amount of UO_2OH^+ was estimated using EQ3/6. A detailed description of the data analysis is given in [4]. The obtained complexation data are summarized in Tab. 1.

Tab. 1: Complexation data for the interaction of HA with U(VI) at pH 7.

Method	$[HA(I)]_{tot}$ = 100%	CNM [3]	
	log β [a]	LC [a]	log β [a]
TRLFS	6.58 ± 0.24 [b]	0.76 ± 0.28	6.95 ± 0.10
fs-TRLFS	6.33 ± 0.20	n.a. [c]	n.a. [c]

[a] ± 2σ. [b] Recommended value. [c] n.a.: not applied.

TRLFS and fs-TRLFS yield comparable log β values which agree with that from $UO_2(OH)_2$ solubility studies in presence of HA (log β = 6.8) [1]. Differences in the definition of $[HA(I)]_{free}$ give only minor differences in log β. A stability constant log $\beta_{0.1M}$ of 14.7 ± 0.2 was derived for the total reaction of U(VI) with HA (Eq. (5)), which agrees with log $\beta_{0.1M}$ = 15.2 given in [1].

$$UO_2^{2+} + OH^- + HA(I)^- \leftrightarrow UO_2(OH)HA(I) \qquad (5)$$

ACKNOWLEDGEMENT. The German Federal Ministry of Economics and Labor funded this work (02E9673).

REFERENCES

[1] Pashalidis, I. (2004) *Report FZKA 6969*, p. 319-330.
[2] Geipel, G. *et al.* (2004) *Spectrochim. Acta* **60**, 417-424.
[3] Kim, J.I. *et al.* (1996) *Radiochim. Acta* **73**, 5-10.
[4] Sachs, S. *et al.,* (2006) *Radiochim. Acta* (submitted).
[5] Wolery, T.J. (1992) *Report UCRL-MA-110662 Part 1,* LLNL.

Reduction of U(VI) with gallic acid in $HClO_4$ and H_2SO_4 solutions

R. Steudtner, G. Geipel

The reduction of U(VI) with gallic acid (GA) in $HClO_4$ and H_2SO_4 solutions was studied under various conditions.

In this study gallic acid (GA) was used as model substance for natural organic compounds. Natural organics (humic acid, lignin) show an influence on the oxidation state of uranium [1]. The redox behavior of GA towards Cr(VI) was studied already [2,3].

EXPERIMENTAL. The reduction of U(VI) in 4 M perchloric acid was studied at two different uranyl (0.05 and 1 mM) and GA (0.1 and 10 mM) concentrations in the presence of a 1 % wt. Pt/SiO_2 catalyst [4]. In sulfuric acid the uranyl concentration was 1 mM and the GA concentration 10 and 15 mM. The sulfuric acid concentration was adjusted to 2, 4 and 8 M. The 1 % wt. Pt/SiO_2 catalyst was used in one series. In the absence of GA a reduction of U(VI) in both mediums could not be observed.
The measurement of the U(IV) concentration was performed by laser-induced photoacoustic spectroscopy (LIPAS) and by UV-vis spectroscopy.

RESULTS. The photoacoustic spectrum of the uranium(IV) formed during the reduction is shown in Fig. 1. Fig. 2 shows the increase of the U(IV) concentration in 4 M $HClO_4$ as a function of the reaction time.

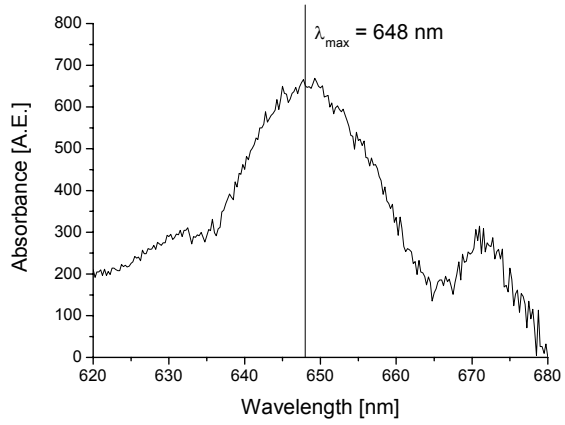

Fig. 1: Photoacoustic spectrum of U(IV).

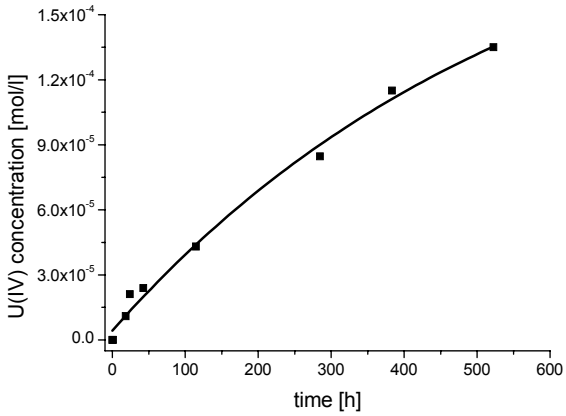

Fig. 2: Increase of the U(IV) concentration in $HClO_4$ with time.

By the reduction of 0.05 mM U(VI) with 0.1 mM GA 79.6 % of U(VI) were converted into U(IV) within 956 h. By the reaction of 1 mM U(VI) with 10 mM GA 13.5 % of U(VI) were reduced to U(IV) within 523 h.
The results of the reduction of 1 mM U(VI) in sulfuric acid under various conditions are summarized in Tab. 1.

Tab. 1: Reduction of 1 mM U(VI) in sulfuric acid.

c (H_2SO_4) [M]	c (GA) [mM]	Application of Pt/SiO_2	c (U^{4+}) [mM]
2	10	no	0.01
4	10	no	0.10
8	10	no	0.16
2	10	yes	0.04
4	10	yes	0.09
8	10	yes	0.23
4	30	yes	0.08

The amount of reduced uranium(IV) in the studies with and without 1 % wt. Pt/SiO_2 was enhanced with increasing sulfuric acid concentration. The application of 1 % wt. Pt/SiO_2 shows a negligible influence on the U(VI) reduction. The reduction of U(VI) in sulfuric acid was most efficient in the presence of the catalyst in 8 M H_2SO_4. Under these conditions 22.8 % of U(VI) were reduced to U(IV) within 505 h. The increase of the U(IV) concentration in sulfuric acid under the various conditions is shown in Fig. 3.

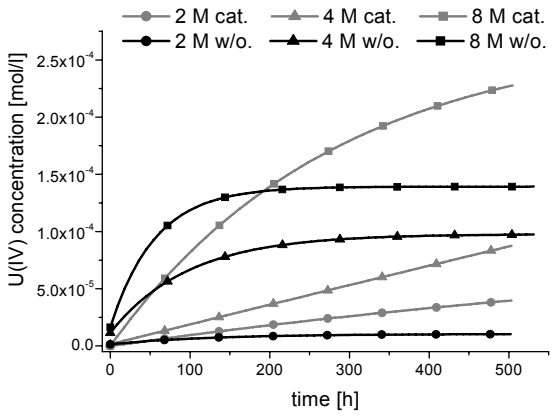

Fig. 3: Time-dependent increase of the U(IV) concentration in sulfuric acid.

The increase of the concentration of the reduced U(IV) on time shows that the reduction occurs only until a concentration limit. This provides evidence that gallic acid has a maximum redox capacity upon reduction of U(VI) to U(IV).

REFERENCES

[1] Abraham A. (2000) *Thesis*, Dresden University of Technology.
[2] Arakawa H. *et al.* (1998) *Bull. Chem. Soc. Jpn.* **71**, 1993-1998.
[3] Arakawa H. *et al.* (2001) *Bull. Chem. Soc. Jpn.* **74**, 1075-1082.
[4] Ananiev A.V. *et al.* (2003) *Radiochim. Acta* **91**, 499-503.

Influence of the particle size on the solubility products of different modifications of uranium dioxide

K. Opel, S. Weiß, H. Zänker, G. Bernhard

Neglecting the particle size of colloids investigated in solubility studies can cause a significant overestimation of the solubility product. In this study, the effect is quantified for colloids consisting of the crystalline and the amorphous modification of uranium dioxide.

Determining correct solubility data of U(IV) is essential for thermodynamic databases used for safety assessments of nuclear waste repositories and abandoned uranium ore mines.

EXPERIMENTAL. $UO_2(ClO_4)_2$ solutions of various concentrations were electrochemically reduced at pH < 1. Subsequent coulometric titration led to the formation of U(IV) colloids when the solubility of U(IV) was exceeded. The onset of colloid formation was detected by laser-induced breakdown detection (LIBD).

RESULTS AND DISCUSSION. The concentration of H^+ at the onset of colloid formation and [U] are evaluated as described in [1]. The arising solubility products of the U(IV) colloids, log K_{sp}^0(coll.), are given in Tab. 1.

Tab. 1: Influence of the particle diameter d_P on the solubility product K_{sp}^0 of uranium dioxide for various uranium concentrations.

log [U]	log K_{sp}^0(coll.)	d_P / nm	log K_{sp}^0
-3.0	-57.0	12.5	-58.9
-3.5	-57.1	7.7	-60.3
-4.0	-54.1	79.6	-54.4
-4.5	-54.2	149.9	-54.3

It can be distinguished between two groups of experiments. Uranium concentrations of log [U] ≤ -4.0 lead to a log K_{sp}^0(coll.) of -54.1. This value is close to the value of -54.5 evaluated for amorphous uranium dioxide, $UO_2 \cdot xH_2O$(am), from experimental data of other authors in a study by Neck and Kim [2].
Data of the experiments with log [U] ≥ -3.5 yield K_{sp}^0 values which are about three orders of magnitude lower indicating the formation of another modification of UO_2. However, log K_{sp}^0 = -57.0 differs from the value given by Rai et al. for crystalline UO_2 (-60.2 [3]) by another three orders of magnitude. To explain these deviations, the diameter d_P of the colloids determined by LIBD is taken into account. For this purpose the distribution of breakdown events in the focal area of the laser beam is evaluated according to the procedure described in detail in [4]. Briefly, breakdown events induced by larger particles can be detected in a wider range of the focal area than those induced by smaller particles. The range in beam propagation direction where breakdown events can be observed is called the effective focal length z. It depends on d_P according to the following empirically determined equation which is valid for our LIBD system:

$$\log z = 2.87 + 0.22 \log d_P \qquad (1)$$

The resulting d_P values are given in Tab. 1. Low particle diameters lead to an increased surface energy compared to a bulk solid of the same mineralogical composition. Due to this increased surface energy, colloids of a given composition are more soluble than their respective bulk. According to a study by Schindler et al. [5], the increased solubility product can be quantified by equation (2):

$$\log K_{sp}^{\ 0} = \frac{\log K_{sp}^{\ 0}(coll.)}{1 - \frac{M\alpha}{4N_A \pi \rho d_P \sum r(i)^2}} \qquad (2)$$

Inserting Avogadro's number N_A, a geometric factor α of 6 and the specific values of crystalline uranium dioxide with ρ = 10.95 g/cm^3 [6], r(U^{4+}) = 0.100 nm and r(O^{2-}) = 0.138 nm [7] leads to the solubility products, log K_{sp}^0, given in Tab. 1, corresponding to the bulk solids of our experiments.
The influence of particle diameters up to d_P = 30 nm on the solubility product of uranium dioxide is shown in Fig. 1.

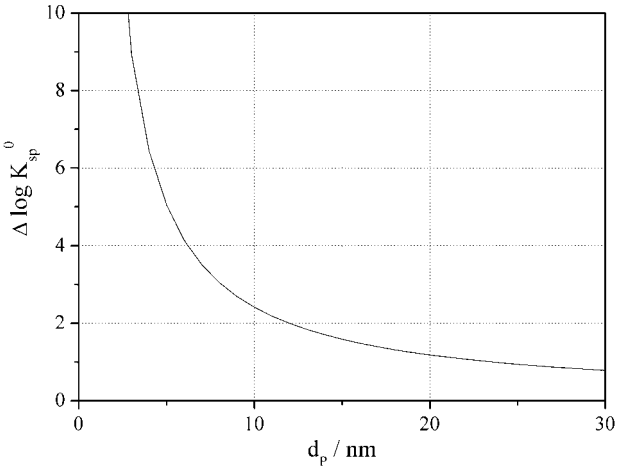

Fig. 1: Influence of the particle size on the solubility product of colloids consisting of crystalline uranium dioxide.

It can clearly be seen that particle diameters of less than 10 nm lead to deviations of K_{sp}^0(coll.) from the corresponding bulk value, log K_{sp}^0, of more than two orders of magnitude. In our experiments this applies to the coulometric titrations with log [U] ≥ -3.5. The correction of log K_{sp}^0(coll.) yields an average value of 59.6 for the bulk solid. This is in fair agreement with log K_{sp}^0 = -60.2 determined by Rai et al. for UO_2(cr) [3]. The formation of microcrystalline UO_2 for log [U] = -3.0 is supported by EXAFS measurements [8].
Since the particles formed in the experiments with log [U] ≤ -4.0 are noticeably larger, their influence on log K_{sp}^0 of the respective bulk is nearly negligible. Thus, the formation of the amorphous modification is confirmed for these titrations.

REFERENCES

[1] Opel, K. *et al.* (2005) *Report FZR-419*, p. 14.
[2] Neck, V. *et al.* (2001) *Radiochim. Acta* **89**, 1-16.
[3] Rai, D. *et al.* (2003) *J. Solution Chem.* **32**, 1-17.
[4] Bundschuh, T. *et al.* (2001) *Colloids Surf. A* **180**, 285-293.
[5] Schindler, P.W. *et al.* (1965) *Helv. Chim. Acta* **48**, 1204-1215.
[6] Wasserstein, B. (1951) *Nature* **168**, 380.
[7] Shannon, D. (1976) *Acta Cryst. A* **32**, 751-767.
[8] Ulrich, K.U. *et al.* this report, p. 17.

Characterization of colloidal U(IV) oxide by EXAFS spectroscopy and XRD

K.-U. Ulrich, K. Opel, S. Weiß, A.C. Scheinost

We studied the mineralogy of intrinsic U(IV) colloids by extended X-ray absorption fine structure (EXAFS) spectroscopy and X-ray diffractometry (XRD). We found X-ray amorphous crystallites with a highly ordered local atomic environment, transforming to more crystalline uraninite (UO_2) or β-U_3O_7 with aging.

EXPERIMENTAL. Intrinsic U(IV) colloids were generated in a N_2 flushed glovebox ($pO_2 < 1$ Pa) by electrochemical reduction of 1 mM $UO_2(ClO_4)_2$ solution to U(IV) at an ionic strength of 0.2 M $HClO_4/NaClO_4$ (pH ~ 0.7) and subsequent coulometric titration as described in [1]. At pH > 1.0, colloids formed and aggregated with rising pH. At pH 2.5, the flocs were concentrated to a wet paste by ultra-centrifugation and filled into a 35 µL polyethylene vial that was stored in liquid N_2 to avoid sample alteration by oxidation. A He cryostat (30 K) was used for recording X-ray absorption between 16940 and 18044 eV (range of U L_{III} edge) at the ESRF synchrotron in Grenoble (Rossendorf Beamline). Thus, from sample preparation up to the EXAFS measurement any contact with molecular oxygen has been avoided. We used standard methods for EXAFS data reduction. Shell fitting of the structural data was based on ab-initio phase and amplitude functions of the mineral uraninite [2]. XRD (Bruker D8 Advance, Cu Kα radiation) was recorded at 40 kV and 40 mA in the 2θ range of 10°(0.05)60° by rotating ~5 mg of dry matter on a glass slide at 15 rpm.

RESULTS AND DISCUSSION. The k^3 weighted EXAFS spectrum and corresponding Fourier transform (Fig. 1) show that the experimental data have rather low noise and tightly match the fit data up to 15 $Å^{-1}$. The coordination number (*N*) and bond distance (*R*) of the U-O shell derived from EXAFS agree with the structural data of crystalline uraninite excellently (Tab. 1). The same applies to the U-U bond distance of 3.86 Å. Taking an accuracy of ± 30 % into account, the calculated coordination number of the U-U shell is much below the crystallographic value of 12 valid for uraninite. Though the measured EXAFS data reflect a highly ordered local atomic environment, X-ray diffraction signals were missing (data not shown) due to the low crystal size. A particle size of ~12 nm was determined by laser-induced breakdown detection [3] but the true size of single crystallites even may have been smaller. This fact could explain the reduced coordination number of the U-U shell in the U(IV) colloid sample.

About eight months after preparation of the U(IV) colloid paste, a repeated XRD analysis showed broad reflections at the 2θ positions typical of crystalline uraninite. This result suggests crystal growth of the uraninite with aging of the wet uranium dioxide sample. However, the reflections correspond to β-U_3O_7 as well. Since the measurement took 16 h at ambient atmosphere, the formation of higher oxides on the crystal surface cannot be excluded [4].

ACKNOWLEDGEMENTS. We thank A. Scholz (Inst. of Ion Beam Physics and Materials Research) for XRD.

Tab. 1: Structural data on the U(IV) colloid sample from the EXAFS shell fit compared with crystalline uraninite (in brackets) [2].

Shell	N	R (Å)	σ^2 [a] ($Å^2$)	ΔE_0 [b] (eV)
U-O	8.1±2.4 (8)	2.34±0.02 (2.37)	0.0093	3.87
U-U	6.3±1.9 (12)	3.86±0.02 (3.86)	0.0027	6.34

[a] Debye-Waller factor, [b] Energy shift

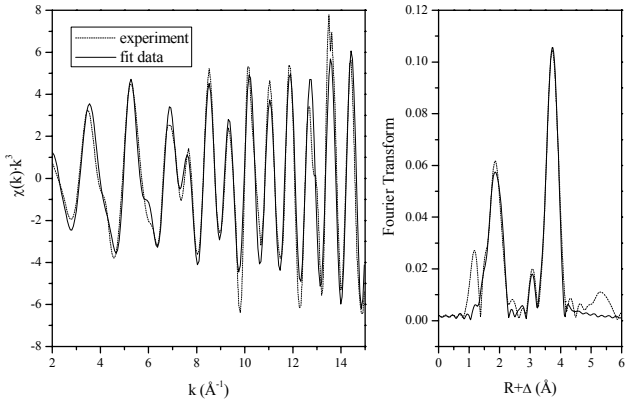

Fig. 1: U L_{III}-edge EXAFS spectrum and Fourier transform of intrinsic U(IV) colloid sample. Dotted line: experiment, full line: fit data.

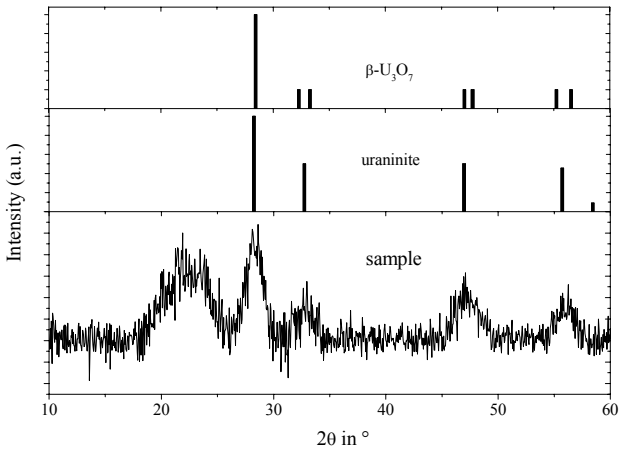

Fig. 2: X-ray diffraction pattern (Cu Kα radiation) of the intrinsic U(IV) colloid sample after eight months aging as a wet paste in N_2 atmosphere at 23 ± 2 °C. The broad underground reflection at 20-25° 2θ is due to the sample holder (glass slide).

REFERENCES

[1] Weiß, S. *et al.* (2005) *Report FZR-419*, p. 13.
[2] Wasserstein, B. (1951) *Nature* **168**, 380.
[3] Opel, K. *et al.* this report, p. 16.
[4] Nowicki, L. *et al*. (1997) *Phys. Rev*. **56**, 534-542.

Influence of iron-rich colloids on uranium(VI) in mine waste rock piles

H. Zänker, S. Weiß

There is a mechanism of direct colloid formation at rock-water interfaces due to the weathering of the rock. Colloids produced by this mechanism can influence the behavior of uranium in the environment.

In [1,2] we showed that there is a mechanism of direct secondary mineral colloid generation at the water-rock interfaces by the weathering of rock. It is of importance in the unsaturated zone as for instance in mine waste rock piles. Here we demonstrate that colloids generated by this mechanism can influence the behavior of contaminants. The behavior of U(VI) serves as an example.

EXPERIMENTAL. The weathering of phyllite from an abandoned uranium mine was simulated. Tab. 1 in [1] gives the mineralogical composition of this phyllite. The phyllite was jaw-crushed and sieved. The ground phyllite, grain size fraction 63 to 200 µm, was suspended in MilliQ water (40 g/L). The material was "prewashed" twice by centrifugation and re-suspension. For the weathering the suspension was shaken for 90 h during which period the colloids were formed (oxic conditions, pH 8.4). Thus, the ground phyllite was used as a "colloid generator" for the subsequent experiments. The bulk of the ground phyllite was separated from the colloids by centrifugation at 1,000 x g. The particle size cut-off of this particle separation is about 10^2 nm (cf. [3]). The supernatant of the 1,000 x g centrifugation (separated by pipetting) was analyzed by ICP-MS and/or by AAS for its concentrations of Al, Fe, K, Mg, Mn, Si and Y. This solution was used as the colloidal suspension for the sorption experiments. A $NaHCO_3$ concentration of 105 mg/L, a U concentration of 50 µg/L and pH values of 8.2 - 4.7 were adjusted. The samples were allowed to equilibrate for 1 day. Finally, the major fraction of the colloids was removed by ultracentrifugation (170,000 x g, separation by pipetting again). The maximum hydrodynamic diameter of the particles still present in the supernatant after this centrifugation is about 10^1 nm (cf. [3]). The supernatant solutions from the ultracentrifugations were analyzed by ICP-MS and/or AAS.

RESULTS. Information on the inventories of colloids of the size class 10^1 to 10^2 nm and the chemical composition of the colloids of this size class can be derived from the differences of the ICP-MS/AAS results after the 1,000 x g and the 170,000 x g centrifugations, $c_{1,000xg} - c_{170,000xg}$. It follows from the differences $c_{1,000xg} - c_{170,000xg}$ that the colloidal solution produced by the weathering of the phyllite contained a total of > 10 mg/L of colloids of the size class 10^1 to 10^2 nm. Fig. 1 shows the chemical composition of these colloids. In [1,2] we described a method to correct the secondary mineral colloid inventories for residuals of ultrafine primary mineral particles of unreacted ground phyllite based on the colloid-borne fractions of K, Mg, and Na in the solution and on the stoichiometry of the phyllite primary minerals given in Tab. 1 of [2]. This correction shows that more than 60 % of the colloid-borne iron, the most important colloidal sorbent of U(VI), is attributable to secondary minerals (most probably ferrihydrite) and not to traces of iron-containing primary mineral particles. The influence of the colloids on the behavior of U(VI) can be seen from Fig. 2. The figure shows the colloid-borne uranium fraction (percentage of the total U) as determined by the differences $c_{1,000xg} - c_{170,000xg}$ for uranium as a function of pH. Note that U(VI) would be truly dissolved in these simulated natural waters in the absence of colloids, either due to low pH or due to the influence of carbonate complexation. However, the presence of the colloids makes most of the uranium colloid-borne in the middle pH region.

CONCLUSIONS. The colloids produced by the weathering of phyllite are able to keep large fractions (up to 90 %) of the uranium(VI) in a colloid-borne form in the pH region of 5.0 to 7.5. In the absence of colloids, this U(VI) would be truly dissolved. The consequences of this colloid influence on uranyl speciation depend on the specific conditions in a geological environment. In a mine waste rock pile both situations are possible: the iron-rich colloids increase U(VI) mobility by preventing UO_2^{2+} attachment at interfaces and the colloids immobilize U(VI) by scavenging, colloid aggregation, colloid deposition, formation of crusts etc.

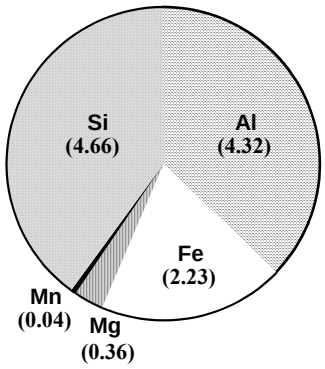

Fig. 1: Concentration differences $c_{1,000xg} - c_{170,000xg}$ (mg/L) of the colloid-forming elements as a measure of the colloid constituent concentrations (colloid particle size range 10^1 to 10^2 nm)

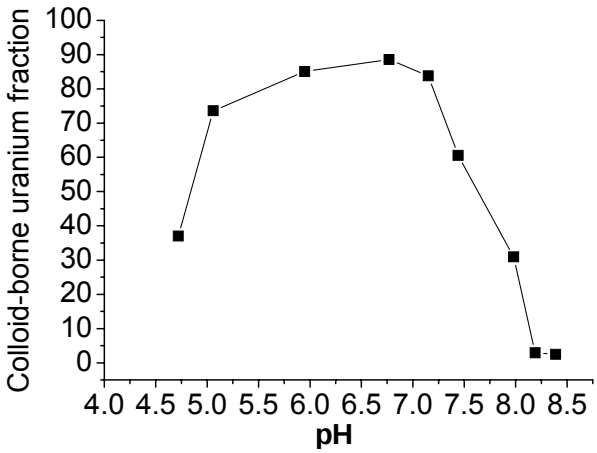

Fig. 2: Colloid-borne fraction of total U in the colloidal solution produced by the weathering of phyllite in dependence on pH (50 µg/L U, 105 mg/L $NaHCO_3$).

REFERENCES

[1] Zänker, H. *et al.* (2006) *Aquatic Geochem.* (accepted).
[2] Zänker, H. *et al.* (2004) *Report FZR- 419*, p. 16.
[3] Zänker, H. *et al.* (2003) *Report FZR-400*, p. 48.

Characterization of the colloidal inventory of mineral waters and physiological salines by laser-induced breakdown detection (LIBD)

K. Opel, H. Zänker, G. Bernhard

The capability of LIBD to quantify size and concentration of colloids present in nearly particle-free solutions was demonstrated at physiological salines and mineral waters.

The migration of contaminants in the environment or of pharmaceutic agents in human organisms can significantly be influenced even by traces of colloids. Therefore, the quantification of these colloidal traces can be of interest.

EXPERIMENTAL. Samples were analyzed by LIBD without prior treatment in flow mode at laser pulse energies of 1.5 mJ. The setup is described in detail in [1]. Breakdown events induced by 14,000 (mineral waters) or 30,000 (salines) laser pulses were detected acoustically and optically. The system was calibrated with suspensions of standard particles consisting of polystyrene latex.

MINERAL WATERS. In the course of a study aimed at the uranium speciation in mineral waters the colloids of these waters were investigated to clarify whether the uranium is attached to them [2]. Though it was shown that the uranium is not colloid-borne, particle sizes and concentrations could be determined by LIBD. The results are given in Tab. 1.

Tab. 1: Concentration c_P and mean diameter d_P of particles present in mineral waters determined by evaluation of LIBD results (p_{BD}: breakdown probability, z_F: focal length).

Water	p_{BD}	z_F / µm	d_P / nm	c_P / ppb
Hunyadi Janos	0.181	1438	20	0.04
Margon Medium	0.381	1540	30	0.60
Margon Still	0.133	1514	25	0.05
San Pellegrino	0.052	1459	20	0.01

Although all waters contain only small particles in relatively low concentrations – San Pellegrino is even comparable to the ultrapure water used in our lab - they could be distinguished by LIBD. Photon correlation spectroscopy as a classical characterization method for colloidal solutions was not able to determine the particle size in any of the samples.

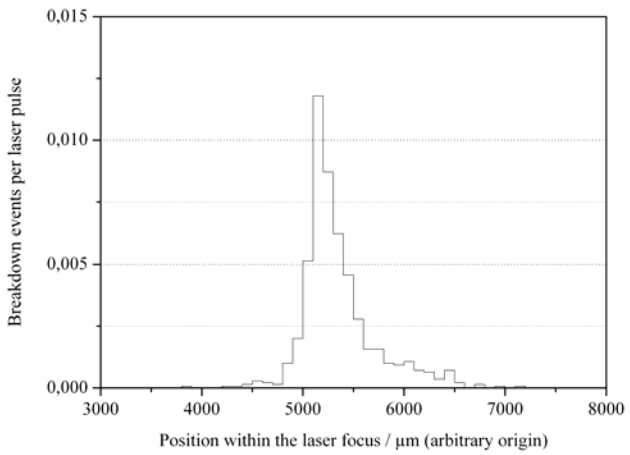

Fig. 1: Frequency distribution of breakdown events in the focal area of the laser beam (San Pellegrino; 14,000 laser pulses at 1.5 mJ).

However, it should be mentioned that the LIBD only yields the mean diameter when the focal length z_F is measured. To resolve bimodal particle size distributions, the frequency distribution of breakdown events in certain parts of the laser focus has to be evaluated. Such a distribution is shown in Fig. 1 for San Pellegrino. Monomodal particle size distributions would yield one nearly Gaussian peak. In Fig. 1 two overlapped peaks of this type are distinguishable. "Fitting by eye" gives a z_F of about 800 µm for the narrower peak corresponding to a particle diameter of less than 5 nm. A more accurate deconvolution of the peaks requires a better calibration of the system with bimodal suspensions of standard particles.
The low particle concentrations of the mineral waters are attributed to the de-ironing of such waters. The de-ironing is intended for separating the iron but removes almost all the particles, iron and non-iron ones.

PHYSIOLOGICAL SALINES. Physiological salines contain 9 g/L sodium chloride. Since sodium chloride is completely soluble in this concentration range, physiological salines should not contain any solid particles. Nevertheless, investigation of the salines by LIBD revealed distinctive differences between the solutions of various suppliers. The results are shown in Tab. 2.

Tab. 2: Concentration c_P and mean diameter d_P of particles present in physiological salines determined by evaluation of LIBD results (p_{BD}: breakdown probability, z_F: focal length).

Saline	p_{BD}	z_F / µm	d_P / nm	c_P / ppb
L1: DeltaSelect, Pfullingen	0.156	2185	150	2
L2: Serumwerk Bernburg	0.075	1873	80	0.3
L3: Fresenius, Bad Homburg	0.169	1844	100	0.7
L4: Baxter, Unterschleißheim	0.067	1862	80	0.3
L5: Braun, Melsungen	0.073	1619	30	0.06

Though the overall colloid content is low, the particle mass concentrations of the solutions partly differ by a factor of 30. The solutions L1 and L3 contain considerably more colloids than our ultrapure water. A specific influence of the container material could not be observed. L1 and L5 were stored in polyethylene bags, L3 and L4 in glass bottles.

REFERENCES

[1] Hübener, S. *et al.* (2004) *Report FZR-400*, p. 46.
[2] Zänker, H. *et al.* this report, p. 56

Formation of stable Cu(II)-complexes with hexadentate bispidine ligands

S. Juran[1], H. Stephan[1], J. Steinbach[1], G. Geipel, G. Bernhard
[1]Institute of Radiopharmacy, FZR, Dresden, Germany

Time-resolved laser-induced fluorescence spectroscopy (TRLFS) has been used to determine the formation constants of bispidine ligands with copper(II). The formation of very stable 1:1 complexes has been proven.

Bispidines (bispidine = 3,7-diazabicyclo[3.3.1]-nonane) show interesting complexation behavior towards transition metals [1]. Considerably high complex stabilities towards Cu(II) have been found particularly in the case of pyridine-containing ligands [2]. The complex stability achieved for copper complexes with bispidines lying in the same range as found for macrocyclic compounds offers the possibility to apply such complexes for diagnostic and therapeutic purposes ($^{64/67}$Cu). Furthermore, the bispidine structure opens suitable chemical approaches to introduce bio-molecules into the skeleton. That is important in view of the targeting of such complexes.
Time-resolved laser-induced fluorescence spectroscopy (TRLFS) [3] has been applied to determine formal stability constants of the hexadentate bispidine ligands N_2Py_4, N_2Py_4-OH and the macrocyclic tetraamine cyclam (Fig. 1).

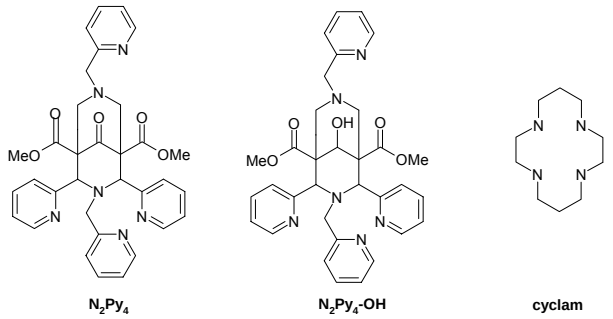

Fig. 1. Bispidine ligands N_2Py_4 and N_2Py_4-OH,and the macrocyclic tetraamine cyclam.

RESULTS AND DISCUSSION. Cyclam was purchased from Aldrich. N_2Py_4 was prepared according to the known procedure [2]. Reduction of N_2Py_4 with $NaBH_4$ in dioxane gave the mono-ol N_2Py_4-OH. TRLFS experiments were performed as described recently [4]. The slope of the "Stern-Volmer-Plot" gives the formal stability constant [5]. Fig. 2 displays the fluorescence spectra of N_2Py_4 in methanol and N_2Py_4-OH in water at different copper(II) concentrations. With adding copper(II) to the solution the fluorescence is almost completely quenched. This effect is characteristic for high stability constants. The formation constant of a 1:1 complex of N_2Py_4 with Cu(II) was found to be log K_{11} = 5.94 ± 0.09 in methanol. This is a remarkable result. The formation constant of N_2Py_4⊂Cu(II) is more than one order of magnitude higher compared to cyclam (log K_{11} = 4.61 ± 0.21 [6]) that forms one of the most stable complexes with Cu(II) at all. Even in water the bispidine ligand N_2Py_4-OH forms a very stable Cu(II)-complex (log K = 5.74 ± 0.10).

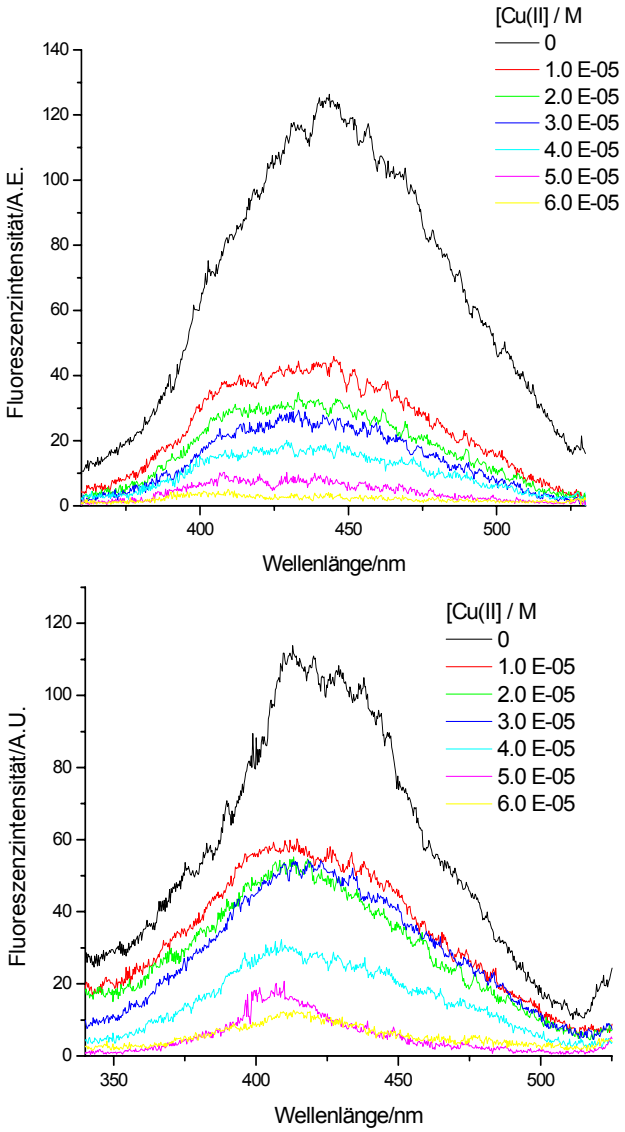

Fig. 2: Time-resolved fluorescence spectra of bispidine ligands N_2Py_4 (methanol, $Cu(CF_3SO_3)_2$) and N_2Py_4-OH (H_2O, $Cu(NO_3)_2$) in dependence of Cu(II) concentration.

REFERENCES

[1] Comba, P. *et al.* (2003) *Coord. Chem. Rev.* **238-239**, 21-29.
[2] Bleiholder, C. *et al.* (2005) *Inorg. Chem.* **44**, 8145-8155.
[3] Geipel, G. *et al.* (2003) *Report FZR-349,* p. 53-60.
[4] Geipel, G. *et al.* (2001) *Report FZR-343*, p. 7.
[5] Geipel, G. *et al.* (2004) *Spectrochim. Acta Part A* **60**, 417-424.
[6] Stephan, H. *et al.* (2005) *Tetrahedron Lett.* **46**, 3209-3212.

Complexation of Cu(II) by glycodendrimers

A. Röhrich[1], H. Stephan[1], J. Steinbach[1], G. Geipel, G. Bernhard, G. Bergamini[2], V. Balzani[2]
[1]Institute of Radiopharmacy, FZR, Dresden, Germany, [2]University of Bologna, Bologna, Italy

Kinetics and stability of Cu(II) complexation by glycodendrimers have been explored. Slow formation of stable 1:1 complexes was found.

Cyclam and its derivatives form very stable complexes in particular with transition and rare earth metal ions [1]. Metalloradio-pharmaceuticals of the metallic radionuclides $^{64/67}$Cu, ^{99m}Tc, $^{186/188}$Re and ^{90}Y are used for diagnostic and therapeutic purposes [2]. In this nexus, we want to develop dendritic ligands having both enhanced complex stability and improved bioavailability. Thus, we built up two glycodendrimers possessing a cyclam core modified with thiourea-linked sugar residues at the surface (Fig. 1). D-glucose and 2-acetamido-2-deoxy-D-glucose have been chosen as sugar moieties. The latter one is frequently a part of metabolites of aberrant glycosylation on cancer cells [3].

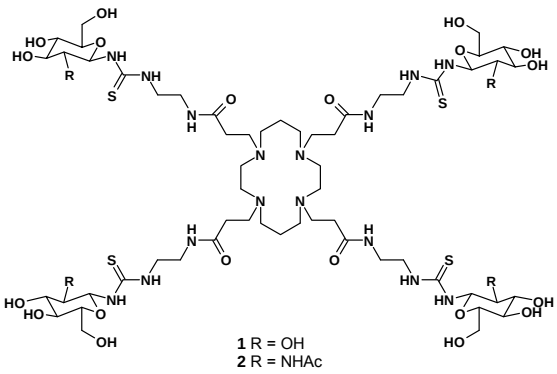

Fig. 1: Glycodendrimers **1** and **2**.

RESULTS AND DISCUSSION. The glycodendrimers **1** and **2** were prepared by glycosylation of the tetraamino-functionalised cyclam core precursor [4] using the O-acetyl-protected glucosyl isothiocyanates. Deacetylation with MeONa in MeOH gave compounds **1** and **2**. Purification was obtained by size exclusion chromatography. Preliminary experiments have been performed in order to achieve information about the kinetics and stability of complex formation of Cu(II) with these glycodendrimers. Kinetics of complex formation of **1** and **2** with Cu(II) was monitored by the change of absorbance at 320 nm (Fig. 2). The maximum of absorbance was obtained at a ratio of 1 between metal to ligand concentration indicating the formation of 1:1 complexes. A slow attainment of complexation equilibrium was observed at room temperature, significantly accelerated at 37 °C. Kinetic constants were found to be 185 ± 8 $M^{-1}\cdot sec^{-1}$ (25 °C), 492 ± 8 $M^{-1}\cdot sec^{-1}$ (37 °C) for **1⊂Cu(II)**, and 340 ± 30 $M^{-1}\cdot sec^{-1}$ (25 °C), 1580 ± 20 $M^{-1}\cdot sec^{-1}$ (37 °C) for **2⊂Cu(II)**.
To estimate the stability of the complexes formed, TRLFS experiments have been carried out [5]. Formal association constants were determined to be $\log K_{11} = 4.51 \pm 0.51$ (**1⊂Cu(II)**), and $\log K_{11} = 4.60 \pm 0.50$ (**2⊂Cu(II)**).

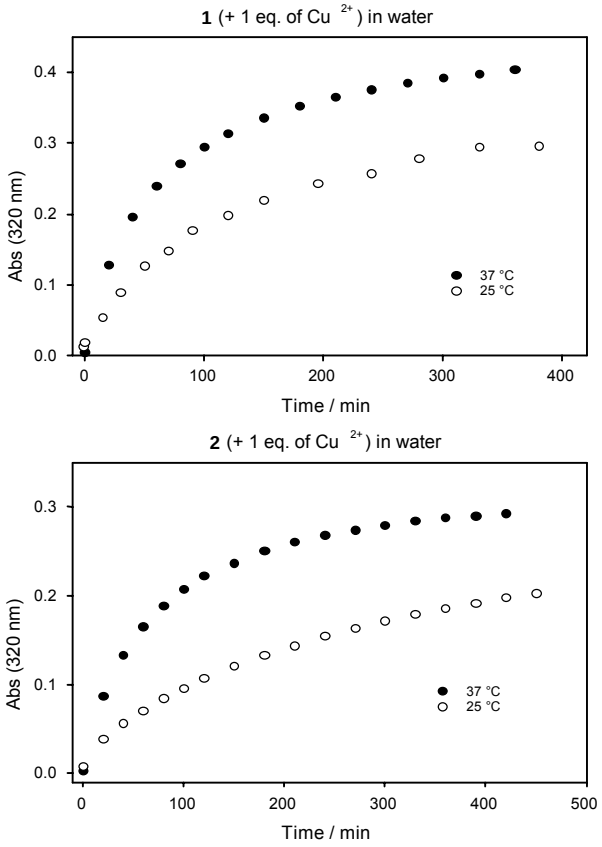

Fig. 2: Absorbance of Cu(II) complexes with the glycodendrimers **1** and **2** as a function of time and temperature.

REFERENCES

[1] Izatt, R.M. *et al* (1991) *Chem. Rev*. **91**, 1721-2085.
[2] Liang, X. *et al* (2004) *Chem. Soc. Rev.* **33**, 246-266.
[3] Vannucci, L. *et al*. (2003) *Int. J. Onc.* **23**, 285-296.
[4] Stephan, H. *et al*. (2005) *Tetrahedron Lett.* **46**, 3209-3212.
[5] Geipel, G. *et al* (2004) *Spectrochim. Acta A* **60**, 417-424.

Part 2:

Actinides in bio-systems

Interaction of U(VI) with *Chlorella vulgaris*

A. Günther, J. Raff, G. Bernhard

Laser-induced fluorescence spectroscopy and ICP-MS measurements were used to study the interaction of U(VI) with cells of the green algae *Chlorella vulgaris* and the properties of the formed uranyl complexes at pH 3 and 6. The spectroscopic results of experiments at pH 3 are more similar to spectra of carboxylic than to spectra of phosphate bound uranium. By contrast, phosphate groups are mainly responsible for the immobilization of U(VI) at pH 6.

EXPERIMENTAL. *Chlorella vulgaris* was grown in a liquid algae full medium [1] under air supply and light until the end of the exponential growth phase. The algae biomass was harvested by centrifugation and washed with 0.9 % $NaClO_4$ solution. The purity of algae culture was verified by light microscope. Than the cells were stored at –20°C. For the sorption experiments the algae biomass was contacted 144 h with U(VI) solution at pH 3 and 6. The experiments were performed in 0.9 % $NaClO_4$ solution. The concentration of resuspended algae biomass in each reaction solution was 0.75 g dry mass / L and the uranium concentration was $1 \cdot 10^{-4}$ M. The pH values of the solutions were adjusted with $HClO_4$ or NaOH. The fluorescence emission spectra were recorded from 350 to 664 nm using an excitation wavelength for the uranium of 266 nm.

RESULTS. Calculation of the U(VI) speciation in the starting solutions with the computer program EQ3/6 using NEA data base showed that the uncomplexed uranyl ion UO_2^{2+} dominate the U(VI) speciation at pH 3 (initial solution A). $(UO_2)_3(OH)_5^+$, $(UO_2)_4(OH)_7^+$ and $(UO_2)CO_3(OH)_3^-$ are the main species in the initial solution B at pH 6.

Figs. 1 and 2 show the uranyl fluorescence spectra of the contaminated algae biomass in comparison to the uranyl spectra of the solutions before and after the experiment at pH 3 and 6, respectively.

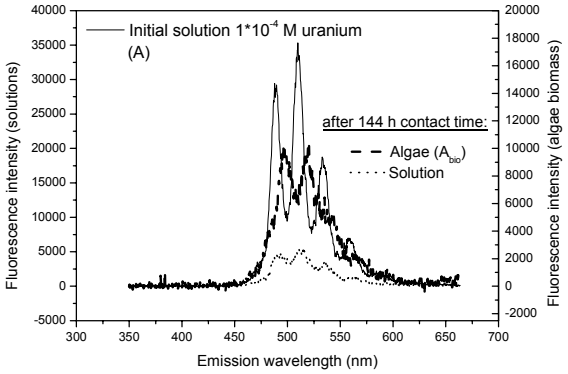

Fig. 1: Fluorescence spectra of different samples of the U(VI) / algae system at pH 3.

The fluorescence intensity of the uranyl species in the initial solutions decreases strongly after contact with algae. ICP-MS analysis demonstrated that 36.5 % of uranium in the initial solution was sorbed /accumulated by the algae biomass at pH 3. But approximately only a third of the dissolved uranium could be detected at a stable pH value and without a shift of the emission bands at the end. A possible reason therefore may be the release of substances from algae forming uranyl complexes which show no fluorescence or which quench the fluorescence.

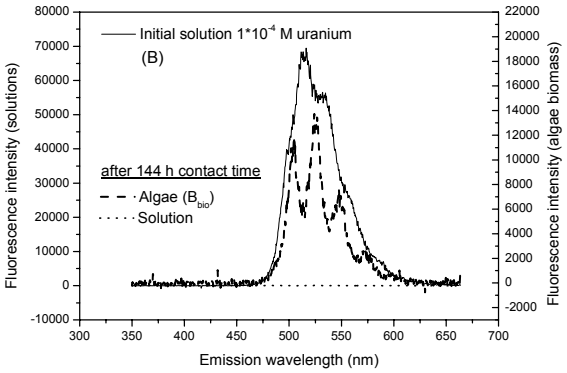

Fig. 2: Fluorescence spectra of different samples of the U(VI) / algae system at pH 6.

Tab. 1: Fluorescence emission bands of uranyl species in the algae biomass of *Chlorella vulgaris* in comparison to the bands of the uranyl species in the initial solutions.

Sample	Emission bands (nm)					
Initial-solution (A)	472.3	489.1	510.2	533.3	558.7	586.9
Algae (A_{bio})	481.8	497.8	518.5	540.4	566.6	592.2
Initial-solution (B)		497.3	514.6	535.1	557.1	584.9
Algae (B_{bio})		503.6	525.1	548.4	573.5	601.3

The binding of uranium on the algae cells at pH 6 is almost complete under the experimental conditions. In this case no fluorescence spectrum of the solution was obtained. Uranyl species were detected in the algae biomass in both experiments which means that uranium remained predominantly in the +VI oxidation state after the interaction with algae cells. The emission maxima of the uranyl species in the algae samples A_{bio} and B_{bio} shifted to higher wavelengths compared to the spectral maxima of the free uranyl ion in the initial solution A and to the spectral lines of the hydroxides in the initial solution B, respectively (see Tab. 1). This indicates that the uranium speciation in the initial solution and on and/or inside the cells of *Chlorella vulgaris* is different. In addition, spectral differences were found in the spectra of the uranium containing algae biomass A_{bio} and B_{bio}. The identification of the formed uranyl species at pH 3 is not yet clear. The formation of uranyl complexes with carboxylic ligands is possible. The positions of the uranyl emission bands in the spectrum of algae at pH 6 are comparable with those obtained for uranium containing higher plant samples, where uranium is mainly coordinated to inorganic and/or organic phosphate groups [2].

REFERENCES

[1] Esser, K. (2000) *Kryptogamen*, Springer Verlag Berlin, Heidelberg, New York.

[2] Günther, A. *et al.* (2003) *Radiochim. Acta* **91**, 319-328.

The use of a redox potential microsensor to determine geochemical heterogeneity within a multi-component biofilm

E. Krawczyk-Bärsch, K. Großmann, T. Arnold, S. Hermann[1], W. Vonau[1]
[1]Kurt-Schwabe-Institut für Mess- und Sensortechnik Meinsberg e.V., Meinsberg, Germany

Microsensors created by the Kurt-Schwabe-Institut für Mess- und Sensortechnik e.V. Meinsberg (Germany) were used to measure the redox potential in a heterogeneous multi-component biofilm and in a nutrient solution. In the biofilm an average redox potential of +170 mV was measured and in the nutrient solution a value of +243 mV was determined.

Bacteria in nature occur in large communities of bacteria glued together by Extracellular Polymeric Substances (EPS), called biofilm. For more information see *e.g.* Costeron *et al.* [1] and Flemming [2]. In these microbial systems, the redox potential (E_h) is primarily determined by the energy-yielding reactions of bacterial cells [3]. Different E_h values are attributed to the metabolic activity of the bacteria and the metabolic processes with different energy-yielding levels [4]. Our aim was to study the redox potential stratification in and outside of biofilms by microsensors.

EXPERIMENTAL. We generated heterogeneous biofilms composed of different bacterial species in a rotating annular bioreactor [5] on biotite platelets. The nutrient solution contained *Pseudomonas stutzeri, Pseudomonas fluorescens, Flavobacterium aquatile* and *Bacillus thuringiensis*. It was pumped through the rotating annular bioreactor for 6 weeks with a pump rate of 0.02 mL/min. The experiments were performed at a temperature of 20 °C. During the six weeks the biofilm grew to a thickness of approximately 170 µm, which was determined by confocal laser scanning microscopy (CLSM).
Parallel to these experiments redox potential microsensors were created in the Kurt-Schwabe-Institut für Mess- und Sensortechnik e.V. Meinsberg (Germany). The technical construction included an electrochemical microsensor forming a unit with an integrated micrometer screw that enables the microsensor to move vertically in the biofilm in µm-steps. Because of the horizontal and vertical variability of the redox potential within the biofilm redox sensors with extreme small diameters were required. For the glass coated Pt sensor an outer diameter of 300 µm and a sensitive area of 80 µm in diameter were realized. The wax/resin covered sensor had an outer diameter of 120 µm and a sensitive area of 80 µm in diameter.
The sensor systems consist of an indicator electrode and a reference electrode. The reference electrode is arranged side-wise, possessing a ceramic diaphragma. To minimize electrical interference, the measurement setup was shielded with a Faraday cage.
The E_h measurements were carried out in the following way. At first an E_h measurement was conducted in the overlaying medium and monitored for 38 minutes. Subsequently the microsensor was inserted vertically into the biofilm with a micromanipulator and the E_h was measured for 50 minutes.

RESULTS. During our experiments significant differences were observed between the redox potential in the overlaying medium and in the biofilm underneath. The results from the redox potential measurements are shown in Fig. 1. They can be described as follows:

- The nutrient solution (medium) shows an average redox potential of +243 mV.
- The average redox potential in the biofilm decreased to a value of +170 mV, clearly indicating that the redox potential is influenced by microbial processes in the biofilm.

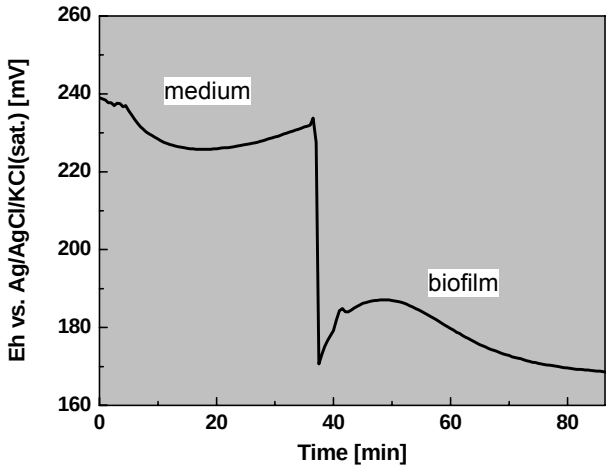

Fig. 1: Redox potential measurements over time in the nutrient solution (medium) and in the biofilm.

The results show that we were able to measure changes of the redox potential over time in a living biofilm with the newly developed microsensors. The values are in agreement with values reported by Bishop and co-workers [3]. The changes are attributed to microbial metabolic activity within the biofilm. These results also clearly indicate that heterogeneous Eh conditions within biofilms may have a severe influence on the permanent and temporal immobilisation of redoxsensitive radionuclides such as U, Pu or Np. Biofilms may influence heavy metal transport by changing the geochemical conditions within the biofilm or simply by adsorption onto the microbial cell wall [6]. They have to be considered in risk assessments.

REFERENCES

[1] Costerton, J.W. *et al.* (1987) *Ann. Rev. Microbiol.* **41**, 435-464.
[2] Flemming, H.C. *et al.* (2002) *The Encyclopedia of Environmental Microbiology* **3**, p. 1223-1231, John Wiley & Sons, New York.
[3] Bishop, P.L. *et al.* (1999) *Wat. Sci. Tech.* **39**, 179-185.
[4] Brock, T.D. *et al.* (1994) *Biology of Microorganisms* **95**, 576.
[5] Lawrence, J.R. *et al.* (2000) *J. Microb. Meth.* **42**, 215-224.
[6] Moore, C.M. *et al.* (2002) *The Encyclopedia of Environmental Microbiology* **4**, p. 1902-1912, John Wiley & Sons, New York.

Spectroscopic evidence of U(VI) in *Pseudomonas stutzeri* biofilms

K. Großmann, T. Arnold, E. Krawczyk-Bärsch, G. Bernhard

Particles were visualized by Confocal Laser Scanning Microscopy (CLSM) in a mature confluent *Pseudomonas stutzeri* biofilm growing on a glass-surface. These particles were spectroscopically identified as uranium(VI) compounds.

More than 99% of all microorganisms in nature usually do not occur as single individual cells but rather in large communities of bacteria glued together by Extracellular Polymeric Substances (EPS) [1]. Such aggregates are called biofilms. Besides *Alcaligenes, Acinetobacter, Arthrobacter, Bacillus, Flavobacterium, Nocardia, Sphingomonas* and *Agrobacter* species, *Pseudomonas* species are well-known biofilm-inhabiters [2]. In addition to strictly abiotic reactions metals can be transformed by microbially mediated reactions [3]. These reactions may lead to temporal or permanent immobilizations of heavy metals within living biofilms and therefore have to be considered for risk assessments.

EXPERIMENTAL. A biofilm was cultured in an annular rotating biofilm reactor [4] at near-neutral pH conditions. During the experiment the nutrient flow rate was 15 ml/min and the rotation velocity of the inner cylinder was 14 rpm. Glass slides were used as substratum for the growing biofilm. The bacteria suspension contained *Pseudomonas stutzeri* and standard nutrient medium. The experiments were not performed under sterile conditions. Therefore the biofilm is a mixed culture biofilm dominated by *Pseudomonas stutzeri.* After 3 to 5 weeks of pumping the bacteria suspension through the biofilm reactor a mature confluent biofilm was established on the glass slides. Then uranium(VI) was added to the nutrient solution to obtain a final uranium(VI) concentration of $5 \cdot 10^{-6}$ M. After an incubation time of at least 2 weeks the resulting biofilm was studied by CLSM. During the CLSM investigations no fluorescence markers for labeling microorganisms, EPS or uranium were used. For visualization, the samples were excited with a diode laser using an excitation wavelength of 408 nm and the emitted fluorescence signal was recorded. The Leica objective HC PL FLUOTAR 10x/0,3 was used.

RESULTS. The thickness of the *Pseudomonas stutzeri* dominated biofilm was determined by CLSM to be 43 µm. The diffuse regions of the CLSM image (see Fig. 1) are attributed to emitted auto-fluorescence light of the microorganisms and associated EPS. In addition, very bright particles of approximately 1 to 5 µm diameter were detected within the biofilm. To spectroscopically analyse these particles, they were irradiated with an excitation wavelength of 408 nm and the emitted fluorescence light was recorded (see Fig. 2) It showed a characteristic uranium(VI) fluorescence signal from 490 to 560 nm, similar to the emission spectra of uranium(VI) with *Thiobacillus ferrooxidans* described by Panak *et al.* [5]. These uranium(VI) particles were observed inside the biofilm. In regions with minor or without microbial populations on the substratum no uranium particles were observed.

CONCLUSION. The results show that we were able to visualize uranium particles inside biofilms by CLSM.

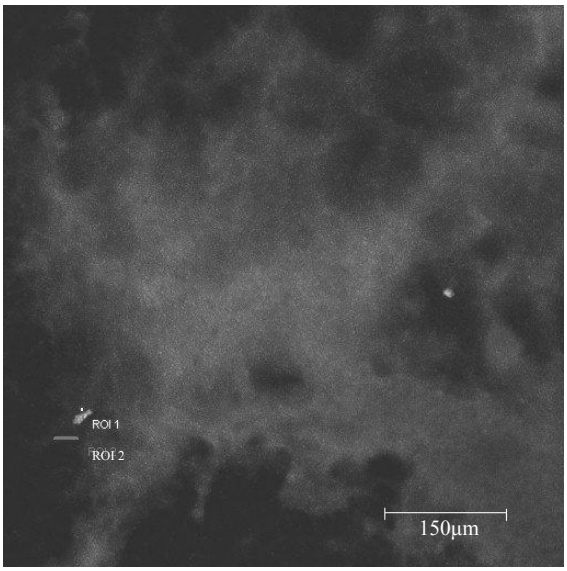

Fig. 1: Confocal image of a *Pseudomonas stutzeri* dominated biofilm. Diffuse regions are attributed to biofilms. ROI 1 and ROI 2 are regions of interest for spectral investigations (see Fig. 2).

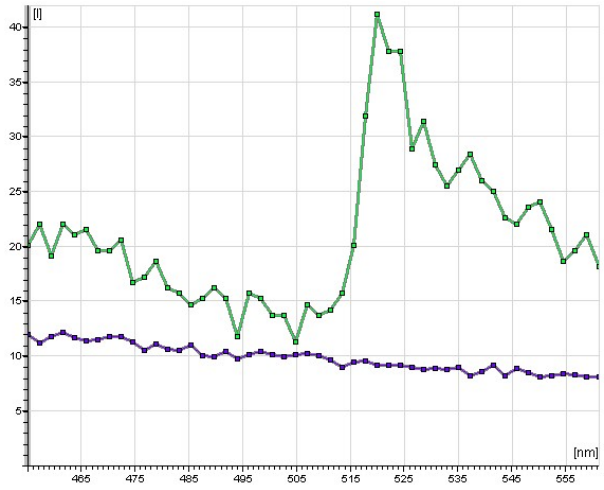

Fig. 2: Emitted fluorescence light (465-555 nm) of small uranium particles (upper line, ROI 1) and the background fluorescence (lower line, ROI 2) by CLSM [xyλ-mode].

REFERENCES

[1] Flemming, H.-C. *et al.* (2000) *Vom Wasser* **94,** 245-266.
[2] Flemming, H.-C. *et al.* (1998) *gwf-Wasser/Abwasser* **139**, 65-72.
[3] Moore, C.M. *et al.* (2002) *The Encyclopedia of Environmental Microbiology* **2**, p. 821-835, John Wiley & Sons, New York.
[4] Lawrence, J.R. *et al*. (2000) *J. Microbiol. Methods* **42**, 215-224.
[5] Panak, P. *et al.* (1998) *Radiochim. Acta* **84**, 183-190.

Transmission electron microscope analysis of U(VI) accumulated by different bacterial isolates from extreme habitats

M. Merroun, M. Nedelkova, G. Bernhard, S. Selenska-Pobell

The cellular localization of U(VI) accumulated by cells of bacterial strains isolated from extreme habitats at different pH values are investigated using transmission electron microscope (TEM) and energy-dispersive X-ray (EDX) analysis. The results showed that the cells precipitate U(VI) a uranium mineral phase at pH 4.5. However, at pH 2 uranium formed complexes with organically bound phosphates of the cell surface.

This paper summarizes the effect of pH on the cellular localization of uranium bound by bacterial strains isolated from the S15 deep-well montoring site, located at the Siberian radioactive subsurface depository Tomsk-7, Russia. Previous EXAFS studies demonstrated that at very acidic pH (pH 2.0) uranium forms complexes with organically bound phosphate of the cell surface while at pH 4.5 in the presence of inorganic phosphate, this radionuclide is precipitated as an m-autunite-like phase [1].

EXPERIMENTAL. After incubation with uranium, the bacterial cells were fixed in 2.5 % glutaraldehyde in 0.1 M cacodylate buffer (pH 7.2) for 2 h at 4°C and then washed three times with the same cacodylate buffer. The cell pellets were fixed for 60 min. at 4 °C in 1 % OsO_4 in cacodylate buffer before being dehydrated with ethanol and embedded in Spurr resin. The samples were thin-sectioned (0.25 µm) using a diamond knife on a Reichert Ultracut S ultramicrotome, and the sections were supported on copper grids and coated with carbon. Samples were examined with a high resolution Philips CM 200 transmission electron microscope at an acceleration voltage of 200 kV under standard operating conditions with the liquid nitrogen anticontaminator in place. EDX analysis was performed at 200 kV using a spot size of 70 Å, and a live counting time of 200 s.

RESULTS. TEM observations of the cells of the two isolates exposed to U solution at pH 2 and 4.5 revealed significant differences on the U accumulation profile for the two pH values. At pH 2, small amounts of U are bound to bacterial cell surfaces of both isolates (Fig. 1). No uranium was detected associated with intracellular or extracellular space.

At pH 4.5, we note the presence of electron dense accumulations extracellularly and on the cell surface of *Microbacterium oxydans* S15-M2. *Sphingomonas* sp. S15-S1 accumulated U in form of precipitates at the cell membrane, and also intracellularly in electron dense granules.

The present study describes different kinds of interaction mechanisms between U and bacterial strains isolated from an extreme habitat as a function of pH. Precipitation of uranium at pH 4.5 in the presence of the bacterial cells studied in this work produces a chemically stable species which can be described as an m-autunite-like phase. This formation is obviously not limited to reducible metals. The results obtained might be useful in predicting the fate and transport of actinides in near-surface environments as well as in using these bacteria for bioremediation of actinide-contaminated sites.

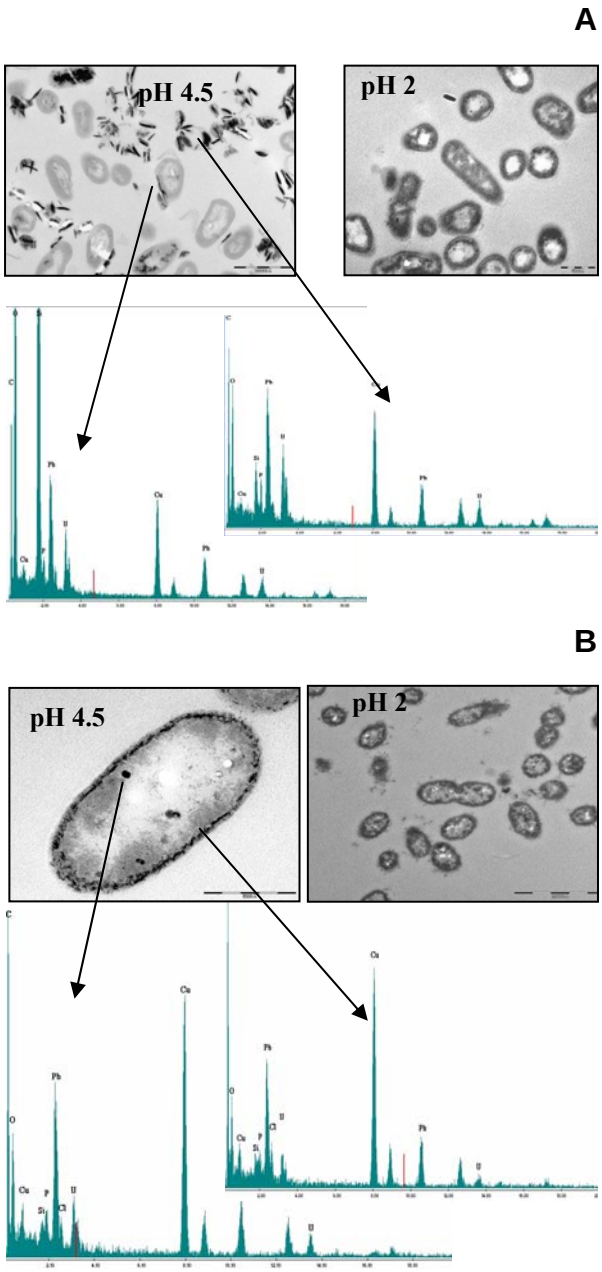

Fig. 1: Transmission electron micrographs of thin sections of *M. oxydans* S15-M2 (A) and *Sphingomonas* sp. S15-S1 (B) cells treated with uranium at pH 2 and 4.5 and EDX spectra of the uranium accumulates.

ACKNOWLLEDGEMENTS. This work is supported by grant FIKW-CT-2000-001105 "BORIS" from the EU and grant D/04/39988 from DAAD.

REFERENCES

[1] Merroun, M. *et al.* (2005) *Radiochim. Acta* (in press).

Uranium binding by S-layer carrying isolates of the genus *Bacillus*

J. Raff, S. Berger, S. Selenska-Pobell

Several *Bacillus*-isolates, recovered from a uranium (U) mining waste pile, were screened for the expression of surface-layer (S-layer) proteins. The S-layer positive isolates were used to determine the U binding capacity of intact bacterial cells and of purified S-layer proteins. At pH 4.5 U binding capacities were measured from 11.6 ± 2.5 to 229 ± 24.54 mg U/g dry weight (dw) for the intact cells and between 42.5 ± 2.5 and 411.7 ± 0.3 mg U/g dw for the purified S-layers.

During the last years the interaction of U with the isolate *B. sphaericus* JG-A12, recovered from the uranium mining waste pile "Haberland" near Johanngeorgenstadt (JG), Saxony, Germany, was intensively studied. It was demonstrated that *B. sphaericus* JG-A12 cells, spores and S-layer bind U selectively and reversibly in amounts of 64.0, 109.5 and 19.5 mg U/g dw *via* phosphate and carboxyl groups [1,2]. The S-layer of the JG-A12 isolate posseses higher affinity to U than the S-layer of the *B. sphaericus* strain NCTC 9602, recovered from air samples [3]. In the present work several *Bacillus* isolates were studied, recovered from the same uranium mining waste pile but from another almost 5 times more contaminated with uranium site (site B).

EXPERIMENTAL. The *Bacillus* waste pile isolates were grown in nutrient broth (5 g/L peptone, 3 g/L meat extract) supplemented with $MnSO_4$ (10 mg/L $MnSO_4$ x $1H_2O$) to the late logarithmic growth phase. After washing the cells, the biomass was split into two parts, one for the U binding experiments with intact cells and the other part for isolatatin of S-layers. The S-layers were extracted with modified protocols according to [1]. In some cases extra solubilization steps, using 6 M guanidine hydrochloride, ammonium sulfate precipitation steps and multiple dialyzes of the S-layers were necessary to get purified S-layer proteins. For the binding experiments 20 mg dw cell biomass and 5 or 20 mg dw of S-layer proteins were used. In all cases the biomass was equilibrated to a pH of 4.5. After transferring the biomasses to 12.5 or 50 mL of $UO_2(NO_3)_2$ x $6H_2O$ solutions, containing 400 mg/L U (cell experiments) or 200 mg/L U (S-layer experiments) in 0.9 % $NaClO_4$, pH 4.5, the samples were shaken for 48 h at 30 °C. Finally all samples and controls were centrifuged at 10.000 g for 15 min and the U content of all supernatants was measured by inductive coupled plasma mass spectroscopy (ICP-MS).

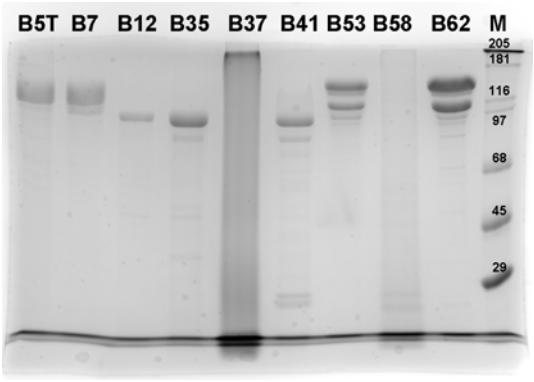

Fig. 1: 10 % SDS polyacryl-amide gel of the purified S-layer proteins from the studied *Bacillus* isolates. M: Marker (M_r in kDa).

RESULTS. The screening of 21 *Bacillus* waste pile isolates revealed the presence of S-layer proteins in 9 cases, namely the isolates JG-B5T, B7, B12, B35, B37, B41, B53, B58 and B62. All S-layers were successfully isolated (see Fig. 1). But the S-layer proteins of B37 and B58 are unstable and the isolates B53 and B62 seem to express two different S-layer proteins. To identify all obtained proteins as S-layer proteins, further analyzes will include the N-terminal sequencing of all proteins in order to check for the presence of SLH-domains, characteristic for the *Bacillus* S-layer proteins. U binding experiments showed, that most of the S-layer proteins have higher binding capacities than the intact cells, except the S-layer of the isolates B53 and B5T (see Fig. 2).

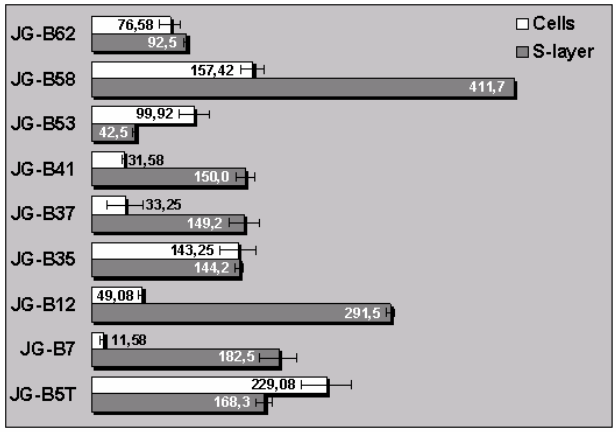

Fig. 2: Uranium binding (in mg U/g dw) by cell or S-layer biomass of different *Bacillus* isolates.

In the case of B5T a very robust capsule is protecting the cells, that may also be involved in the binding of U. B53 and B62 were identified as *B. sphaericus* strains (data not shown) and are therefore the closest relatives to *B. sphaericus* JG-A12. In particular, the cells and the S-layer of B53 have only slightly higher binding capacities to those of the JG-A12 isolate. Interestingly all S-layer proteins of the strains isolated from the more contaminated with U soil sample have higher binding capacities than the S-layer of *B. sphaericus* JG-A12. In addition, all studied S-layer proteins of the B-isolates, again apart from B53, possess a higher phosphorous (P) content than the S-layer of JG-A12. But there is no direct correlation between the amount of bound U molecules and the number of P molecules present in the proteins. The question is, which molecular mechanisms are responsible for the extremely high uranium binding capacity of some S-layers of the B-isolates. Beside this fundamental question, the S-layer protein of B12 and possibly that of B58 are excellent candidates for the construction of a filter material for the removal of dissolved U from drinking water.

ACKNOWLEDGEMENTS. We thank U. Schaefer for the ICP-MS analyses.

REFERENCES

[1] Raff, J. *et al.* (2003) *Chem. Mater.* **15**, 240-244.
[2] Merroun, M. *et al.* (2005) *Appl. Environ. Microbiol.* **71**, 5532-5543.
[3] Raff, J. *et al.* (2004) *Report FZR-400*, p. 24.

Formation of gold nanoclusters by DMAB in the presence of cells and S-layer protein of *Bacillus sphaericus* JG-A12

M. Merroun, K. Pollmann, A. Rossberg, A.C. Scheinost, S. Selenska-Pobell

Cells and S-layer sheets of *B. sphaericus* JG-A12 were used as templates for the deposition of metallic gold nanoclusters using dimethyl amino borane (DMAB) as reducing agent. Gold L_{III}-edge XAS measurements confirmed the formation of Au(0) nanoclusters in both cases.

A combination of X-ray absorption spectroscopy (XAS) and Iterative Target Test Factor Analysis [1] was used previously to characterize the gold nanoparticles formed on the cells and S-layer protein of *B. sphaericus* JG-A12 using H_2 as reducing agent. The results demonstrated that only 67 % and 37 % of the Au(III) was reduced to Au(0) on the cells and S-layer protein of this bacterium, respectively [2]. The present study was undertaken in order to optimize the Au reduction process using another reducing agent dimethyl amino borane (DMAB).

EXPERIMENTAL. *B. sphaericus* JG-A12 cells were grown in a batch culture to mid exponential phase and harvested by centrifugation. The preparation of S-layer protein was performed as described in [3]. For sorption of Au(III), 15 mg of dialysed protein and 20 mg of cells were incubated in 150 mL and 30 mL of a solution of 2 mM $HAuCl_4$ x $3H_2O$, respectively. After 3 hours incubation at room temperature under shaking in the darkness the samples were centrifuged (20 min, 10000 × *g*) and the pellets were resuspended in H_2O. Residual salts were removed by dialysis of the metallized proteins and cells against H_2O. Au(III) was reduced by the addition of DMAB to produce Au(0)-nanoparticles. The metallized cells and protein samples were centrifuged (20 min, 10000 × *g*) and dried in a vacuum oven (48 h, 80 °C).

RESULTS. Figure 1 shows the XANES regions of the EXAFS spectra obtained with Au-treated S-layer and cells after addition of DMAB and for reference compounds containing two oxidation states of gold: Au(III) (solution of 2 mM $HAuCl_4$ x $3H_2O$) and metallic Au (gold foil). Comparison of the experimental spectra to the reference spectra clearly shows that Au is present mainly as metallic Au in the Au-treated S-layer and cells. To determine the relative amounts of Au(0) and Au(III) present in the biological samples, we applied Iterative Transformation Factor Analysis. The calculation revealed a mixture of 89 % metallic Au and 11 % Au(III) for the Au-loaded cells sample and 81 % metallic Au and 19 % Au(III) for the S-layer sample.
Gold L_{III}-edge EXAFS spectra of cells and S-layers of *B. sphaericus* JG-A12 in presence of DMAB are shown together with Au foil in Fig. 2. In these samples Au is present mainly as metallic phase where the interatomic distances found are comparable with the one of metallic foil. The coordination numbers (N) are different from the bulk ones, showing the presence of small metal particles. The reduction of the coordination number of the first shell is used to estimate the average particle. The coordination number of the Au-Au found in this work (8.7 ± 0.3 for the S-layer and 6.3 ± 0.4 for the cells sample) is not the real coordination number of the Au per nanoparticles. This value corresponds to the coordination number of Au-Au per sample. The coordination number of the bond distances per nanoparticle is weighted by the atomic percentage of Au atoms in the metallic phase. Using the cubic (FM3-M) structure of elemental gold, the average cluster size was estimated. It was found that the nanoparticles deposited on the cells and S-layer protein have a mean diameter of about 0.6 – 0.8 nm and 1.5 – 2.5 nm, respectively.

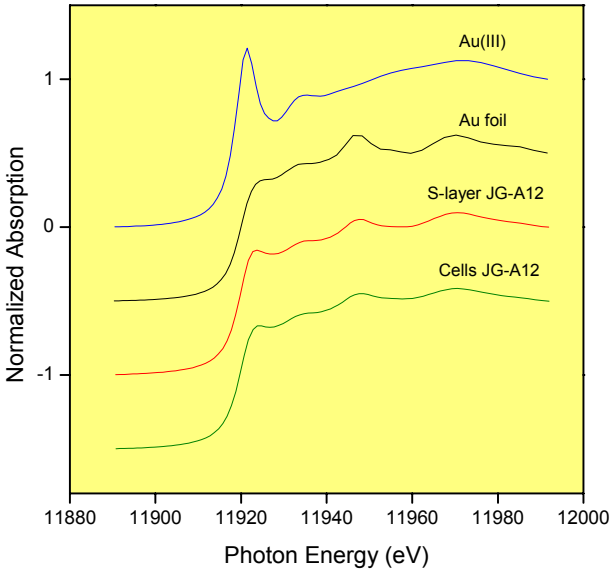

Fig. 1: XANES region of EXAFS spectra of the Au L_{III}-edge in reference compounds and for Au-loaded cells and S-layer of *B. sphaericus* JG-A12.

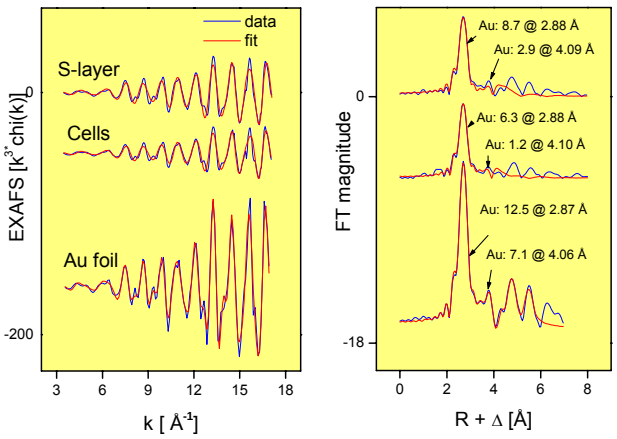

Fig. 2: Au L_{III}-edge EXAFS spectra and their FT of Au- treated cells and S-layer of *B. sphaericus* JG-A12 and gold foil.

ACKNOWLLEDGEMENTS. This work is supported by SMWK Grant N° 7531.50-03.0370-1/5.

REFERENCES

[1] Rossberg, A. *et al.* (2003) *Anal. Bioanal. Chem.* **376**, 631-638.
[2] Merroun, M. *et al.* (2006) *Mater. Sci. Engin. C* (submitted).
[3] Raff, J. (2002) *Report FZR -358*.

Construction of an S-layer with enhanced Ni-binding capacity

K. Pollmann, S. Matys[1], S. Selenska-Pobell
[1]Max Bergmann Center of Biomaterials, Dresden, Germany

An S-layer protein with enhanced Ni-binding capacity was produced by cloning and expression of the S-layer protein gene *slf*B of *Bacillus sphaericus* JG-A12 in *Escherichia coli*. The recombinant S-layer protein monomers reassembled into a regular three-dimensional structure which differs from that of the wild-type S-layer.

The proteinaceous surface layer (S-layer) of the cells of the uranium mining waste pile isolated *Bacillus sphaericus* JG-A12 is able to bind selectively and reversibly high amounts of heavy metals such as U, Pb, Cu, Al, Ga, and Cd [1]. The S-layer is composed of protein monomers with the ability to self-assemble into regular paracrystalline arrays. These characteristics make the S-layer interesting for biotechnological applications [2].
Previously, the S-layer protein gene of the strain *B. sphaericus* JG-A12 was cloned and heterologously expressed in *Escherichia coli* [3]. The protein was modified by the addition of six Ni-binding histidine residues at the N- and C-termini, enabling the purification by Ni-chelating chromatography [3]. In the present work, we studied the Ni-binding capacity of the purified modified S-layer protein in comparison to the wild-type S-layer protein of the strain JG-A12 and investigated the structure of the re-assembled modified S-layer by REM imaging.

EXPERIMENTAL. The S-layer protein gene of *B. sphaericus* JG-A12 was cloned into the vector pET30 Ek/Lic and heterologously expressed in *E. coli* Bl21(DE3). The expression of the gene was induced by addition of IPTG. The recombinant protein, carrying six histidine residues each at the N- and C-termini, was purified by Ni-chelating chromatography using a XK-26/20 column (Amersham) packed with Ni-Sepharose High Performance (Amersham) under denaturating conditions.
The Ni-binding capacity of the recombinant S-layer protein in comparison to the wild-type protein was investigated. Sorption experiments were carried out in dialysis tubes each containing 1 mg of protein. The tubes were shaken at 30 °C for 48 hours in a volume of 5 ml of a solution of 2 mM or 1 mM $NiCl_2$. The amount of sorbed Ni was calculated by the determination of the Ni-concentration in the supernatants using ICP-MS-analysis. All experiments were done in triplicate samples and repeated two times.
AFM images were taken from the wild-type S-layer and REM images were taken from the S-layer composed of the recombinant proteins.

RESULTS. As evident from the results presented in Fig. 1 the recombinant S-layer protein modified with 12 additional histidine residues possesses a significantly enhanced Ni-binding capacity in comparison to the wild-type protein, removing the double amount of Ni from a solution of 2 mM $NiCl_2$ in comparison to the wild-type S-layer. Histidine residues are well known for their strong interactions with Ni^{2+}. The present results demonstrate that a re-assembled S-layer protein with enhanced Ni-binding capacity could be engineered by the addition of His residues.

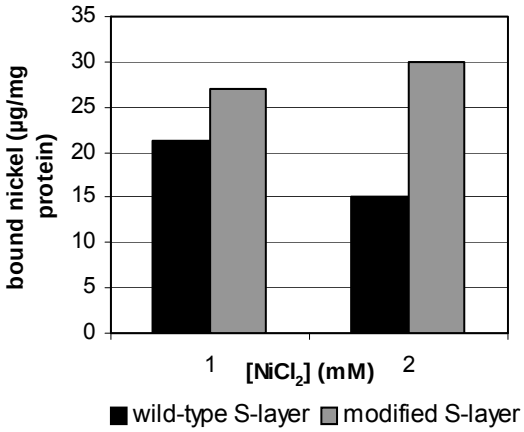

Fig. 1: Ni^{2+}-binding by the wild-type and recombinant S-layer proteins of *B. sphaericus* JG-A12. The proteins were incubated with solutions of 1 mM or 2 mM $NiCl_2$.

As shown in Fig. 2, the wild-type S-layer of JG-A12 tends to reassemble into regular tubes of a size of about 4×20 µm (A) or sheets (B). Such structures were not found in case of the modified S-layer protein, but the His-tagged protein re-assembled into regular spheres with a diameter of about 1-2 µm (C). REM images demonstrated that these spheres are formed by small regular sheets of a size of about 0.3×1 µm (D).

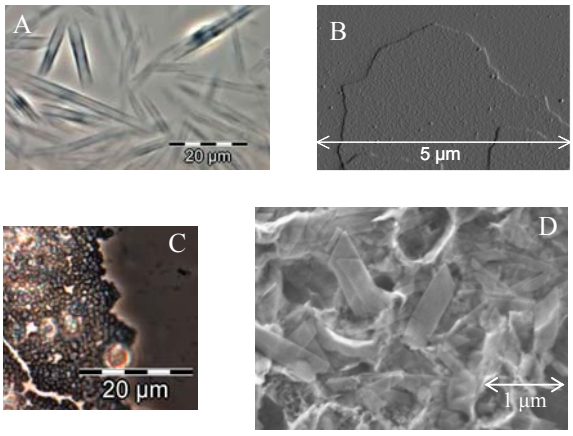

Fig. 2: Purified and re-assembled wild-type (**A** and **B**) and recombinant (**C** and **D**) S-layer of *B. sphaericus* JG-A12. **A, C** Light microscopic image; **B** AFM image; **D** REM image.

ACKNOWLEDGEMENTS. This study was supported by grant DFG/SE 671/7-2 from DFG, Bonn, and by EC grant GRD1-2001-40424.

REFERENCES

[1] Selenska-Pobell, S. *et al.* (1999) *FEMS Microbiol. Ecol*. **29**, 59-67.
[2] Pollmann, K. *et al.* (2006) *Biotechnol. Adv*. **24**, 58-68.
[3] Pollmann, K. *et al.* (2005) *Report FZR-419*, p. 38.

Interaction of actinides with *Desulfovibrio äspöensis* (DSM 10631^T). Part IV: Plutonium

H. Moll, M. Merroun, S. Selenska-Pobell, G. Bernhard

This study presents new results on the interaction of Pu(VI) and Pu(IV)-polymers with cells of the sulfate-reducing bacterial (SRB) strain *D. äspöensis*. The interaction mechanism includes five processes which have different time scales. Solvent extractions showed that 97 % of the initially present Pu(VI) is reduced to Pu(V) due to the activity of the cells within the first 24 h of contact time.

Microbes are widely distributed in nature and they can strongly influence the migration of actinides in the environment. This work continues our studies on microbial interactions of *D. äspöensis* with selected actinides in different oxidation states. This SRB-strain frequently occurs in the aquifer system of the Äspö HRL, Sweden [1]. In contrast to Cm(III) and U(VI), plutonium species are more redox active and can coexist in several oxidation states, *i.e.*, +3, +4, +5 and +6, in aqueous solution under environmental conditions [2]. It is unknown in which way *D. äspöensis* interacts with plutonium.

EXPERIMENTAL. The plutonium oxidation state distributions were determined by solvent extraction. As extracting agents theonyl-trifluoro-acetone (TTA, 0.5 M) in xylene, and di(2-ethylhexyl)phosphoric acid (HDEHP, 0.5 M) in toluene were taken according to [3,4]. All plutonium concentrations were measured by liquid scintillation counting (LSC). Cells of *D. äspöensis* were grown to the mid-exponential phase. The collected biomass was 0.9 ± 0.1 $g_{dry\ weight}$/L. The experiments were performed at pH 5 under N_2 atmosphere at 25 °C. As a background electrolyte 0.154 M NaCl was used. The $[^{242}Pu]_{initial}$ was varied between 7.6 and 254 mg/L. The separation of cells from the supernatant solution was performed by centrifugation.

RESULTS. The Pu oxidation state distribution of the blanks remains relatively unchanged as 47 ± 6 % Pu(VI) and 32 ± 3 % Pu(IV)-polymers (see Fig. 1A). 77 ± 5 % of the Pu occurs in the pentavalent oxidation state in the supernatant (see Fig. 1B).

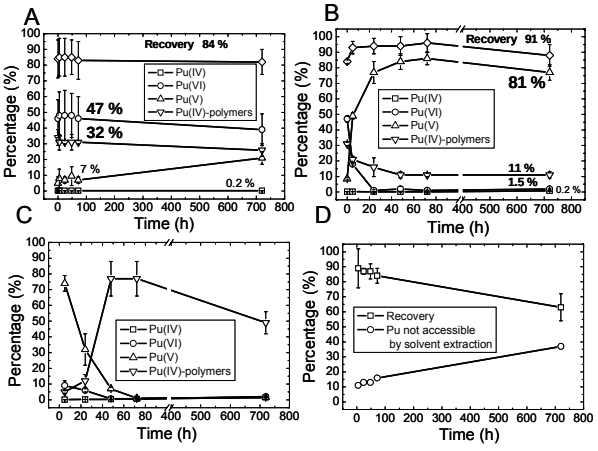

Fig. 1: Summary of the solvent extraction experiments showing the change of the ^{242}Pu oxidation state distribution in (A) the blank, (B) the supernatant and (C and D) the biomass samples.

The cell-bound ^{242}Pu consist of 49 ± 7 % Pu(IV)-polymers and a certain amount of Pu, 37 ± 6 %, which is not accessible by solvent extraction (see Fig. 1C and 1D). This study demonstrates that there is a strong interaction of the main plutonium species, Pu(VI) and Pu(IV)-polymers, with cells of *D. äspöensis*. On the basis of our results and taking into consideration the work of Panak and Nitsche [5], we developed a model which describes the ongoing processes (see Fig. 2) in the system Pu - *D. äspöensis*.

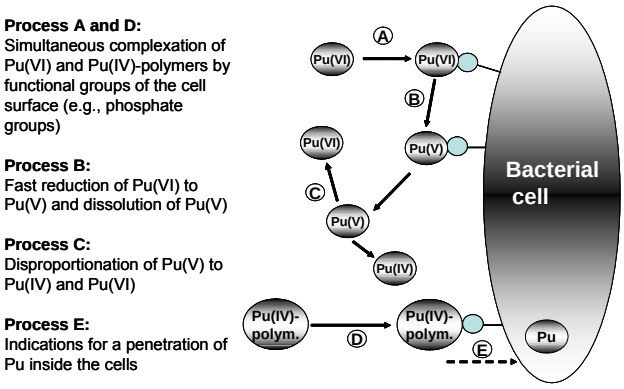

Fig. 2: Illustration of the different processes describing the interaction of Pu with *D. äspöensis* based on the schema developed by Panak and Nitsche in [5].

In the first step, the Pu(VI) and Pu(IV)-polymers are bound to the biomass. The biosorbed Pu(VI) was reduced in a fast direct enzymatic reaction to Pu(V). Most of the formed Pu(V) dissolves back to the aqueous solution due to the weak complexing properties of plutonium in this oxidation state. The dissolved Pu(V) disproportionates to Pu(IV) and Pu(VI). We conclude from the increased Pu amount which is strongly bound and not accessible for solvent extractions a penetration of Pu species (*e.g.*, Pu(IV)-polymers) inside the bacterial cell.
The observed processes cause changes of the oxidation state of Pu which have an impact on its migration behavior. The reduction of the Pu(VI) to Pu(V) by the bacteria leads to an increased dissolution of the cell bound plutonium. In contrast to the release of Pu(V) from the cell surface into the surrounding solution, we observed an immobilization of Pu as Pu(IV)-polymers by the bacteria.

ACKNOWLEDGEMENTS. This work was funded by the BMWi under contract number: 02E9491.

REFERENCES

[1] Motamedi, M. *et al.* (1998) *Int. Syst. Bacteriol.* **48**, 311-315.
[2] Neu, M.P. *et al.* (2005) *Radiochim. Acta* **93**, 705-714.
[3] Nitsche, H. *et al.* (1988) *J. Radioanal. Nucl. Chem. Articles* **124**, 171-185.
[4] Nitsche, H. *et al.* (1994) *Radiochim. Acta* **66/67**, 3-8.
[5] Panak, P.J. *et al.* (2001) *Radiochim. Acta* **89**, 499-504.

Desulfovibrio äspöensis (DSM 10631^T) and plutonium. XAS results

H. Moll, C. Hennig, A. Roßberg, M. Merroun, S. Selenska-Pobell, G. Bernhard

X-ray absorption near edge structure (XANES) spectroscopy in combination with extended X-ray absorption fine structure (EXAFS) were applied at the Pu L_{III}-edge in order to verify the plutonium oxidation state distribution and to determine the structure of the bound plutonium on cells of the SRB strain *D. äspöensis*. The results demonstrated that the accumulated Pu(IV)-polymers are interacting with the biomass.

X-ray absorption spectroscopy (XAS) is a powerful tool to characterize the speciation of heavy metals in a broad range of systems. The two parts, XANES and EXAFS, are giving in combination element specific information concerning the oxidation state and local structure of an absorbing metal. In this study, XAS was used for a detailed characterization of the microbial processes taking place in the system Pu – *D. äspöensis*. This strain predominates the indigenous SRB population at the Äspö aquifer system in Sweden.

EXPERIMENTAL. The spectrum from the Pu(VI) reference sample (0.05 M in 1 M HNO_3) was taken from earlier measurements [1]. The Pu(IV) reference sample (0.08 M in 1 M $HClO_4$) was prepared as described in [2]. 1 mL of the bacterial suspension in 0.9 % NaCl was incubated with 5 mL of ^{242}Pu, 127 mg/L, at pH 5. After shaking the samples for 96 h under N_2 atmosphere, the biomass was separated by centrifugation, washed with 0.9 % M NaCl, and sealed in a polyethylene cuvette. The bacterial sample was measured as wet paste. The Pu XAS data were recorded at the Rossendorf Beamline (ROBL, BM20) at the ESRF in Grenoble, France.

RESULTS. The low intensity of the white line (WL) and the feature near 18080 eV are indicating dominating plutonyl species in the blank, the supernatant and in the Pu(VI) reference (see Fig. 1).

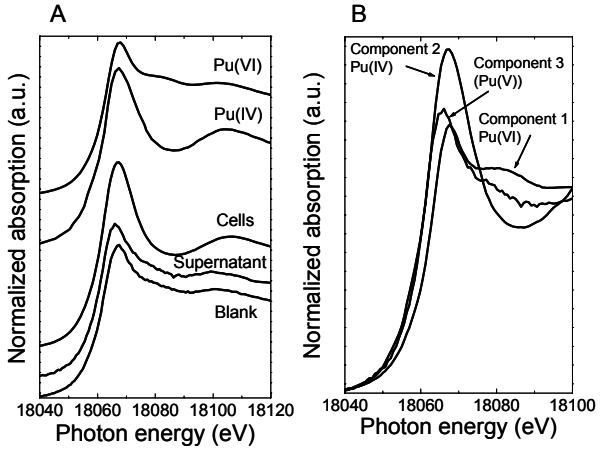

Fig. 1: (A) XAS data of the blank solution, the supernatant, the biomass and from the Pu(IV) and Pu(VI) reference samples. (B) Single component XANES spectra as a result from the iterative transformation factor analysis (FA).

This shoulder above the WL results from multiple scattering processes of the photo electron wave between Pu and the two axial oxygens. The Pu accumulated by *D. äspöensis* occurs in the tetravalent oxidation state. The characteristic changes in the absorption spectra were used to determine the relative concentrations of the Pu species by applying the iterative transformation factor analysis (FA). The calculations showed that every spectrum in Fig. 1A can be described by a combination of three independent components (see Fig. 1B).

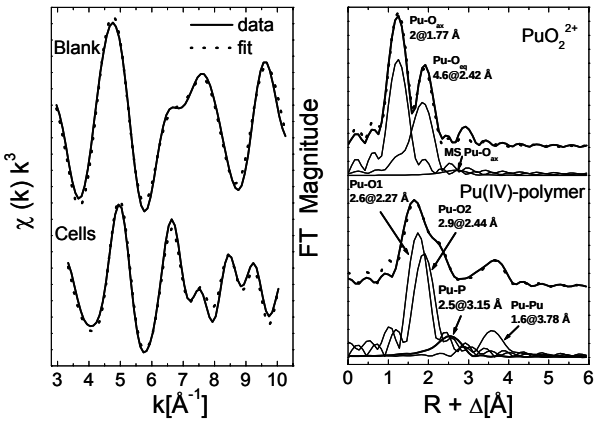

Fig. 2: Pu L_{III}-edge k^3-weighted EXAFS spectra (left) and the corresponding Fourier transforms (right) of the blank and the biomass sample and the theoretical fits (dotted line). The data were FT filtered using a Gaussian window (0.3 Å^{-1}).

The Pu in the blank is surrounded by two close axial oxygen atoms at 1.77 Å and approximately five equatorial oxygen atoms at 2.42 Å (see Fig. 2). These values are in very good agreement with published data [1]. Unfortunately, we cannot present structural parameters of Pu in the supernatant solution. Changes in the XANES from scan to scan showed that the sample was not stable in the synchrotron beam. The EXAFS oscillation of the cell-bound Pu show close similarities to the spectra of colloidal Pu(IV) species published in [3]. The presence of an additional symmetric EXAFS oscillation yielding a FT peak at R + Δ of approx. 2.8 Å gives evidence for an interaction of the Pu(IV)-polymers with light atoms of the biomass. The best fit result could be obtained using P which points to an interaction with organic phosphate groups of the cell membrane structure as postulated for Cm(III) in [4]. The relatively short Pu–P distance at 3.15 Å indicates a bidentate coordination of the phosphate group to plutonium. In conclusion, the XANES/EXAFS investigation of the Pu bound by cells of *D. äspöensis* confirmed the results of the solvent extraction experiments [5]. The cell-bound Pu exists as Pu(IV)-polymers which are interacting with the biomass.

ACKNOWLEDGEMENTS. This work was funded by the BMWi under contract number: 02E9491. The Pu(IV) reference sample was used by courtesy of Ch. Den Auwer (CEA Marcoule, France).

REFERENCES

[1] Reich, T. *et al.* (2001) *Report FZR-322*, 27-32.
[2] Charrin, N. *et al.* (2000) *Radiochim. Acta* **88**, 25-31.
[3] Rothe, J. *et al.* (2004) *Inorg. Chem.* **43**, 4708-4718.
[4] Moll, H. *et al.* (2004) *Environ. Sci. Technol.* **38**, 1455-1459.
[5] Moll, H. *et al.* this report, p. 32.

Influence of U(VI) on *Bacillus sphaericus* natural isolates as demonstrated by two-dimensional gel electrophoresis

D. Regenhardt, S. Selenska-Pobell

Addition of uranium to culture medium increased the lag period of the *Bacillus sphaericus* isolates JG-A12 and JG-B62 in comparison to cultures incubated without U(VI). Analysis by two-dimensional gel electrophoresis (2-D PAGE) of total proteins showed different profiles between the treated and the control cells.

The intensive uranium mining and processing during the last decades for nuclear energy and nuclear weapon programs resulted in enormous pollution of the environment with radionuclides (especially uranium) and other heavy metals. The toxicity potential of this element for biological systems is based on its chemical properties more than on its radiation [1,2]. To survive in metal polluted environments bacteria must have the capacity to avoid or to detoxify them. Consequently they synthesize proteins that counteract or remove the stressful factors or repair the damages. The 2-D PAGE is an ideal tool for monitoring the alterations in the protein profile. It offers the possibility to identify individual proteins involved in stress responses and the entire response of the cell to its environment [3]. To date little is known about the changes in the protein profile caused by uranium in bacteria. The analysis of the uranium stress response in bacteria will offer the possibility to identify responding proteins and protein groups and to provide a framework to the mechanisms of uranium toxicity and cellular protection against this toxic metal.

EXPERIMENTAL. The *Bacillus* isolates were maintained as batch cultures in nutrient broth supplemented with $MnSO_4$ at 30 °C with constant shaking. Culture growth was monitored by measuring the optical density at 600 nm. Both bacterial cultures grown with or without U(VI) proceeded without medium replenishment.
For protein extraction, rehydration buffer (4 % CHAPS, 30 mM DTT, 20 mM Tris base, 7 M urea, 2 M thiourea) was added to the harvested cells and the suspension was sonicated on ice (Ultrasonic Cell Disruptor, Branson Ultraschall, Germany). For nucleic acids digestion, 1/1000 of Benzonase® Nuclease (Novagen) and $MgCl_2$ (1-2 mM) were added and the tubes were incubated at 20 °C for 1 h. In order to remove salts, DNA and other contaminating substances the supernatants were extracted with cold phenol. For protein precipitation ice-cold acetone was added and centrifuged. The resulting protein pellets were washed twice with ice-cold acetone, air-dried, resuspended in up to 500 µL rehydration buffer and the protein concentration was determined. The 2-D PAGE was carried out as previously described [4].

RESULTS. Additon of U(VI) increased the lag period of the strains (Fig. 1).
The response of *B. sphaericus* JG-A12 cells to U(VI) was examined using genome expression profiling through proteomics (Fig. 2). All conditions were maintained through the growth period of the cultures, *i.e.* the treatments were not administered as transient or shock effect. Preliminary results of the the 2-D gel approach revealed proteins that were differentially expressed and one protein only synthesized in the untreated cells (Fig. 2, white open arrow). Proteins down-regulated in treated cells (open arrows) showed molecular weights between 35 and 55 kDa and neutral isoelectric points (pIs). Four of the five proteins up-regulated under the influence of U(VI) showed molecular weights between 50 and 60 kDa with pIs ranging from pH 5.5 to 7 (closed arrows). Interestingly, the largest protein spot (M_w 126 kDa) with enhanced expression was identified as the S-layer protein which indicates that it plays probably a protective role for the cells against U(VI).
Efforts to identify the detected proteins influenced by the addition of U(VI) are in progress in our laboratory.

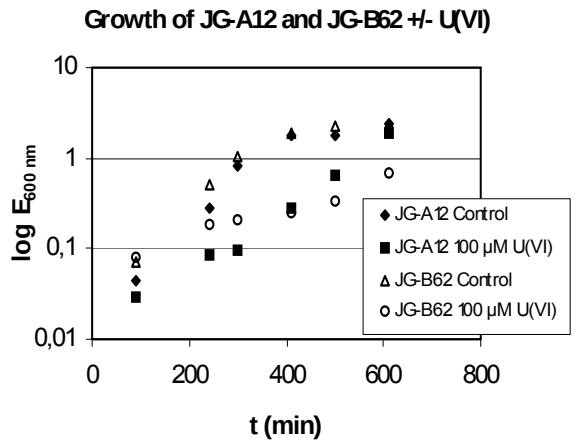

Fig. 1: Growth curves of *Bacillus sphaericus* natural isolates JG-A12 and JG-B62. The cells grown with added U(VI) show an extended lag phase in comparison to their controls.

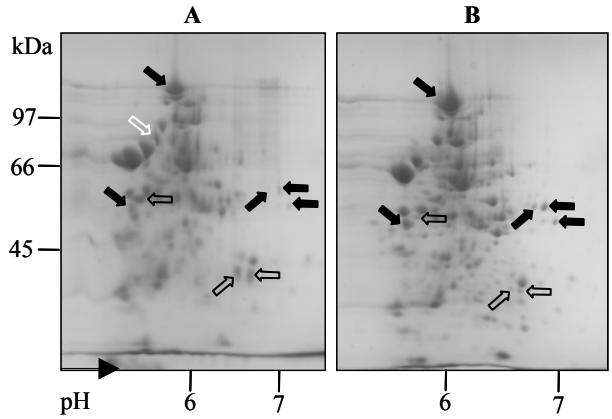

Fig. 2: 2-D PAGE of proteins extracted from *B. sphaericus* JG-A12 cells grown in media containing no added U(VI) (A) or 100 µM U(VI) (B). The closed arrows indicate proteins up-regulated and the open black arrows indicate proteins down-regulated under the influence of U(VI). The open white arrow shows a protein only synthesized in the control cells (A).

REFERENCES

[1] Miller, A.C. *et al.* (2002) *J. Inorg. Bio.* **91**, 246-252.
[2] Yazzie, M. *et al.* (2003) *Chem. Res. Toxicol.* **16**, 524-530.
[3] Neidhardt, F.C. *et al.* (2000) *Bacterial Stress Responses*, ASM Press, Washington, D.C.
[4] Regenhardt , D. *et al.* (2005) *Report FZR-419*, p. 34.

Uranyl and sodium nitrate induced changes in indigenous bacterial community of a uranium mining waste pile

A. Geissler, J. Tschikov, M. Schlömann[1], S. Selenska-Pobell
[1]Interdisziplinäres Ökologisches Zentrum, TU Bergakademie Freiberg, Freiberg, Germany

Bacterial diversity in a soil sample from a uranium mining waste pile was investigated before and after supplementation and incubation with uranyl or sodium nitrate by using the 16S rDNA retrieval. A shifting in natural bacterial community from *Acidobacteria, Alpha- and Deltaproteobacteria* in the untreated sample to *Betaproteobacteria*, *Bacteroidetes, Actinobacteria,* and *Gammaproteobacteria* was observed depending on the salt solutions added and on the aeration conditions.

Bacteria possess different mechanisms to interact with metals and radionuclides [1]. Therefore, they can influence their fate and their migration in contaminated sites. The aim of the present work was to investigate and compare the influence of high levels of uranium (up to 300 mg U/kg) on a natural bacterial community of a uranium mining waste pile under anaerobic and aerobic conditions.

EXPERIMENTAL. The studied soil sample (JG35-2) was collected from a depth of 2 m from the uranium mining waste pile Haberland located near the town of Johanngeorgenstadt, Germany. The sample was supplemented with 1 mM uranyl nitrate (pH 4.0) to achieve a final uranium content of 300 mg U/kg [2]. One portion of the uranium treated sample, called U3, was incubated for 14 weeks in the dark, at 10 °C, and under anaerobic conditions which corresponded to the natural environmental conditions of the sample. A second portion of the sample, U2A, was handeled in a similar way as U3 but under aerobic conditions. To investigate the influence of nitrate on the natural bacterial community of the studied sample two controls (K1 and K2) each supplemented with 2 mM sodium nitrate (pH 4.0) were incubated under aerobic and anaerobic conditions, respectively. The bacterial diversity of the untreated sample (JG35-2), containing 26 mg U/kg, and of the samples supplemented with uranyl nitrate (U3 and U2A) or with sodium nitrate (K2 and K1) was estimated *via* the 16S rDNA retrieval as described in [2].

RESULTS. It is evident from the results presented in Fig. 1 that the incubations with sodium or uranyl nitrate influence the structure of the natural bacterial community of the sample in a very specific way. Moreover, the changes in both cases were strongly dependent on the aeration conditions. In the sample U3, which was incubated at conditions closest to the natural, a propagation of betaproteobacterial denitrifyers and nitrate reducers was highly favored by the addition of uranyl nitrate. The populations of *Acidobacteria* and *Deltaproteobacteria,* which were predominant in the untreated sample JG35-2, were notably reduced in the U3 sample where representatives of *Firmicutes* (*Clostridium* spp.) and *Actinobacteria* (*Arthrobacter* spp.) appeared after the incubation with uranyl nitrate. Interestingly, representatives of the latter two bacterial genera are known for their tolerance to heavy metals and radionuclides [3,4,5,6]. Some clostridia were described to be even able to reduce U(VI) to U(IV) [6].

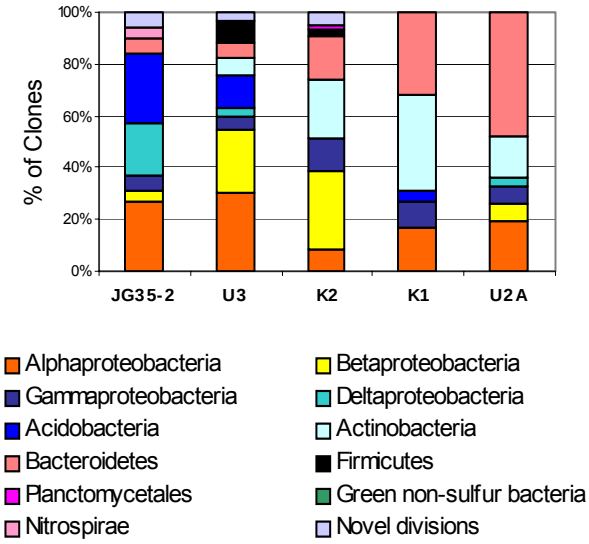

Fig. 1: Predominant bacterial populations (in %) in the original sample JG35-2; in the uranyl nitrate treated samples, U3 (anaerobic) and U2A (aerobic); and in the sodium nitrate treated controls K2 (anaerobic) and K1 (aerobic).

The addition of sodium nitrate to the anaerobic control sample K2 induced a strong propagation of *Betaproteobacteria, Arthrobacter* spp., *Bacteroidetes*, and *Gammaproteobacteria* which had overgrown most of the alphaproteobacterial and the acidobacterial populations predominating the original sample. However, significant parts of these denitrifying and nitrate reducing populations seem to be sensitive to U(VI) because their sizes were significantly smaller in the sample U3 suplemented with uranyl nitrate (compare K2 with U3).
The bacterial community structures of the samples incubated with uranyl nitrate (U2A) and with sodium nitrate (K1) under aerobic conditions differed significantly from those of the above mentioned anaerobically treated samples U3 and K2 (Fig. 1). Under aerobic conditions the propagation of the *Bacteroidetes*, and *Actinobacteria*, especially of the *Arthrobacter* spp. populations was more strongly induced by the addition of sodium nitrate than under anaerobic conditions (compare K1 to K2). In agreement with the results obtained under anaerobic conditions, a large part of the *Arthrobacter* spp. seemed to be sensitive to the added U(VI) (compare K1 with U2A). In contrast, the size of the *Bacteroidetes* populations was extremely large in the aerobically treated uranium supplemented sample U2A.
Our results demonstrate that natural bacterial communities possess a very high flexibility and potential to sense and possibly to interact with U(VI) at various environmental conditions.

REFERENCES

[1] Selenska-Pobell, S. (2002) *Interactions of Microorganisms with Radionuclides*, p. 225-253, Elsevier Science Ltd, Oxford.
[2] Geissler, A. *et al.* (2006) *Geobiology* (in press).
[3] Fredrickson, J.K. *et al.* (2004) *Appl. Environ. Microbiol*. **70**, 4230-4241.
[4] Suzuki Y. *et al.* (2004) *Geomicrobiol. J.* **21**, 113-121.
[5] Suzuki Y. *et al*. (2004) *Radiochim. Acta* **92**, 11-16.
[6] Francis A.J. *et al.* (1994) *Environ. Sci. Technol.* **28**, 636-639.

Part 3:

Interaction of actinides with solid phases

Cesium sorption on montmorillonite and bentonite

C. Nebelung, S. Brockmann[1], J. Mibus

[1]Faculty of Mechanical and Process Engineering, University of Applied Science, Dresden, Germany

The sorption characteristics of cesium on bentonite and montmorillonite were investigated in batch experiments for understanding the near-field behavior in geological nuclear repositories. The retention of cesium is small and only caused by cation exchange.

EXPERIMENTAL. The batch sorption experiments were carried out using 100 mg montmorillonite SWy-1 (Source Clay Repository) and bentonite MX 80 in 40 mL 0.1 M $NaClO_4$ and pore water [1], respectively. The solids and liquids were conditioned for 4-5 weeks. In this time the pH-value had to be adjusted several times. After cesium addition the samples were carefully shaken for five days. The samples were centrifuged (30 min, 3500 rpm). An aliquot of the supernatant was prepared for direct liquid scintillation measurement. After filtration through a 30 kD filter to separate potentially existing colloids another aliquot was taken.
Three parallel samples were prepared for studying the pH-dependence. 1 µM $^{133}CsCl$ spiked with $^{137}CsCl$ (4000 Bq in each sample = $2.3 \cdot 10^{-10}$ M) was given to samples of pH between 3 and 11 in 0.5 steps.
The effect of Cs concentration was investigated between $3 \cdot 10^{-9}$ M and $1 \cdot 10^{-4}$ M CsCl. The natural Cs content at low Cs concentrations has to be considered. The sorption was investigated at pH 8.

RESULTS. The distribution coefficient (K_D) and the sorption isotherms were determined for the batch sorption experiments. The K_D in mL/g is given as:

$$K_D = \frac{V}{m} \cdot \frac{c_0 - c_{eq}}{c_{eq}} \quad (1)$$

where V volume [mL]
m mass of the solid [g]
c_0 initial concentration of Cs [mol/L]
c_{eq} equilibrium concentration of Cs [mol/L]

The sorption isotherms give a better characterization than K_D values alone. In this study the Freundlich isotherm was used to describe the sorption:

$$\log \frac{c_{sorb}}{m} = \log k + \frac{1}{n} \log c_{eq} \quad (2)$$

where c_{sorb} concentration of sorbed Cs [mol/kg]
m mass of the solid [kg]
c_{eq} equilibrium concentration of dissolved Cs [mol/L]

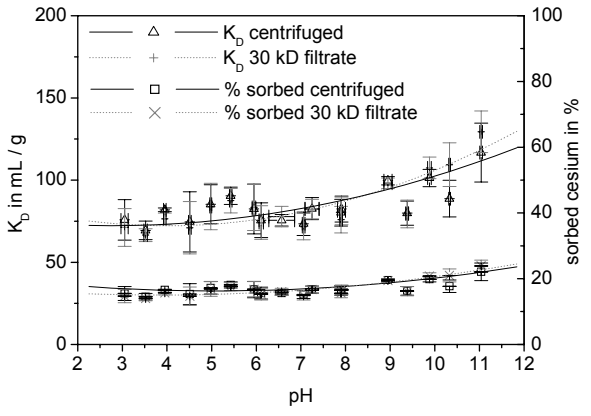

Fig. 1 Cesium sorption on montmorillonite, dependence of pH.

The pH dependence of the Cs sorption is very small (Fig. 1). In the region from pH 3 to 8 no significant differences were measured. A marginal higher sorption was found at pH ≥ 9. No significant colloidal fraction was determined at all pH values.
The dependence of the K_D value on the Cs concentration is shown in Fig. 2. The Cs sorption on montmorillonite in $NaClO_4$ is higher than on bentonite in pore water (PW). Sorption decreases with increasing ionic strength.

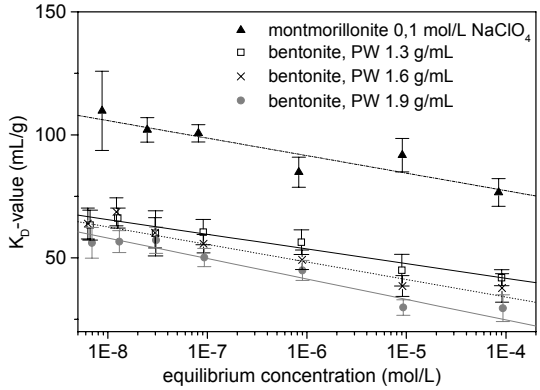

Fig. 2: Cesium sorption on montmorillonite and bentonite, dependence of cesium concentration.

From the linearity of the sorption isotherms (Fig. 3) it is concluded that only one binding type is present. With the high cation exchange capacity of 78.7 meq / 100 g [1] (upper line in fig. 3) and 85 meq / 100 g [2] all Cs retention is caused by ionic exchange, even for the highest initial Cs-concentration.

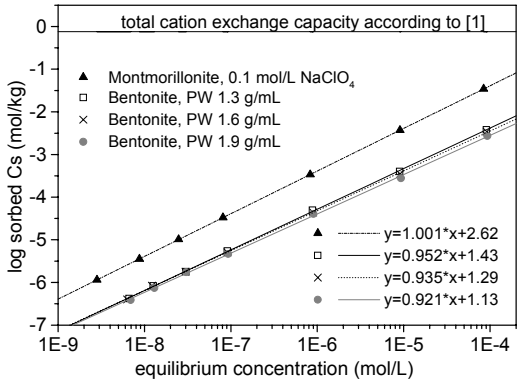

Fig. 3: Comparison of Cs-sorption isotherms for bentonite with three pore water types and montmorillonite with 0.1 M $NaClO_4$.

The retention of Cs in the concentration range between $3 \cdot 10^{-9}$ and $1 \cdot 10^{-4}$ mol/L on bentonite (K_D between 30 and 64 mL/g, 7 – 14 % sorption) and on montmorillonite (K_D between 77 and 189 mL/g, 16 – 31 % sorption) is not high.

ACKNOWLEDGEMENTS. Funding by the European Commission (NF-PRO C2-ST-C-01) is gratefully acknowledged.

REFERENCES

[1] Bradbury, M.H. *et al.* (2002) *PSI-Report 02-10*, Paul-Scherrer-Institute Villigen, Switzerland.
[2] Wanner, H. *et al*. (1996) *Fresenius J. Anal. Chem*. **354**, 763-769.

Uranium sorption on montmorillonite

C. Nebelung

The sorption of uranium onto montmorillonite was investigated. Sorption maxima were found between pH 5.5 to 6 and pH > 10.5. The linear sorption isotherm indicates only one binding type.

EXPERIMENTAL. The batch sorption experiments were carried out using 100 mg montmorillonite Swy-1 (Source Clay Repository) in 40 mL 0.1 mol/L $NaClO_4$. The surface area of montmorillonite was 30.1 m^2/g (measured by BET). The solids and liquids were conditioned 4-5 weeks in air atmosphere. Within this period the pH-value had to be adjusted 6 times. After addition of uranium the samples were carefully shaken for five days. The samples were centrifuged (30 min, 3500 rpm). An aliquot of the supernatant was prepared for direct liquid scintillation (LS) measurement. After filtration through a 30 kD filter to remove potentially existing colloids another aliquot was taken.
Three parallel samples were prepared for studying the pH-dependence. 2155 Bq ^{234}U was added to samples in the pH range of 3 to 11 (in 0.5 steps) to get concentrations of $1 \cdot 10^{-6}$ mol/L ^{234}U.
The variation of the uranium concentration (also three parallel samples) was investigated between $1 \cdot 10^{-9}$ mol/L and $1 \cdot 10^{-3}$ mol/L uranium. The natural uranium concentration dissolved from the montmorillonite has to be considered at low uranium concentrations. For the preparation of the samples with $1 \cdot 10^{-9}$ mol/L to $1 \cdot 10^{-6}$ mol/L uranium, pure ^{234}U was used. For the samples with $1 \cdot 10^{-5}$ mol/L to $1 \cdot 10^{-3}$ mol/L uranium, 2155 Bq ^{234}U was added to the adequate amount of ^{238}U. The sorption was investigated at pH 5.5.

RESULTS. The distribution coefficient (K_D) and the sorption isotherms were determined in batch sorption experiments. The use of sorption isotherms gives a better characterization than K_D values alone. In this study the Freundlich isotherm was used to describe the sorption [1].
The pH dependence of the uranium sorption has a characteristic shape (Fig. 1). A similar shape was found for natural uranium dissolved from the solid montmorillonite (Fig. 1). Between pH 5.5 and 6.5 the lowest uranium concentration was found in both cases.
The K_D values have the same trend: the highest K_D was determined between pH 5 and 6.5 with the maximum at pH 5.5 (Fig. 2). For the high K_D at pH 11 there is no explanation so far. At low uranium concentration in solution and high K_D values a colloidal fraction of maximal 31 % (at pH 11) was determined. At low K_D values (≤ 2000 mL/g) no colloidal fraction was found.

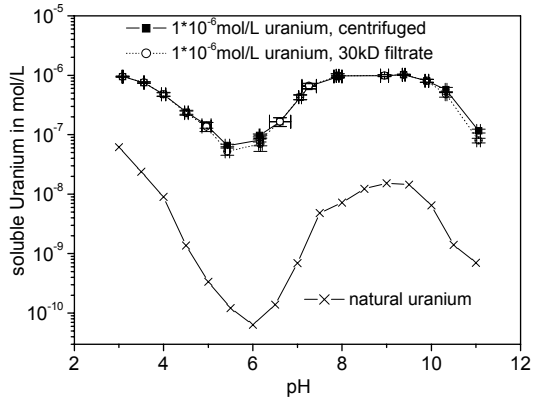

Fig. 1: Soluble uranium after sorption on montmorillonite, comparison with natural uranium, pH dependence.

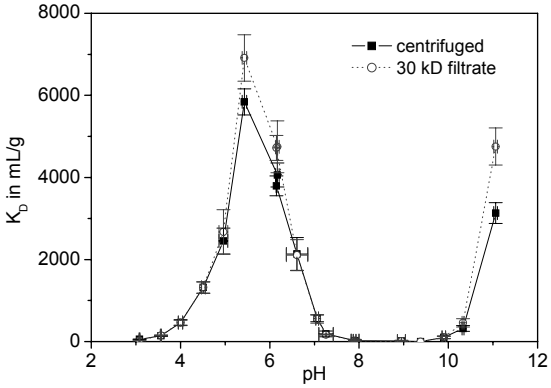

Fig.2: Uranium sorption on montmorillonite, dependence of pH.

In Fig. 3 the sorption dependence of uranium concentration is shown in terms of sorption isotherms. In case of the sorption of $1 \cdot 10^{-9}$ mol/L uranium solution, all uranium was sorbed and the uranium content was below the detection limit of the LS measurement of $1.2 \cdot 10^{-10}$ mol/L uranium. The linear sorption isotherm indicates only one binding type. The determined slope of 0.77 corresponds well with the parameter of 0.79 in [2]. The retention of uranium on montmorillonite at pH 5.5 is between 100 % (at low uranium concentration) and 50 % (at high concentrations). The K_D values ranged between 430 and 31500 mL/g. The retention of uranium is considerably higher than in the case of cesium sorption [1].

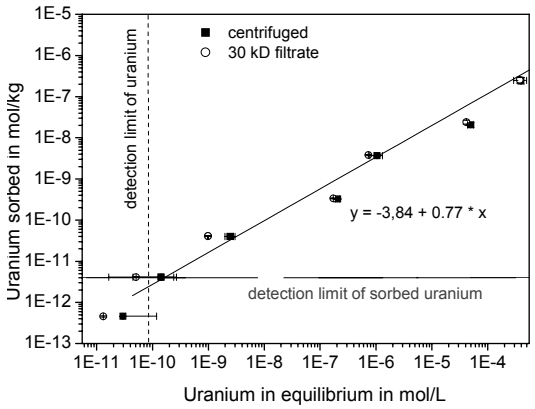

Fig. 3: Uranium sorption on montmorillonite, Freundlich sorption isotherm.

ACKNOWLEDGEMENTS.
Funding by the European Commission (NF-PRO C2-ST-C-01) is gratefully acknowledged.

REFERENCES

[1] Nebelung, C. *et al.* this report, p. 39.
[2] Hull, L.C. *et al.*(2004) A*ppl. Geochem.* **19,** 721-736.

EXAFS investigations of U(VI)/humic acid/kaolinite interaction

A. Křepelová, S. Sachs, T. Reich[1], A. Roßberg, G. Bernhard
[1]Institute of Nuclear Chemistry, Johannes Gutenberg-Universität Mainz, Mainz, Germany

We investigated the influence of humic acid (HA) on the near-neighbor surrounding of U(VI) in kaolinite surface complexes. The results of our EXAFS experiments show that HA has no influence on structure parameters of U(VI) adsorbed on kaolinite.

Determination of structure parameters is important for the modeling of U(VI) sorption onto kaolinite. Batch experiments [1] were combined with spectroscopic measurements to obtain molecular-level information on the interaction of U(VI) with HA and kaolinite in natural systems.

EXPERIMENTAL. The reference clay kaolinite KGa-1b (Washington County, Georgia) [2] was obtained from the Clay Minerals Society Source Clay Repository. Synthetic HA type M42 was used. It was synthesized as described in [3]. U(VI) was adsorbed under the following conditions: [U(VI)]: $1 \cdot 10^{-5}$ M, [HA]: 10 mg/L, S/L ratio: 4 g/L, I: 0.1 M $NaClO_4$. Four samples at pH: 5, 6, 7, and 8.5 were prepared on air ($p(CO_2) = 10^{-3.5}$ atm). To study the influence of carbonate, the sample at pH 8.5 was prepared also under N_2-atmosphere. The samples were measured as wet pastes. EXAFS data were collected at ROBL (ESRF, BM20) at room temperature in the fluorescence mode. The ionization potential of the uranium L_{III}-edge was defined as 17,185 eV. Multiple scans were measured for all samples. The EXAFS spectra were analyzed according to standard procedures including statistical weighting of the 13 fluorescence channels and their dead-time correction.

RESULTS. Fig. 1 shows uranium L_{III}-edge k^3-weighted EXAFS oscillations and their corresponding Fourier transforms - FT - (not corrected for phase shift). All examined samples exhibit comparable EXAFS oscillations and FT. The structural model for fitting the experimental data was derived from EXAFS investigations of the binary system U(VI)/kaolinite KGa-1b [4].
Structural parameters obtained from EXAFS analysis are summarized in Tab. 1. They show no remarkable differences. There is a drop in the U-O_{eq} distance from 2.34 Å to 2.31 Å in the absence of CO_2. From this it is suggested that U(VI) interacts with carbonate also in the presence of HA. However, this effect is less pronounced than in the binary system. From comparison of our results with the results obtained for the binary system [4] and with other model systems [5-8] (Tab. 2), we conclude that HA has no significant influence on the near-neighbor surrounding of U(VI) in kaolinite surface complexes. U(VI) prefers sorption on the HA-uncovered surface of kaolinite (this is supported by XPS measurements). It was also possible to fit the Si shell with a radial U–Si distance longer than 2.71 Å. In this case the resulting average U–Si distance was 3.06 Å, but the fits did not improve significantly.

ACKNOWLEDGEMENT. This work was financially supported by the BMWA under contract No. 02E9673.

REFERENCES

[1] Křepelová, A. *et al.* (2004) *Report FZR-419*, p. 50.
[2] Pruet, R.J. *et al*. (1993) *Clays Clay Miner.* **41**, 514-519.
[3] Sachs, S. *et al.* (2004) *Report FZR-399*, p. 4.

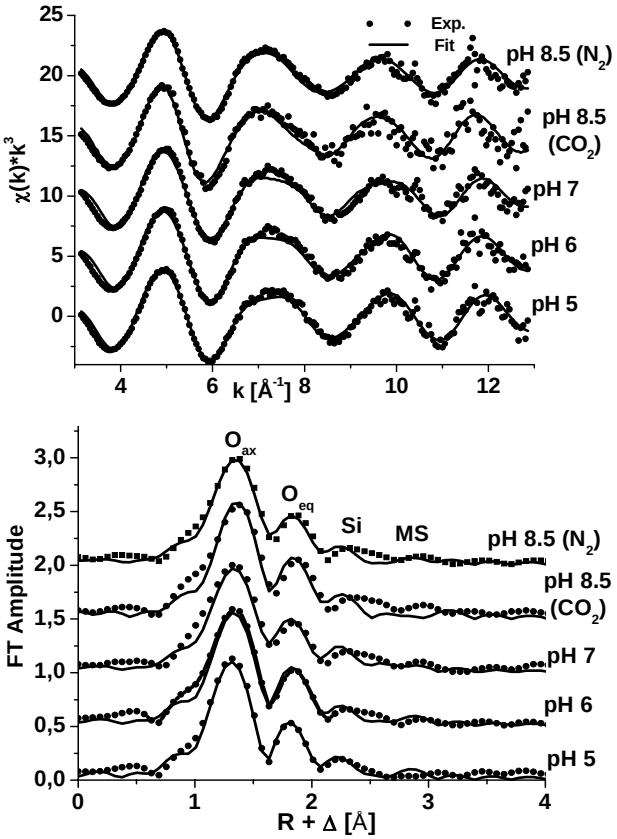

Fig. 1: Uranium L_{III}-edge k^3-weighted EXAFS spectra (top) and corresponding Fourier transforms (bottom) of U(VI) adsorbed onto kaolinite in the presence of HA.

Tab. 1: EXAFS structural parameters for U(VI) adsorbed onto kaolinite in the presence of HA at different pH values. Coordination numbers for the axial oxygen and silicon atom were held constant during the fitting procedure.

Sample	2 x U–O_{ax}		U–O_{eq}			1 x U–Si	
	R^a[Å]	σ^2[Å^2]	N	R^a[Å]	σ^2[Å^2]	R^b[Å]	σ^2[Å^2]
pH 5	1.76	0.002	4.7 ± 1.5	2.32	0.012	2.73	0.007
pH 6	1.78	0.003	4.2 ± 1.4	2.34	0.010	2.74	0.008
pH 7	1.77	0.004	4.9 ± 1.7	2.32	0.012	2.73	0.005
pH 8.5 (CO_2)	1.79	0.003	5.0 ± 2.4	2.34	0.011	2.73	0.007
pH 8.5 (N_2)	1.78	0.003	5.0 ± 1.5	2.31	0.012	2.70	0.009

[a] ± 0.02 Å [b] ± 0.04 Å

Tab. 2: Comparison of EXAFS results of this study with literature.

System	References	U–O_{ax} R [Å]	U–O_{eq} R [Å]	U–Si R [Å]
Silica	[5]	1.79	2.26/2.51	2.72
Silica	[6]	1.76	2.26/2.48	3.08
$UO_2SiO_4H_2$	[7]	1.80	2.14	2.88
Kaolinite KGa-2	[8]	1.80	2.29/2.47	3.3
Kaolinite KGa-1b	[4]	1.78	2.35	2.72
Kaolinite KGa-1b	This study	1.77	2.32	2.73/3.06

[4] Reich, T. *et al.* (in preparation).
[5] Reich, T. *et al.* (1998) *J. Electron Spectrosc. Related Phenom.* **96** 237-243.
[6] Sylwester, E.R. *et al.* (2000) *Geochim. Cosmochim. Acta* **64**, 2431-2438.
[7] Wheaton, V. *et al*. (2003) *Chem. Phys. Lett.* **371**, 349-359.
[8] Thompson, H.A. *et al.* (1998) in: *Adsorption of Metals by Geomedia*, p. 349-370, Academic Press, San Diego.

Adsorbed U(VI) surface species on muscovite by TRLFS and HAADF-STEM

T. Arnold, S. Utsunomiya[1], G. Geipel, R.C. Ewing[1], N. Baumann, V. Brendler
[1]Department Geological Sciences, University of Michigan, Ann Arbor, U.S.A.

Time-resolved laser-induced fluorescence spectroscopy (TRLFS) and high-angle annular dark-field scanning transmission electron microscopy (HAADF-STEM) were applied to investigate the species of uranyl(VI) adsorbed onto muscovite platelets and muscovite suspensions.

EXPERIMENTAL. Batch sorption experiments with $1 \cdot 10^{-5}$ M U(VI) sorbing onto muscovite powder (grain size fraction 63-200 µm) and muscovite platelets were conducted and prepared for subsequent TRLFS and HAADF-STEM measurements. The conducted experiments are described in detail in [1].

RESULTS. The deconvoluted TRLF spectra of the adsorbed U(VI) surface species on muscovite edges indicated two surface species with different fluorescence life times. The first species has a fluorescence lifetime of 450 ± 22 ns and the second species a distinctively larger one of 4000 ± 190 ns. Six fluorescence emission bands as reported by Bell and Biggers [2] were used to describe the TRLFS spectra. The resulting emission bands and lifetimes of the fluorescence signals are shown in Tab. 1. The deconvoluted TRLF spectra of the adsorbed U(VI) surface species on muscovite suspensions also indicated two surface species. The first species has a fluorescence life time of 462 ± 33 ns, and the second species a distinctively larger one of 14100 ± 1100 ns. Comparing the adsorbed U(VI) surface species on the muscovite edges with the ones in suspension, it was found that there were slight differences in the positions of the peak maxima. The lifetime of the short-lived species both on the edges and in suspension agree within the errors of the measurements. However, comparing the fluorescence lifetime of the long-lived species, we find a longer lifetime for the species in suspension, indicating a smaller average number of coordinated water molecules.

Tab. 1: Lifetimes and emissions bands of the two U(VI) surface species detected (a.) on the edge-surfaces of muscovite platelets and (b.) in suspensions.

Species	Lifetime [ns]	Fluorescence emission bands [nm]					
a1	450 ± 22	491.4	504.2	521.5	541.6	563.0	588.7
a2	4000 ± 190	487.8	501.7	519.4	538.8	558.8	583.6
b1	462 ± 33	488.4	500.9	517.0	536.1	557.7	582.3
b2	14100 ± 1100	484.5	499.7	519.2	541.1	558.6	573.4

HAADF-STEM revealed that nano-clusters of an amorphous uranium phase were attached to the edge-surfaces of muscovite powder (63 – 200 µm) during batch sorption experiments. These U-nano-clusters were not observed on {00l} cleavage planes of the muscovite. The HAADF-STEM image (Fig. 1) showed a few nanometer-sized clusters with bright contrast, for which semi-quantitative analysis of EDX spectrum revealed a few wt% of U. Because the EDX analysis included the signal from the underlying muscovite, the actual concentration of U is much higher than a few wt%. An electron diffraction pattern selecting the area where several U-rich clusters were present did not show any diffraction maxima except for the pattern of muscovite, indicating that the particles are not crystalline, but nearly amorphous. Probably these clusters are "polymerized" U (oxy-)hydroxyls in a size range of 1-2 nm.

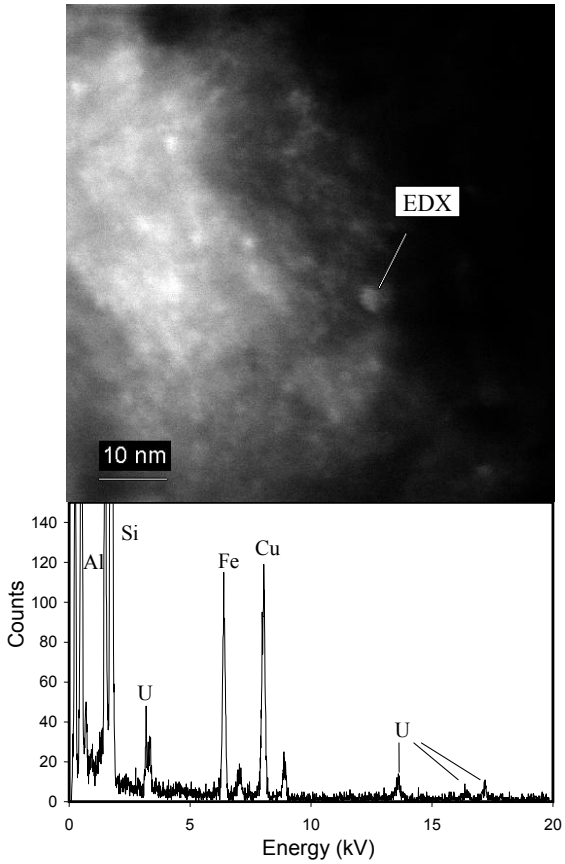

Fig. 1: Uranium nanoparticles on muscovite edge-surfaces (upper) HAADF-STEM image (lower) EDX spectrum.

CONCLUSIONS. The surface species with the shorter fluorescence lifetimes are interpreted as truly adsorbed surface complexes. The surface species with the longer fluorescence lifetimes is interpreted to be an amorphous U(VI) condensate or nanosized clusters of polynuclear uranyl(VI) surface species with a particle diameter of 1 to 2 nm. Depending on the size of these clusters the fluorescence lifetimes vary, *i.e.* the larger the nanosized clusters, the longer is the fluorescence lifetime.

ACKNOWLEDGEMENTS. Financial support through the EU Project ACTAF (Contract No. FIKW-CT-2000-00035) is gratefully acknowledged. The work at the University of Michigan (RCE and SU) was supported by the Office of Science and Technology and International (OSTI) of the Office of Civilian Radioactive Waste Management (DE-FE28-04RW12254).

REFERENCES

[1] Arnold, T. *et al.* (2006) *Environ. Sci. Technol.* (submitted).
[2] Bell, J.T. *et al.* (1965) *J. Mol. Spectrosc.* **18**, 247-275.

A TRLFS study of the influence of humic acid on U(VI) sorption onto kaolinite

A. Křepelová, N. Baumann, V. Brendler, S. Sachs, G. Bernhard

Time-resolved laser-induced fluorescence spectroscopy (TRLFS) was combined with batch experiments to study the influence of humic acid (HA) on U(VI) sorption onto kaolinite. Two fluorescence lifetimes could be observed.

TRLFS measurements follow the EXAFS investigations [1] in the system U(VI)/HA/kaolinite to obtain molecular information about the influence of HA on the formation of U(VI) surface complexes onto kaolinite.

EXPERIMENTAL. The experiments were performed using kaolinite KGa-1b [2] and synthetic HA M42 [3]. Four samples of U(VI) adsorbed onto kaolinite in the absence of HA and four of U(VI) adsorbed in the presence of HA were prepared under the following conditions: $[U(VI)]_0$: $1 \cdot 10^{-5}$ M, $[HA]_0$: 10 mg/L, S/L ratio: 4 g/L, I: 0.1 M $NaClO_4$, pH: 5, 6, 7, 8, $p(CO_2) = 10^{-3.5}$ atm, for details see [4]. After an equilibration time of 60 h, the supernatant solutions were removed by centrifugation. Kaolinite samples with adsorbed U(VI) and HA were resuspended in 10 mL of a $NaClO_4$ solution with pH and ionic strength identical to the original solution (without U(VI) and HA). A Nd:YAG diode laser (Spectron) was used. Time-resolved spectra were recorded with ICCD-camera (Spectron) in the wavelength range between 446 nm and 617 nm (delay times: 0.03 - 6.53 µs, pulse energy: 0.3 mJ, excitation wavelength: 266 nm).

Tab. 1: U(VI) content in the solutions after sorption and percentage of U(VI) adsorbed onto kaolinite.

pH	Sample	$U_{supernatant}$ [µg/L]	$U_{supernatant}$ [mol/L]	$U_{adsorbed}$ [%]
5	U(VI)	1440	$6.05 \cdot 10^{-6}$	38.92
	U(VI) + HA	138	$5.80 \cdot 10^{-7}$	93.39
6	U(VI)	340	$1.43 \cdot 10^{-6}$	84.25
	U(VI) + HA	27.4	$1.15 \cdot 10^{-7}$	96.95
7	U(VI)	170	$7.14 \cdot 10^{-7}$	91.48
	U(VI) + HA	40.9	$1.72 \cdot 10^{-7}$	95.39
8	U(VI)	425	$1.78 \cdot 10^{-6}$	81.43
	U(VI) + HA	324	$1.36 \cdot 10^{-6}$	84.22

RESULTS. The results of U(VI) adsorption onto kaolinite in the absence and presence of HA are summarized in Tab. 1.

As an example, the original spectrum of U(VI) adsorbed onto kaolinite in the absence and presence of HA at pH 7 is shown in Fig. 1. The relative fluorescence yields (RFY) of the samples are summarized in Tab. 2.

The RFY significantly decreases in the presence of HA (factor 2 - 3). The difference in RFY between samples with and without HA does not depend on the amount of adsorbed U(VI): At pH 7 the presence of HA increases U(VI) sorption by only 4 %, whereas at pH 5 this effect amounts to 54 %.

Tab. 2: Relative fluorescence yields (RFY) and fluorescence lifetimes of the samples. Data represent mean values of two measurements, errors represent 2σ.

pH	Sample	RFY	t_1 [ns]	t_2 [ns]
5	U(VI)	40	700 ± 110	10100 ± 1300
	U(VI) + HA	12	560 ± 140	12600 ± 1600
6	U(VI)	55	940 ± 120	10800 ± 1400
	U(VI) + HA	15	760 ± 140	12400 ± 1700
7	U(VI)	50	880 ± 110	10100 ± 1300
	U(VI) + HA	15	580 ± 80	11600 ± 1500
8	U(VI)	14	720 ± 90	10700 ± 1400
	U(VI) + HA	8	510 ± 80	9900 ± 1300

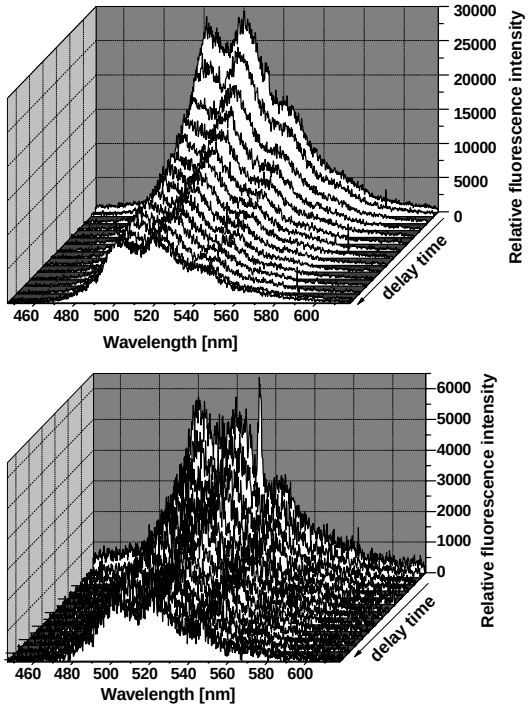

Fig. 1: TRLFS spectra of U(VI) adsorbed onto kaolinite at pH 7 in the absence (top) and presence (bottom) of HA.

Based on the TRLFS spectra, the fluorescence decay function was determined. The best approximation was a bi-exponential decay function (Eq. 1) yielding one short (t_1) and one significant longer (t_2) fluorescence lifetime (Tab. 2).

$$y = A_1 e^{-(x-x_0)/t_1} + A_2 e^{-(x-x_0)/t_2} \quad (1)$$

Obtained lifetimes are comparable for all studied pH values irrespective of the presence or absence of HA. HA shows little influence on the fluorescence lifetimes. t_1 slightly decreases, while t_2 slightly increases in the HA presence.

The RFY of the samples is dependent on pH, which also points to a formation of different uranyl surface complexes. At lower pH a formation of uranyl-humate and/or uranyl-hydroxo-humate surface complexes is expected. A decrease of RFY at pH 8 could be caused by the formation of uranyl-carbonate (absence of HA) or uranyl-carbonato-humate (presence of HA) surface complexes.

The results are comparable with the system U(VI)/Gibbsite [5], where also two uranyl surface species were identified.

ACKNOWLEDGEMENT. This work was financially supported by the BMWA under contract No. 02E9673.

REFERENCES

[1] Křepelová, A. *et al.* this report, p. 41.
[2] Pruet, R.J. *et al.* (1993) *Clays Clay Miner.* **41**, 514-519.
[3] Sachs, S. *et al.* (2004) *Report FZR-399.*
[4] Křepelová, A. *et al.* (2004) *Report FZR-419*, p. 50.
[5] Baumann, N. *et al.* (2005*) J. Colloid Interface Sci.* **290,** 318-324.

Uranium(VI) interactions with hydroxylapatite

V. Brendler, L. Fuchs[1], N. Baumann
[1]University of Applied Sciences Zittau/Görlitz, Germany

U(VI) surface complexation onto hydroxylapatite (HAP) has been investigated by batch sorption experiments and time-resolved laser-induced fluorescence spectroscopy (TRLFS). The surface speciation changes for aged samples within a time frame of eight weeks.

Several apatite minerals have been proposed for the save long-term immobilization of heavy metals and in particular actinides, due to their pronounced ability to sorb and irreversibly incorporate such contaminants. However, the respective reaction paths with changes in speciation and structure are not well understood so far.

EXPERIMENTAL. HAP from Carl Roth GmbH & Co. KG, Karlsruhe, Germany, was fully characterized: high purity was proven by ICP-MS, AAS and ion sensitive electrodes, the specific surface was 67.5 m²/g (BET) at a mean grain size of 5.8 µm. Two batch experiment series (500 mg HAP in 40 mL solution, each sample as duplicate) were performed: at constant $[UO_2^{2+}] = 10^{-5}$ M with pH steps from 5.5 to 9 ($\Delta = 0.5$), and at constant pH 7.5 with the U(VI) concentration varying from $1 \cdot 10^{-7}$ M to $1 \cdot 10^{-4}$ M. All studies were performed in 0.01 M $NaClO_4$ under air. 48 h in an overhead shaker were sufficient to establish sorption equilibrium, thereafter phase separation using a centrifuge with subsequent analysis and sample preparation for TRLFS followed.
The determination of the U(VI) surface speciation immediately after phase separation was performed by TRLFS with a Nd-YAG (excitation wavelength: 266 nm; spectra recording between 446 and 618 nm; delay times: 30 ns - 6 µs, gate time: 2 µs). For more details see [1]. A second TRLFS measurement series was performed for each sample eight weeks after phase separation.

RESULTS. A FITEQL [2] modeling of the acid-base titrations of HAP yielded the two protolysis constants $pK_1 = 6.07$ and $pK_2 = -8.83$ at a surface binding site density of 1.23 nm^{-2}. The batch sorption experiments showed that sorption started at pH 5.5, approaching nearly quantitative sorption at pH 7.0, and keeping this high sorption even until pH 9 (and maybe beyond). Again, FITEQL was used to extract two surface complexation constants $\log K_A = 4.92$ and $\log K_B = -2.82$ for the respective surface reactions:

$$=XOH + UO_2^{2+} \leftrightarrow =XO\text{-}UO_2^{+} + H^{+} \quad (A)$$
$$=XOH + UO_2^{2+} + H_2O \leftrightarrow =XO\text{-}UO_2OH + 2\,H^{+} \quad (B)$$

TRLFS on the fresh samples revealed that there are two surface species distinguishable, with fluorescence lifetimes of $\tau_1 = 615 \pm 84$ ns and $\tau_2 = 5160 \pm 840$ ns. Both species show identical (within the experimental uncertainty) peak maxima, which do not depent on pH. Tab. 1 summarizes the fluorescence properties. After aging the samples for another eight weeks TRLFS indicated some interesting changes in the fluorescence pattern, see Fig. 1 for details. Whereas the former species with a fluorescence lifetime of about $\tau_1 = 615$ nm vanishes completely for pH values above 6, the species with a lifetime of about $\tau_2 = 5160$ ns has now a lifetime of only $\tau_2 = 2140 \pm 400$ ns. And there is a new species emerging over the whole experimental pH range with a very short lifetime of only $\tau_3 = 206 \pm 51$ ns and its spectrum is ~8 nm blue-shifted. The presence of aqueous uranyl phosphates can be ruled out because their lifetime would be much higher, around 12000 ns [3].

Tab. 1: Fluorescence peak maxima of uranyl surface species on HAP in fresh and aged samples (grouped by lifetime, see text).

Peak position	Fresh samples	Aged samples	
	τ_1 & τ_2	τ_3	τ_1 & τ_2
	Peak maxima in nm [a]		
1st	486.0 ± 0.6	478.8 ± 0.4	485.7 ± 0.3
2nd	502.3 ± 0.2	493.3 ± 0.2	501.8 ± 0.1
3rd	523.7 ± 0.3	513.2 ± 0.6	522.4 ± 0.1
4th	545.9 ± 0.2	538.8 ± 0.2	545.4 ± 0.1
5th	571.2 ± 0.5	559.0 ± 0.6	570.8 ± 0.3
6th	600.0 ± 0.9	585.6 ± 2.0	599.1 ± 0.3

[a] ± 2σ.

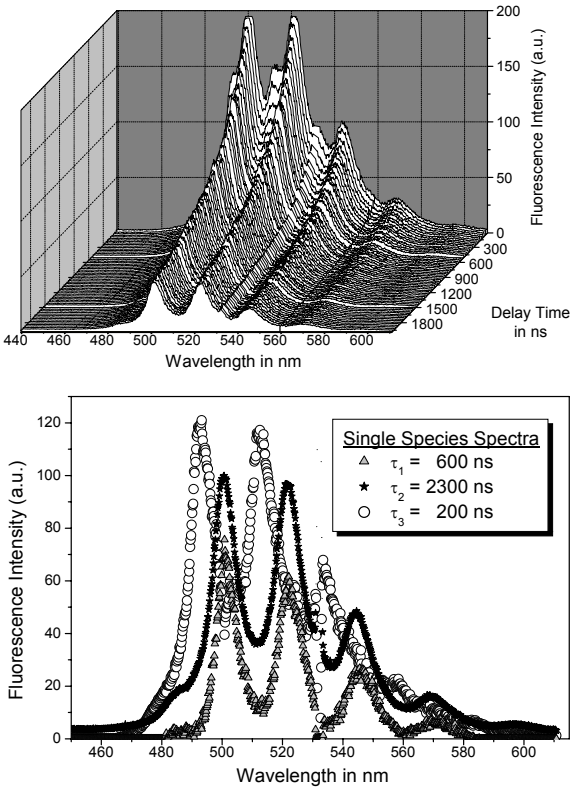

Fig. 1: Aged U(VI) sorbate onto HAP at pH 5.5: 3D-TRLFS spectra (upper) and de-convoluted single species spectra (lower).

REFERENCES

[1] Geipel, G. *et al.* (1996) *Radiochim. Acta* **75**, 199-204.
[2] Herbelin, A.L. (1996) *Report 96-01,* Depart. Chem., Oregon State University, Corvallis, U.S.A.
[3] Brendler, V. *et al.* (1996) *Radiochim. Acta* **74**, 75-80.

TRLFS fingerprint of the uranium silicate boltwoodite $HKUO_2SiO_4 \cdot 1.5\ H_2O$

N. Baumann, T. Arnold, S. Amayri[1]

[1]Institute of Nuclear Chemistry, Johannes Gutenberg-Universität Mainz, Germany

To enlarge a collection of uranium reference minerals with defined spectroscopic features, synthetically prepared boltwoodite was characterized with time-resolved laser-induced spectroscopy (TRLFS). The spectra show six fluorescence emission bands at 485.1, 501.5, 521.2, 543.0, 567.4, and 591.4 nm and two fluorescence lifetimes of 490 ns and 2400 ns.

A database of TRLFS spectra for a variety of uranium minerals is currently in progress. By a fingerprinting procedure it will then be possible to obtain structural information about the coordination environment of sorbed uranium species. This supports the spectroscopic evidence for the presence of uranium surface complexes on geological substrates or the formation of secondary uranium phases. In this study boltwoodite, a naturally occurring uranium silicate mineral, is investigated by TRLFS. It is a suitable substrate to better understand the chemical environment of adsorbed U(VI) species on silicate minerals.

EXPERIMENTAL. Boltwoodite was synthesized from a solution of $UO_2(NO_3)_2$ and KCl together with quartz chunks using a method described by [1]. The purity of the obtained crystals was verified by XRD and EDX measurements. TRLFS measurements were carried out with dry crystals. The TRLFS system consists of a Nd:YAG diode laser with an excitation wavelength of 266 nm. For further details concerning the set-up of the TRLFS equipment and operation modes see [2]. The acquired TRLFS spectra displayed a high signal-to-noise ratio and sharp emission bands. Fig. 1 shows a typical TRLFS spectrum of boltwoodite.

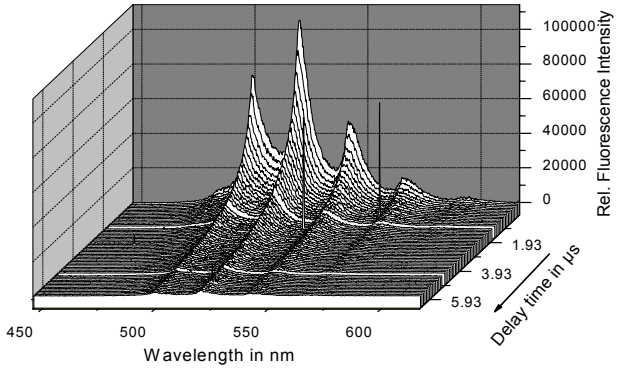

Fig. 1: Fluorescence spectra of Boltwoodite as a function of delay time.

RESULTS. The deconvoluted fluorescence spectrum of boltwoodite (see Fig. 2) shows six emission bands at 485.1, 501.5, 521.2, 543.0, 567.4, and 591.4 nm. Compared to the spectra from the free UO_2^{2+} ion in solution the peak maxima of boltwoodite (see Tab. 1) are shifted towards higher wavelengths. This shift decreases from 14 nm for the 1st peak to 6 nm for the 6th peak.
Based on the measured TRLFS spectra, the fluorescence decay function was determined (see Fig. 3). The time-resolved spectrum is best described with two lifetimes of 490 ns and 2400 ns.

Tab. 1: Position of emission bands from boltwoodite in nm, in comparison to peak maxima from $UO_2^{2+}{}_{(aq)}$ described by [3]

Boltwoodite	485.1	501.5	521.2	543.0	567.4	591.4
$UO_2^{2+}{}_{(aq)}$	470.1	487.8	509.3	532.7	558.1	585.4
Difference	13.8	12.6	10.7	9.1	8.0	5.9

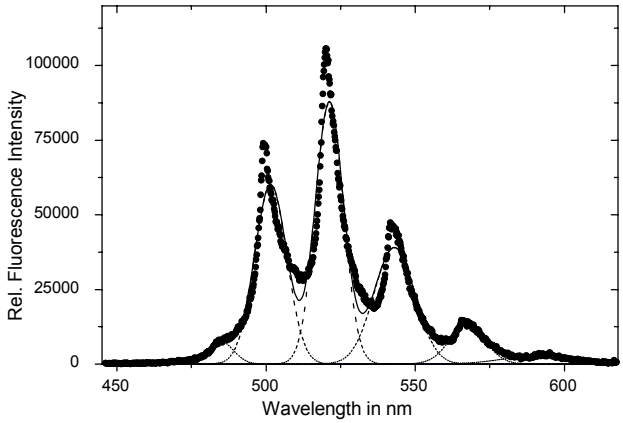

Fig. 2: Deconvoluted fluorescence spectrum of boltwoodite.

It is assumed that the longer lifetime of about 2400 ns is caused by the pure chemical compound $HKUO_2SiO_4 \cdot 1.5\ H_2O$.

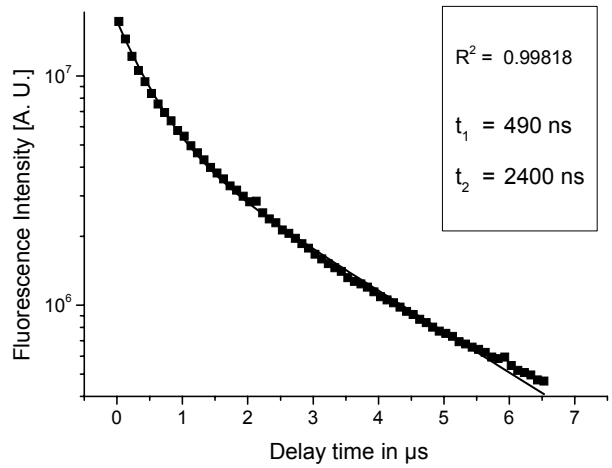

Fig. 3: Fluorescence decay of the uranium(VI) signal from boltwoodite.

The shorter lifetime of about 490 ns is assumed to be a uranium species with almost the same chemical coordination, but with more water molecules in its coordination environment, since water molecules quench the fluorescence lifetime. This may occur on the surface of the crystals.

ACKNOWLEDGEMENTS. This work was conducted within the framework of the EU project FUNMIG.

REFERENCES

[1] Vochten, R. *et al.* (1997) *Can. Mineral.* **35**, 735-741.
[2] Geipel, G. *et al.* (1996) *Radiochim. Acta* **75**, 199-204.
[3] Bell, J.T. *et al.* (1965) *J. Mol. Spectrosc.* **18**, 247-275.

XPS study of humic acid/kaolinite interaction

T. Reich[1], J. Drebert[1], A. Křepelová, S. Sachs
[1]Institute of Nuclear Chemistry, Johannes Gutenberg-Universität Mainz, Mainz, Germany

The interaction of humic acid with kaolinite was studied by X-ray photoelectron spectroscopy (XPS). This study shows that humic acid (HA) does not form a homogeneous coverage of the kaolinite surface. Therefore, significant parts of the kaolinite surface are available for sorption of U(VI).

Previous studies showed that the presence of HA influences the adsorption of U(VI) onto the clay mineral kaolinite [1]. To understand the effect of HA on U(VI) sorption, it is worthwhile to study how HA interacts with the clay surface. XPS is a powerful tool for qualitative and quantitative surface analysis [2].

EXPERIMENTAL. Solutions of 10 mg/L synthetic HA of type M42 [3] in 0.1 M $NaClO_4$ were contacted with kaolinite KGa-1b (Source Clays Repository) at pH 4.0 and 7.5, respectively. 94 % of HA was adsorbed at pH 4.0 corresponding to 2.4 mg HA/g kaolinite (sample HA_4.0). At pH 7.5, the HA uptake by kaolinite was 45 % corresponding to 1.2 mg/g (sample HA_7.5). An additional sample (R11/04KS) resulted from the synthesis of HA in the presence of kaolinite as described in [4]. The uptake of humic substances by kaolinite was 9 mg/g. Kaolinite powder without any treatment was measured as reference.
For XPS measurements, the dry powders were pressed into indium foil without further treatment. XPS spectra were excited by Mg Kα radiation (1253.6 eV). The analyzer pass energy was 50 eV. The vacuum during the measurements was $2 \cdot 10^{-8}$ mbar. The electrostatic charging of the sample surface was corrected by setting the C 1s binding energy to 285.0 eV.

RESULTS. The elements C, O, Al, Si, and minor amounts of Na were detected in the overview spectra of all HA samples. The binding energies and relative intensities of the XPS lines of C, O, Al, and Si were determined from twenty sweeps of each line. Sample HA_7.5 was measured twice. The O 1s, Si 2s, Al 2s, Si 2p, and Al 2p binding energies of the HA/kaolinite samples agree within the experimental uncertainty of ±0.1 eV with each other and with those of the untreated kaolinite sample (see Table 1).
The following conclusions can be drawn from the relative intensities given in Table 2:

1) Relatively small amounts of adsorbed hydrocarbons, *i.e.*, approximately 1 atom% C, were detected at the untreated kaolinite surface. Although the HA uptake by kaolinite varied by a factor of eight (9 mg/g – 1.2 mg/g), the C 1s/Al 2p intensity ratio is nearly constant and does not show any correlation with the HA loading. The surface of the HA/kaolinite samples contains only approximately 5 atom% carbon. This leads to the important conclusion that the surface of the clay particles is not covered by a homogenous HA layer. Part of the HA must be distributed between the particles. This implies that in the ternary system U/kaolinite/HA U(VI) can interact with significant parts of the kaolinite surface that are not covered by HA.
2) All HA/kaolinite samples show the same surface composition with respect to Si, Al, and O as the untreated kaolinite. The chemical composition of the kaolinite surface was not altered by HA adsorption or during HA synthesis.
3) The experimental intensity ratios Si 2p/Al 2p and O 1s/Al 2p agree with the theoretical values that were calculated according to the chemical composition of kaolinite, *i.e.*, $\{Al_2[Si_2O_5(OH)_4]\}$.
4) After sputtering sample HA_7.5 10 min with Ar^+ ions, the C 1s/Al 2p intensity ratio decreased from 0.47 to 0.18 (Table 2). This means that a significant amount of carbon, *i.e.*, approximately 60 %, could be removed by Ar^+ sputtering from the surface of the clay particles. However, the C 1s/Al 2p intensity ratio after sputtering was nearly twice that of the untreated kaolinite surface. This indicates that the remaining HA may not be bound to the kaolinite surface but could be located between the clay particles (*cf* first conclusion).

ACKNOWLEDGEMENTS. This work was supported by BMWA grants No. 02 E 9653 and 02 E 9673.

REFERENCES

[1] Křepelová, A. *et al.* (2005) *Report FZR-419*, p. 50.
[2] Briggs, D. *et al.* (2003) *Surface Analysis by Auger and X-ray Photoelectron Spectroscopy*, IM Publications, West Sussex.
[3] Sachs, S. *et al.* (2004) *Report FZR-399*.
[4] Sachs, S. *et al.* (2005) *Report FZR-419*, p. 49.

Tab. 1: Binding energies E_b of O 1s, Si 2s, Al 2s, Si 2p, and Al 2p XPS lines in eV. E_b(C 1s) = 285.0 eV. Error ±0.1 eV.

Sample	O 1s	Si 2s	Al 2s	Si 2p	Al 2p
HA_4.0	531.9	153.6	119.0	102.6	74.3
HA_7.5	532.0	153.8	119.1	102.7	74.4
HA_7.5	531.9	153.7	119.0	102.6	74.3
HA_7.5[a]	531.8	153.5	119.4	102.5	74.6
R11/04KS	532.0	153.7	119.0	102.7	74.3
KGa-1b[b]	532.2	153.9	119.3	102.9	74.6

[a]) after 10 min Ar^+ sputtering (4000 V, 10 – 15 μA)
[b]) untreated kaolinite.

Tab. 2: Relative XPS line intensities and uptake of humic substances by kaolinite. Error ±5 %.

Sample	mg/g	C 1s/Al 2p	Si 2p/Al 2p	O 1s/Al 2p
HA_4.0	2.4	0.61	1.60	20.6
HA_7.5	1.2	0.45	1.55	20.0
HA_7.5	1.2	0.47	1.62	20.1
HA_7.5[a]	-	0.18	1.48	16.6
R11/04KS	9.0	0.52	1.59	20.0
KGa-1b[b]	-	0.10	1.54	19.6
Calculated[c]	-	0	1.52	22.7

[a]) after 10 min Ar^+ sputtering (4000 V, 10 – 15 μA)
[b]) untreated kaolinite; [c]) $\{Al_2[Si_2O_5(OH)_4]\}$.

Design and test of a specific EXAFS mother wavelet: The FEFF-Morlet wavelet

H. Funke, M. Chukalina[1], A.C. Scheinost
[1]Institute of Microelectronics Technology RAS, Chernogolovka, Russia

A new mother wavelet function for EXAFS data analysis was designed, combining a model EXAFS function derived from the ab-initio EXAFS code FEFF8.2, with the complex Morlet wavelet. This new FEFF-Morlet mother wavelet routine allows to generate wavelets well adapted to specific EXAFS problems.

This report is a direct continuation of [1] and [2]. We suggested in [1] to use the appropriate model EXAFS spectra derived from FEFF8.2 to generate an EXAFS adapted wavelet, which is specially designed to increase the resolution at a given distance of interest and for a special backscatterer element.
It turned out, however, that the wavelets generated from the FEFF model spectra are real functions and the resulting WT plots are very difficult to interprete [1]. In order to combine the advantages of the "accurate", *i.e.* ab-initio wavelet function with the descriptive plots of the WT modulus using Morlet wavelets, we propose to generate FEFF-Morlet mother wavelets as follows:

1) Cut out the first maximum of the envelopes of the model spectrum.
2) Model the envelopes with a spline function.
3) Adapt the EXAFS oscillations within the envelopes to the cos function → real part.
4) Add the same function with a phase shift of π/2 → imaginary part.
5) Set the "center of gravity" of the curve to zero.

An example of the result of the construction is shown in Fig. 1.

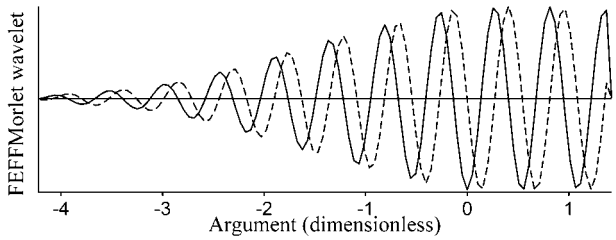

Fig. 1: Real (full line) and imaginary (dashed line) part of the FEFF-Morlet wavelet constructed from the model spectrum Zn-Zn @ 6 Å.

We tested this the new wavelet function by applying it to a well suited test case, the EXAFS spectrum of a Zn-Al Layered Double Hydroxide (Zn-Al LDH) (Fig. 2).

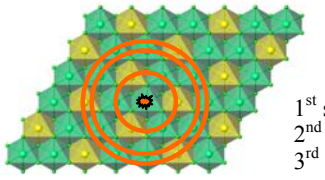

Fig. 2: Model of the octahedral layer of Zn/Al LDH. Zn(OH)6-octahedra are shown in green, those of Al are shown in yellow.

In this model, a maximum fraction of 1/3 of all metal sites is occupied with Al^{3+}, and the remaining 2/3 are occupied with Zn^{2+}. To achieve an even charge distribution, Al^{3+} cannot occupy neighboring metal centers. Consequently, the second metal shell at 5.2 Å contains only Zn atoms, while the third metal shell contains 3 Zn and 3 Al atoms (Fig. 2).
The EXAFS spectrum of this LDH sample has been investigated using the wavelet transform (WT) [1,2]:

$$W_\chi^\phi(k',s) = \sqrt{s}\int \chi(k)k^3\phi(s(k-k'))dk$$

Again we use a scale parameter s instead of the distance r with $s = 1$ if the wavelet is not dilated. Hence, the WT has a maximum for $s = 1$, if the selected model function and the given distance are correct. The relation between the distances and the scale parameter is: $r = r_{opt} \cdot s$, par ex.: r_{opt} = 6 Å.
In order to concentrate the WT analysis to specific distances and specific k ranges, we introduced the power density functions (PDF) $\Phi(k)$ and $\Phi(s)$ depending on either k or s:

$$\phi(k) = \int \left[W_\chi^\psi(k,s)\right]^2 ds, \quad \phi(s) = \int \left[W_\chi^\psi(k,s)\right]^2 dk$$

Now, we will investigate the WT of the LDH spectrum using the following 4 wavelet functions calculated with FEFF: Zn-Zn @ 6 Å, Zn-Al @ 6 Å, Zn-Zn @ 5.2 Å, and Zn-Al @ 5.2 Å. The PDF analysis shows the expected maxima at $s = 1$ for both Zn and Al at ≈ 6Å, confirming that both atoms are present (Fig. 3). At a distance of 5.2 Å, however, only the path involving Zn shows a maximum at $s = 1$, while Al does not (see red circle). This confirms that the second metal shell does not contain Al, indicating an even metal distribution in LDH, in line with a regular charge distribution.

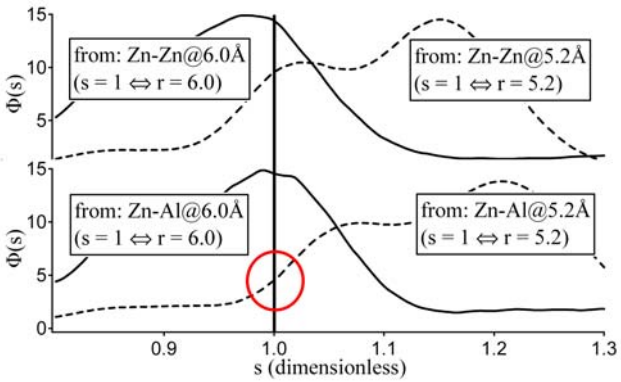

Fig. 3: Four PDF's in the region ≈ 4.8,…, 6.6 Å (see text).

With the previously used Morlet wavelet, it was possible to distinguish Zn and Al in the first shell (~3 Å). However, it was not possible to resolve the two more distant shells at 5.2 and 6 Å simultaneously with respect to wavenumber k (element identity) and the distance r. This problem is now overcome with the newly developed FEFF-Morlet wavelet.

ACKNOWLEDGEMENT. This work is supported by the NATO Collaborative Linkage Grant CBP.NR,CLG 981353.

REFERENCES

[1] Funke, H. *et al*. (2004) *Report FZR-419,* p. 63.
[2] Funke, H. *et al*. (2005) *Phys. Rev B* **71**, 094110.

The local structure of soddyite – EXAFS wavelet analysis and shell fitting

H. Funke, C. Hennig, A. Rossberg, A.C. Scheinost

We measured the EXAFS spectrum of a soddyite sample of Renaud Vochten's collection of uranium minerals (Vo-43) at 30 K. The local structure determined by shell fitting is fairly consistent with crystallographic data. Wavelet analysis clearly resolved the Si and U atoms at distances between 3 and 4 Å.

Many uranyl (U(VI)) minerals have a characteristic layer structure in the equatorial plane due to the strong electrovalence of the two axial oxygen atoms. The XRD structure of such layer minerals is often difficult to determine for two reasons. For structures conatining heavy atoms like U, the XRD patterns are dominated by the backscattering from the heavy atoms, while the positions of light atoms like O or Si may be occasionally inaccurate (0.05 – 0.1 Å). In contrast, EXAFS spectroscopy allows to specifically probe the interatomic distances around U, porviding a distal resolution of 0.01 – 0.02 Å for both light and heavy atoms [1]. Second, layered structures with hydrated interlayers often show irregular cation spacings and turbostratic effects, that might affect the long-range structural determination perpendicular to the layers by XRD. These facts can make the XRD analysis difficult, mainly for obsolete diffraction techniques. In such cases EXAFS spectroscopy may significantly improve the structural analysis.

While conventional EXAFS shell fitting is the method of choice to decipher the local structure of minerals, this method is not well suited to resolve heavy and light back scatterers at the same radial distance from the central atom U. In such cases the EXAFS data evaluation is improved by introducing wavelet analysis [2]. Here we present both conventional shell fitting and wavelet analysis of the local structure of soddyite, $(UO_2)_2{\cdot}SiO_4{\cdot}2(H_2O)$.

In contrast to the layered structure of most other uranyl minerals, soddyite consists of a three-dimensional network of pentagonal bipyramids (Fig. 1). The bipyramids form double-chains by sharing equatorial O atoms. The chains are linked by SiO_4 octahedra, which share edges with bipyramids of adjacent chains. By this arrangement the orientation of the uranyl bipyramids varies by approximately 90° (Fig. 1). Radial distances around the unique U position are given in Table 1.

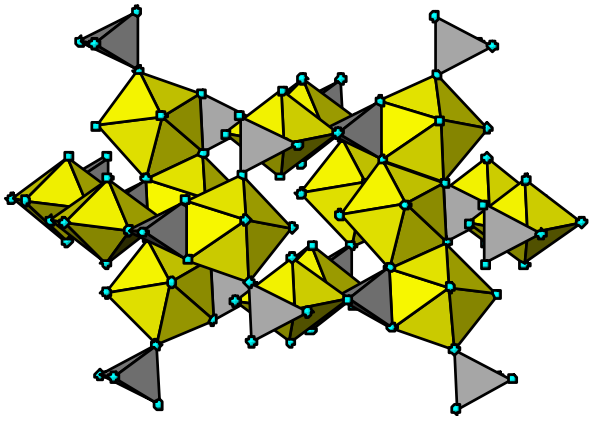

Fig. 1: Polyhedral model of the structure of soddyite [3].

EXAFS spectra were recorded at the Rossendorf Beamline at ESRF at 30 K in transmission mode, resulting in unprecedented spectral quality out to 20 $Å^{-1}$ and 8 Å (Fig. 2). The structural parameters determined by EXAFS shell fitting (EXAFSPAK, FEFF8.2, [3]) are summarized in Table 1.

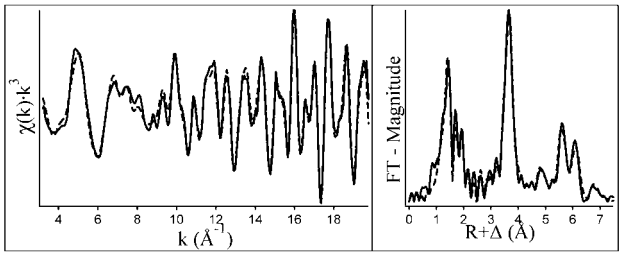

Fig. 2: U L_{III}-edge k^3 weighted EXAFS spectrum (left) and its Fourier transform magnitude (right) of soddyite at 30 K (experiment: full line, fit: dashed line).

Tab. 1: EXAFS structural parameters of soddyite. Radial distances by XRD [3] are given for comparison.

Path	*CN*	*R (Å)*	*DW ($Å^2$)*	*ΔE_0*	*R_{XRD}*
O_{ax}	1.99	1.79	0.0015	-7.91	1.78
MS	3.99c	3.59c	0.0030c	-7.91	3.56
O1	2.10	2.31	0.0031	-7.91	2.31
O2/3	3.10	2.42	0.0047	-7.91	2.43
Si1	1.16	3.14	0.0027	-7.91	3.16
Si2	2.89	3.88	0.0034	-7.91	3.81
U1	2.35	3.58	0.0016	-7.91	3.86
U2	1.61	5.07	0.0025	-14.07	5.15
U3	3.37	5.81	0.0022	-14.07	5.83
U4	3.09	6.37	0.0020	-14.07	6.37
U5	1.68	6.99	0.0020	-14.07	6.99

The radial distances by EXAFS are in fair agreement with those determined by XRD. Significant distal deviations were observed, however, for Si2, U1 and U2 (Table 1). Note that the backscattering of the electron wave from Si2 at 3.88 Å and of U1 at 3.58 Å results in a common Fourier transform peak at 3.8 Å (uncorrected for phase shift), which hides the presence of the much weaker backscatterer Si. The detail wavelet plot, however, clearly reveals the presence of both Si and U atoms at this position by centers at 10 and 18 $Å^{-1}$, respectively (Fig. 3).

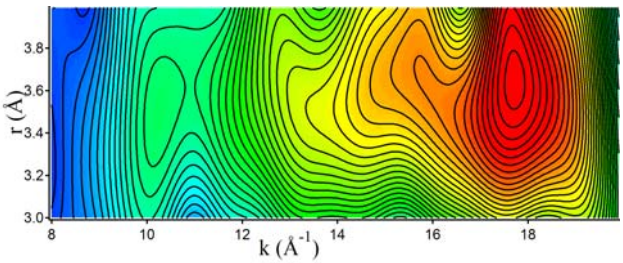

Fig. 3: The detail wavelet of the 30 K soddyite EXAFS spectrum with Morlet parameters η = 05, σ = 1 in the region 3 < r < 4 Å.

REFERENCES

[1] Hennig, C. *et al*. (2003) *Z. Kristallogr.* **218**, 37-45.
[2] Funke, H. *et al*. (2005) *Phys. Rev B* **71**, 094110.
[3] Demartin, F. *et al.* (1992) *Acta Cryst. C* **48**, 1-4.

Photothermal beam deflection spectroscopy on uranyl compounds at the free electron laser facility FELBE

H. Foerstendorf, K. Heim, W. Seidel[1], G. Bernhard
[1]Institute of Nuclear and Hadron Physics, FZR, Dresden, Germany

The commissioning of the free electron laser (FEL) facility FELBE provides a laboratory for investigations of radioactive samples. First results were obtained by photothermal beam deflection spectroscopy (PTBD) on uranyl compounds.

FELBE is an acronym for the free electron laser (FEL) at the Electron Linear accelerator with high Brilliance and low Emittance (ELBE) located at the FZR. This FEL is a source of pulsed, coherent light which is continuously tunable over the infrared wavelength range from 4 to 25 µm. The parameters of the FEL light are given in Tab. 1. The FELBE facility is a member of the EC funded "Integrating Activity on Synchrotron and Free Electron Laser Science (IA-SFS)", which comprises most synchrotron and FEL facilities in Europe and provides financial support to users from the EC and associated states.

Tab. 1: Parameter of the FEL

Wavelength range	**4 – 25 µm (15 – 150 µm)**	U27 (Undulator) (U100; operation 2006)
Pulse energy	**≤ 1 µJ (U27)**	depending on λ
Pulse length	**1 – 10 ps**	depending on λ
Repetition rate	**13 MHz**	3 modes: - cw - Macropulse structure: 0.1 – 36 ms (duration) 1 – 25 Hz (rate) - single-pulse selection: 1 – 2,000 Hz

At the FELBE facility a laboratory suitable for radiochemistry research was installed. This laboratory is classified as a controlled zone for investigations of certain radionuclides obeying to all aspects of radiation protection (Tab. 2). The maximum activity of the investigated radioactive samples can add up to 10^5 times of the admissible limit. A glove box provides the possibility to perform experiments on sensitive samples which have to be kept in an inert gas atmosphere.

Recently we have shown that photothermal beam deflection (PTBD) spectroscopy performed with a pulsed free electron laser (FEL) can provide reliable infrared spectra throughout a distinct spectral range of interest [1]. In our first experiments at FELBE we use uranyl model compounds to obtain absorption spectra showing the antisymmetric stretching vibration (υ_{as}) mode of the UO_2^{2+}-cation since the position and shape of this band can help to identify uranium complexes sorbed on mineral surfaces.

Tab. 2: Table of radionuclides which can be handled at FELBE.

Nuclide	$T_{1/2}$	Molar activity	Max. allowed activity in lab
	[s]	[Bq]	[Bq]
C-14	1.81E+11	2.31E+12	9.00E+04
Tc-99	6.62E+12	6.30E+10	5.73E+05
Th-232sec	4.42E+17	9.46E+05	3.66E+00
Pa-231	1.04E+12	4.01E+11	1.56E+06
Np-237+	6.75E+13	6.19E+09	2.35E+04
U-238sec	1.41E+17	2.96E+06	1.12E+01
Pu-239	7.57E+11	5.52E+11	2.08E+06
Pu-242	1.18E+13	3.53E+10	1.31E+05
Am-243+	2.32E+11	1.80E+12	6.66E+06
Cm-244	5.71E+08	7.31E+14	4.99E+07
Cm-248	1.07E+13	3.89E+10	1.41E+05

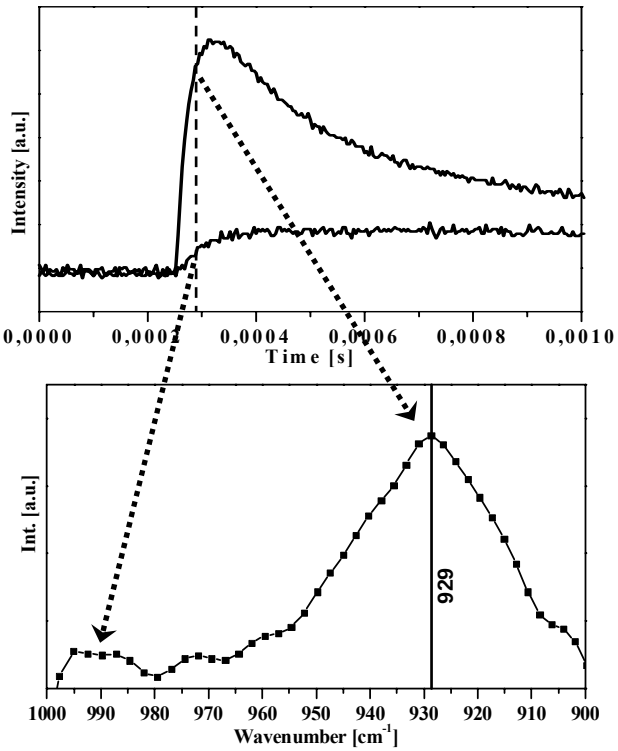

Fig. 1: PTBD signals recorded at the maximum (top, upper trace) and at the edge of the UO_2^{2+}-absorption band (top, lower trace). The amplitudes of the signal provide the spectral intensities after normalization (below).

Fig. 1 shows typical deflection curves of a uranium model compound recorded with different FEL wavelengths. The amplitude of the deflection curves correlates with the absorption coefficient of the sample. Since the wavelength of the FEL light can be tuned over a certain range, absorption spectra can be calculated out of the deflection curves by extracting the values of the amplitude at a certain time and normalizing with the reference signal of the FEL (Fig. 1 bottom). The obtained spectrum is in good agreement to spectra recorded by conventional FT-IR spectroscopy [2].

In further studies we evaluate the minimal concentration of the actinide compounds which will be necessary for detection by PTBD. Another topic will be the investigation of neptunium(V) model compounds at a longer FEL wavelength.

REFERENCES

[1] Seidel, W. *et al.* (2004) *Eur. Phys. J. - Appl. Phys.* **25**, 39-43.
[2] Zazhogin, A.A. *et al.* (1999) *J. Mol. Struct.* **482/483**, 189-193.

Molecular topology of ferrihydrite by EXAFS spectroscopy revisited

K.-U. Ulrich, A. Rossberg, S. Weiß

Iron K-edge EXAFS spectroscopy was applied on wet pastes of pure ferrihydrite, a U(VI)-ferrihydrite coprecipitate, and a mine water related ferrihydrite sample generated at mildly acidic conditions (pH 5.5) to elucidate the molecular structure of fundamental units.

EXPERIMENTAL. Two samples of ferrihydrite (Fh) colloid aggregates (FhN_2 and $FhUN_2$) were prepared in a N_2 flushed glove box (p_{CO2} <0.2 Pa) both in the absence and in the presence of 50 µM $UO_2(NO_3)_2$ by rising the pH of a 1 mM $Fe(NO_3)_3 \cdot 9\ H_2O$ solution with NaOH up to 5.5. The preparation of the mine water related colloid sample M2 containing ~65 % Fh is described in [1]. Using a He cryostat (30 K), Fe K-edge EXAFS spectra were collected at BM20 (ESRF, Grenoble) in transmission mode.

RESULTS. The first peak of the EXAFS Fourier transform (FT) corresponds to five or six oxygen atoms (-OH or -OH_2 ligands) coordinated to the absorbing Fe atom by two different atomic distances (R) (Fig. 1). Up to three O-atoms were found to be coordinated with $R_{Fe\text{-}O1}$ ~1.94 Å and $R_{Fe\text{-}O2}$ ~2.06 Å, respectively (Tab. 1). The second FT peak fits to three Fe-Fe shells with $R_{Fe\text{-}Fe1}$ = 2.89-2.96 Å, $R_{Fe\text{-}Fe2}$ ~3.07 Å, and $R_{Fe\text{-}Fe3}$ = 3.37-3.45 Å. Including a forth Fe shell with $R_{Fe\text{-}Fe4}$ = 3.92-4.00 Å improved the fit of oscillations at higher k values and explained the third FT peak. Neither the EXAFS of sample $FhUN_2$ nor the calculated difference with spectrum FhN_2 give evidence on the adsorbed U(VI) (Fig. 1).

Tab. 1: EXAFS fit parameters. Variable correlated (#) or fixed (*) during the fit to reduce the number of free variables. [a] Coordination number (± 30 %), [b] atomic distance (± 0.02 Å), [c] Debye-Waller factor, [d] Goodness-of-fit parameter.

Sample	Shell	CN [a]	R [b] [Å]	σ^2 [c] [Å^2]	ΔE_0 [eV]	χ_v^2 [d]
M2	Fe-O_1	2.2	1.94	0.0046	-2.86	0.20
	Fe-O_2	3.0	2.07	0.0106	#	
	Fe-Fe_1	1.0	2.89	0.0086	#	
	Fe-Fe_2	2.6	3.07	#	#	
	Fe-Fe_3	0.8	3.37	#	#	
	Fe-Fe_4	0.7	3.92	#	#	
$FhUN_2$	Fe-O_1	3.2	1.94	0.0056	-4.12	0.10
	Fe-O_2	1.7	2.06	0.0042	#	
	Fe-Fe_1	0.5	2.96	0.0041	#	
	Fe-Fe_2	1.0	3.07	#	#	
	Fe-Fe_3	1.1	3.45	#	#	
	Fe-Fe_4	0.3	3.99	#	#	
FhN_2	Fe-O_1	3*	1.93	0.0045	-4.46	0.12
	Fe-O_2	2.1	2.05	0.0038	#	
	Fe-Fe_1	0.5	2.94	0.0051	#	
	Fe-Fe_2	1.3	3.06	#	#	
	Fe-Fe_3	1.5	3.45	#	#	
	Fe-Fe_4	0.3	4.00	#	#	

DISCUSSION. The splitting of the O-shell into two subshells (Tab. 1) is due to the presence of Fe-O and Fe-OH bonds, confirming the formation of octahedral clusters by deprotonation [3]. Although the Fe-Fe distance of 2.89 Å indicates face sharing octahedra in M2, the structural data do not support hematite, but instead a highly polymerized intermediate stage on the transition from Fh to hematite [4]. The Fe-Fe_1 distance of ~2.95 Å cannot be unequivocally attributed to either face sharing or edge sharing linkage (2.95-3.10 Å). Therefore, the calculated distances of 3.00 ± 0.07 Å and ~3.45 Å are explained by edge sharing and double-corner sharing linkage, respectively [2]. Two Fe octahedra sharing a single corner exhibit an Fe-Fe distance of 3.92-4.00 Å [5]. The type and number of linkages were combined (Tab. 2) to a representative basic unit (indicated by dashed circles in Fig. 2) which consists of six $Fe(O,OH)_6$ octahedra in planar arrangement; four of them are coordinated by edges, and two octahedra are linked to this tetrameric unit by sharing double-corners. Each basic unit representing a section of the homogenous network is linked to two other moduls of the same type by sharing a single corner (modified from [2]).

REFERENCES

[1] Ulrich, K.U. *et al.* (2004) *Report FZR-400*, p. 45.
[2] Rose, J. *et al.* (1997) *Langmuir* **13**, 3240-3246.
[3] Combes, J.M. *et al.* (1989) *Geochim. Cosmochim. Acta* **53**, 583-594.
[4] Combes, J.M. *et al.* (1990) *Geochim. Cosmochim. Acta* **54**, 1083-1091.
[5] Manceau, A. *et al.* (1993) *Clay Minerals* **28**, 165-184.

Tab. 2: Number of linkages (CN) for n_{Fe} = 6 octahedra in Fig. 2.

	$CN_{Fe1/Fe2}$ (3.00 ± 0.07 Å)	CN_{Fe3} (3.45 Å)	CN_{Fe4} (3.99 Å)
Fe_i	2 (Fe_j–Fe_l)	0 (Fe_n)	1 (Fe_y)
Fe_j	3 (Fe_i–Fe_k–Fe_l)	1 (Fe_n)	0
Fe_k	2 (Fe_j–Fe_l)	2 (Fe_m–Fe_n)	0
Fe_l	3 (Fe_i–Fe_j–Fe_k)	1 (Fe_m)	0
Fe_m	0	2 (Fe_k–Fe_l)	1 (Fe_z)
Fe_n	0	2 (Fe_j–Fe_k)	0
$CN_{calc} = \Sigma CN/n_{Fe}$	1.67	1.33	0.33
CN_{fit} (FhN_2 + $FhUN_2$)	1.65 ± 0.15	1.3 ± 0.2	0.3

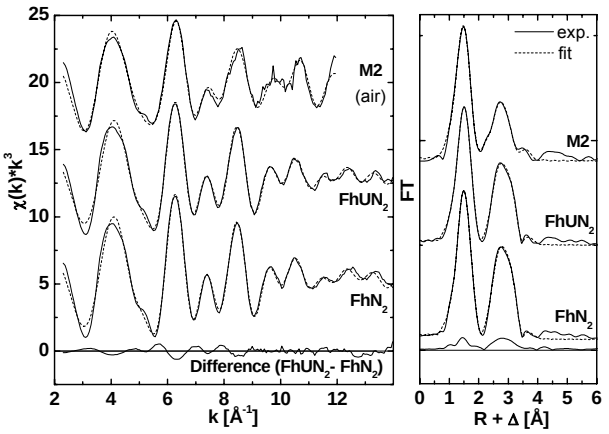

Fig. 1: Fe K-edge EXAFS spectra and FTs (experiment and fit) of ferrihydrite samples (M2: mine water origin; $FhUN_2$ and FhN_2: prepared with and without U(VI) at p_{CO2} < 0.2 Pa.

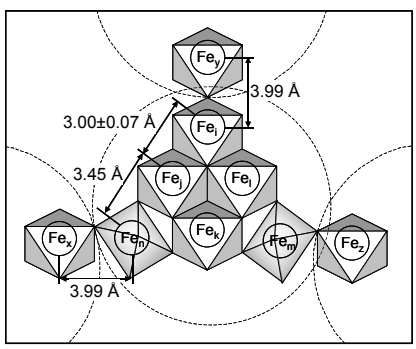

Fig. 2: Molecular topology of ferrihydrite fundamental unit fitting the EXAFS data of the samples FhN_2 and $FhUN_2$ (Tabs. 1 and 2).

Solving the 3-dimensional structure of the binary U(VI)-ferrihydrite sorption complex with EXAFS spectroscopy and MCTFA

A. Rossberg, K.-U. Ulrich, A.C. Scheinost

Applying a novel approach to the data analysis of EXAFS spectra we were able to derive a 3D structural model of the U(VI)-ferrihydrite sorption complex, which is for the first time fully consistent with the experimental data.

Previous EXAFS work has shown that U(VI) adsorbs to the surfaces of the iron oxides ferrihydrite, goethite, and hematite by formation of a bidentate, edge sharing complex [1-5]. However, a spectral contribution at 2.4 Å in the Fourier transform (FT) was not explained by this binary complex. Depending on the preparation conditions (ambient air [1,2,5], CO_2-free atmosphere [3,4], 0.1 M NaCl [4]) the FT peak is controversially discussed as contribution from C, O or Cl atoms, hence involving a ternary complex structure. Here we show that this peak is independent of the preparation conditions. To find an alternative structural model consistent with both the spectroscopic and the experimental data, we employ Monte Carlo Target Transformation Factor Analysis (MCTFA) [6].

EXPERIMENTAL. Ferrihydrite samples were prepared at ambient air atmosphere (sample A) and by using CO_2–free chemicals in a N_2-flushed glovebox (sample B) to prevent any interaction with CO_2 or carbonate. By adding 0.1 - 1.0 M NaOH to solutions of 1 mM $Fe(NO_3)_3 \cdot 9H_2O$ and 12 µM $UO_2(NO_3)_2 \cdot 6H_2O$, the aggregation of ferrihydrite (96 mg/L) and the adsorption/coprecipitation of UO_2^{2+} were initiated. The pH was adjusted to pH 5.5. After settling and ultra-centrifugation the wet pastes were shock-frozen with liquid N_2 and the fluorescence U L_{III}-edge EXAFS spectra were recorded with a 13-element germanium detector at 30 K in a helium cryostat.

RESULTS. The difference spectrum between the EXAFS spectrum of sample A and B shows no significant spectral contributions (Fig. 1). Hence the atmospheric CO_2 has no influence on the local atomic environment of U(VI). In the FT of both spectra a significant spectral contribution at 2.4 Å is visible. The following spectral contributions were identified by shell fitting: two axial O-atoms (O_{ax}) at 1.80 - 1.81 Å (peak 1, Fig. 1), three equatorial O-atoms (O_{eq}) at 2.40 -2.41 Å and two O_{eq} at 2.30 Å (peak 2), one Fe-atom at 3.39 Å (peak 4). According to the experimental conditions and the conformity between spectrum A and B, a contribution of bidentately coordinated carbonate ligands to the peak at 2.4 Å can be excluded. Hence the only possible alternative is an O-atom at a radial distance of 2.86 Å, which improves the fit significantly. In order to derive a 3-dimensional model accounting for all shells, we performed MCTFA. Input data were the Debye-Waller factors taken from the shell fit, an Fe octahedron of hematite and the experimental EXAFS spectrum of sample B. The best match between the MCTFA fit and the spectrum of sample B is shown in Fig. 2, and the corresponding structure in Fig. 3. The MCTFA fit reproduces the experimental spectrum up to 4.7 Å (Fig. 2). It is evident that the peak at 2.4 Å originates from a third O-atom of the Fe octahedron (oh) (Fig. 2, 3). If one considers a regular U(VI) polyhedron with all O_{eq} in one plane normal to the two O_{ax}, a very short distance of 1.77 Å between one O_{ax} and one O_{oh} would arise, requiring an interaction (H-bond) between O_{ax} and O_{oh}. However, longer distances between O_{ax} and O_{oh} are possible if one considers a distortion of the U(VI) polyhedron due to the sterical influence of neighboring Fe octahedra. This is subject to further research.

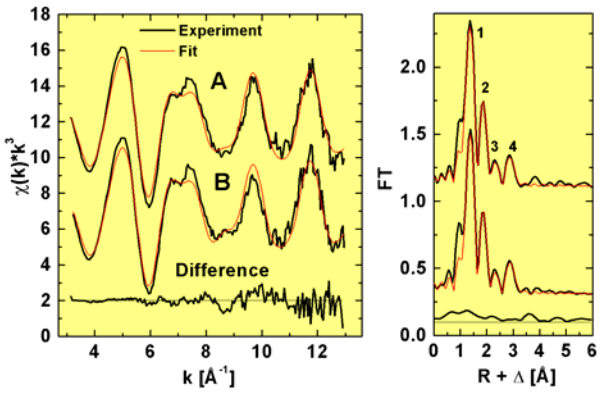

Fig. 1: EXAFS spectra of sample A and B, difference spectrum (A-B) and corresponding Fourier transforms (right).

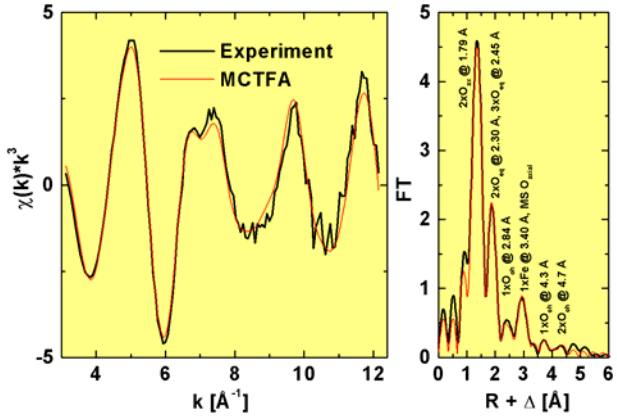

Fig. 2: EXAFS spectrum of sample B and MCTFA fit with corresponding Fourier transform (right). Oh – octahedron, MS – multiple scattering.

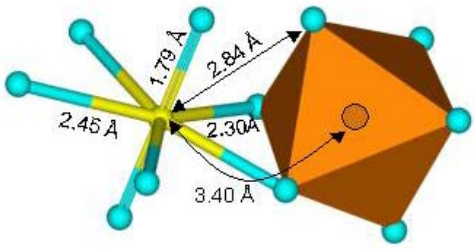

Fig. 3: Structure of the U(VI)-ferrihydrite sorption complex determined by MCTFA. Yellow: U atom, blue: O atoms, brown: Fe atom.

REFERENCES

[1] Waite, T.D. *et al.* (1994) *Geochim. Cosmochim. Acta* **58**, 5465-5478.
[2] Reich, T. *et al.* (1998) *J. Electron Spectrosc. Relat. Phenom.* **96**, 237-243.
[3] Walter, M. *et al.* (2003) *Environ. Sci. Technol.* **37**, 2898-2904.
[4] Redden, G. *et al.* (2001) *J. Coll. and Interface Sci.* **244**, 211-219.
[5] Bargar, J.R. *et al.* (2000) *Geochim. Cosmochim. Acta* **64**, 2737-2749.
[6] Rossberg, A. *et al.* (2005) *Anal. Bioanal. Chem.* **383**, 56-66.

Structural changes of the surface complexes upon U(VI) sorption on ferrihydrite in aqueous solution investigated by ATR FT-IR spectroscopy

H. Foerstendorf, C. Jaidane[1]

[1]Faculty of Mechanical and Process Engineering, University of Applied Sciences, Dresden, Germany

The changes of the carbonate surface complexes upon adsorption of uranium (VI) onto ferrihydrite (Fh) was investigated by attenuated total reflection (ATR) FT-IR spectroscopy. The use of a flow cell allows the *in situ* acquisition of the sorption processes of actinide ions under selected conditions in an aqueous medium.

The structures of the uranyl surface complexes at iron hydroxide mineral phases such as hematite and ferrihydrite (Fh) are still in the focus of recent spectroscopic investigations [1,2]. The infrared spectroscopic approach presented here provides a view on the molecular interactions of dissolved uranium(VI) with a thin Fh-film fixed directly on an ATR crystal by using the flow cell technique (Fig. 1).

EXPERIMENTAL. The preparation of the Fh-films was accomplished directly out of solutions of Fh-suspensions (2.4 g/L) in H_2O. 5 µL of the suspension were put homogeneously on the crystal surface and dried under a gentle stream of nitrogen. According to [3] this procedure was repeated until the thickness of the film was sufficient for the infrared experiments.
After sealing the flow cell (Fig. 1) the Fh-film was equilibrated at a constant flow rate of ~200 µL/min with 20 mM NaCl, pH 5.5, until no changes in the infrared spectra were observed (Fig. 2A). The sorption process was induced by a 50 µM UO_2^{2+} solution containing 20 mM NaCl, pH 5.5. Infrared spectra were recorded continuously by averaging 128 scans at a spectral resolution of 4 cm^{-1} for each spectrum. Difference spectra were calculated immediately after the acquisition time of each spectrum in such a way that positive bands represent the chronological later spectrum.

RESULTS AND DICUSSION. The difference spectra shown in Fig. 2 are obtained at different stages of the sorption process of UO_2^{2+}-ions onto Fh. After equilibration of the freshly prepared Fh-film, *i.e.* before sorption occurs, no bands are observed (Fig. 2A). With the beginning of the UO_2^{2+}-sorption a broad positive band at 903 cm^{-1} with a shoulder around 935 cm^{-1} shows up in the difference spectrum which can be assigned to the υ_{as} stretching modes of UO_2^{2+}-ions sorbed onto Fh [4] and to undefined structural changes of the Fh-film possibly due to the actinide binding, respectively.

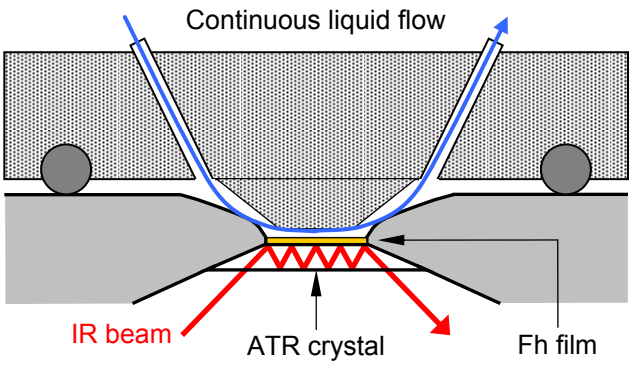

Fig. 1: Scheme of the ATR flow cell.

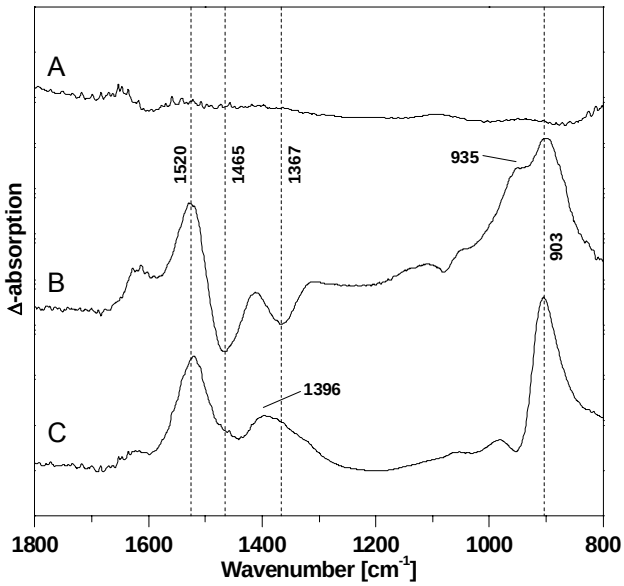

Fig. 2: FT-IR difference spectra of the sorption processes of UO_2^{2+} onto Fh. Spectra recorded after equilibration of CO_2 adsorption and before UO_2^{2+} adsorption occurs (A), at the beginning (B) and after 1 h of UO_2^{2+} adsorption (C), respectively.

Simultaneously, in the region of the CO_3^{2-} stretching vibration (1550 – 1300 cm^{-1}) positive and negative bands are observed representing a change of the CO_3^{2-} surface complexes induced by the UO_2^{2+} ions (Fig. 2B). The negative band at 1465 cm^{-1} representing the υ_{as} (CO_3^{2-}) is shifted to 1520 cm^{-1} upon UO_2^{2+} adsorption whereas a shift of the υ_s mode is not observed possibly due to the overlapping negative band at 1465 cm^{-1}.
The shape of the difference spectra changes during the proceeding sorption of UO_2^{2+} to Fh (Fig. 2C). The positive band at 903 cm^{-1} clearly shows that still additional uranyl is sorbed onto the Fh phase. Moreover, the bands at 1520 and 1396 cm^{-1} indicate the ongoing formation of carbonate complexes at the Fh phase. No further changes of the spectral shapes were observed and only a decreasing amplitude was observed within one hour indicating that the binding capacity of the Fh-film was exhausted.
The adsorption induced ATR FT-IR experiments clearly demonstrate that the carbonate surface complexes on Fh undergo structural changes upon UO_2^{2+} adsorption. This can be deduced from the upshift of the υ_{as} and the υ_s mode of the carbonate anions 1465 to 1520 cm^{-1} and from 1367 to 1396 cm^{-1}, respectively. This upshift can be interpreted as a change from mono- to a bidendate binding of the anions upon UO_2^{2+} adsorption.
In further studies we intend to investigate the sorption mechanism by varying distinct parameters (pH, ionic strength, etc.) and also the desorption behavior of the actinide ions under distinct conditions.

REFERENCES

[1] Bargar, J.R. *et al.* (1999) *Environ. Sci. Technol.* **33**, 2481-2484.
[2] Ulrich, K.-U. *et al.* (2006) *Geochim. Cosmochim. Acta* (submitted).
[3] Voegelin, A. *et al.* (2003) *Environ. Sci. Technol.* **37**, 972-978.
[4] Wazne, M. *et al.* (2003) *Environ. Sci. Technol.* **37**, 3619-3624.

Aqueous phase transformation of ferrihydrite: Influence of coprecipitated UO_2^{2+}

S. Weiß, K.-U. Ulrich, H. Reuther[1], A. Scholz[1]

[1]Institute for Ion Beam Physics and Materials Research, FZR, Dresden, Germany

We studied by Mössbauer spectroscopy the aqueous phase alteration of ferrihydrite to hematite at 70 °C in the absence and presence of UO_2^{2+}. XRD showed no evidence of surface precipitation of schoepite during and after the aging process.

Ferrihydrite (Fh) is a widespread natural iron oxyhydroxide originating from rapid Fe^{2+} oxidation, Fe(III) hydrolysis, and rock weathering. Typical properties are large surface area (>340 m^2/g), low crystallinity and high sorption capacity for U up to 30 % of the dry mass of Fh [1-3]. In a 16-year-experiment at 24 °C, aqueous phase alteration of Fh to hematite (Hm) occurred at pH 4 - 7 [4]. By a similar aging of Fh with coprecipitated U(VI), Hm appeared after 80 d and prevailed after 3 yrs along with goethite [5]. Higher temperatures accelerate the aging process. The conversion of Fh to Hm means a decrease of surface area and an increase of crystallinity both lowering the sorption capacity. Both poisoning of the phase alteration by UO_2^{2+} due to the perfect steric fit of adsorbent and adsorbate by their coordinated oxygen ligands [2], and incorporation of UO_2^{2+} in the aged mineral phase was reported [6,7]. The aim of our experiment was to show the influence of coprecipitated UO_2^{2+} on the aqueous phase alteration of Fh to Hm.

EXPERIMENTAL. We simulated by synthetic groundwater (Tab. 1) the ionic strength and major constituents (except Si due to its inhibiting power [2]) of an aquifer close to the Königstein uranium mine and added 4 mM $Fe(ClO_4)_3 \cdot 10\ H_2O$. Parallel experiments were run without UO_2^{2+} (A) and with 50 µM UO_2^{2+} (B) added from a 1 mM $UO_2(NO_3)_3$ stock solution. In both samples pH 6.1 was adjusted by dropwise adding 1 M NaOH to initiate precipitation of Fh. The suspensions were oven-heated at 70 °C for different time periods. During the aging process pH declined to ~4, but was readjusted to the initial value. After 0, 7, 14, 21 and 28 days of aging, aliquots of the precipitates were separated by ultra-centrifugation (0.5 h, 285000 *g*, Beckman XL-100K) and dried at 22 ± 1 °C in a desiccator. Mössbauer spectroscopy (normal transmission geometry, $^{57}Co(Rh)$ source, sample mass ≥ 10 mg) and X-ray diffraction (Bruker D8 Advance, Cu Kα radiation) were applied at room temperature in order to quantify the Fe mineral phase transformation and to prove secondary (surface) precipitation of U(VI) minerals like schoepite.

RESULTS AND DISCUSSION. The Figs. 1 and 2 show the Mössbauer spectroscopic results. In the absence of UO_2^{2+} (experiment A), more than 50% of Fh converted to Hm within 7 days, and no Fh was left after 28 days. In the presence of UO_2^{2+} (experiment B), most of the Fh converted to Hm within the second week of aging, but after 4 weeks still 17% of Fh was present. Surface precipitation of U minerals (*e.g.*, schoepite) was not detected by XRD after 0, 14, 21, and 28 days of aging. This result is in contrast to similar experiments run with 40 µM UO_2^{2+} in contact with a goethite suspension, showing surface precipitation of schoepite after 1 month at room temperature [8]. Goethite has a higher crystallinity and substantially lower surface area than Fh. Hence we conclude that an excess supply of Fe-OH binding sites amenable to inner-sphere adsorption of UO_2^{2+} prevents the surface precipitation of schoepite, but delays the crystallization of Fh to Hm.

Tab. 1: Ionic composition of the synthetic groundwater.

Ion	c (mmol/L)	c (mg/L)
Ca^{2+}	8.86E-01	35.5
Mg^{2+}	1.27E-01	3.09
Na^{+}	2.09E-01	4.82
K^{+}	4.02E-02	1.57
Cl^{-}	3.58E-01	12.7
HCO_3^{-}	2.49E-01	15.2
SO_4^{2-}	8.34E-01	64.8

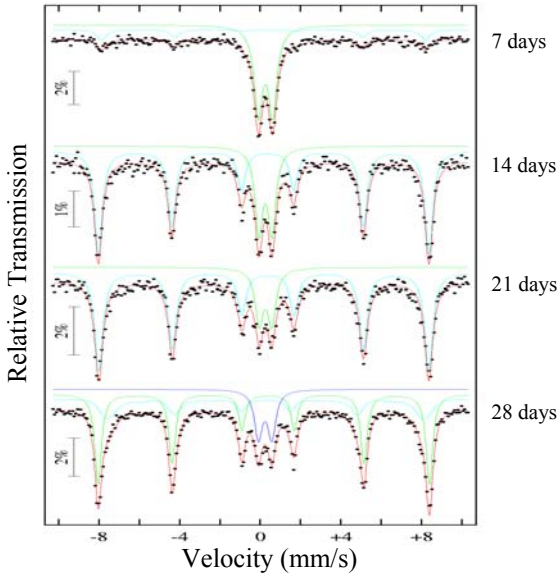

Fig. 1: Mössbauer spectra of different stages of aging ferrihydrite (doublets) to hematite (sextets) in the experiment B.

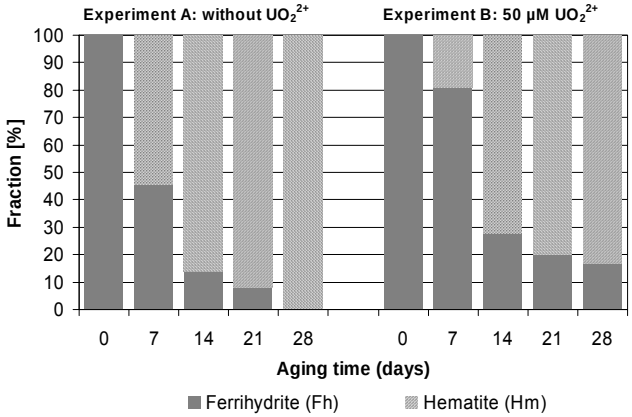

Fig. 2: Percentage of Fe minerals as a function of aging time as determined by Mössbauer spectroscopy.

REFERENCES

[1] Jambor, J.L. *et al.* (1998) *Chem. Rev.* **98**, 2549-2585.
[2] Manceau, A. *et al.* (1992) *Applied Clay Science* **7**, 201-223.
[3] Wazne, M. *et al.* (2003) *Environ. Sci. Technol.* **37**, 3619-3624.
[4] Schwertmann, U. *et al.* (1999) *J. Coll. Interface Sci.* **209**, 215-223.
[5] Bruno, J. *et al.* (1995) *Geochim. Cosmochim. Acta* **59**, 4113-4123.
[6] Payne, T.E. *et al.* (1994) *Radiochimica Acta* **66/67**, 297-303.
[7] Duff, M.C. *et al.* (2002) *Geochim. Cosmochim. Acta* **66**, 3522-3547.
[8] Giammar, D.E. *et al.* (2001) *Environ. Sci. Technol.* **35**, 3332-3337.

Aqueous phase transformation of ferrihydrite: Desorption of coprecipitated UO_2^{2+}

K.-U. Ulrich, S. Weiß, U. Schaefer, H. Zänker

In contrast to ferrihydrite (Fh) where U(VI) sorption is fully reversible, hematite (Hm) as an aged product significantly incorporates U making it resistant to leaching by HCO_3^- solution or substantial pH variation.

The binding stability of U(VI) to Fh during its alteration to more crystalline iron oxides is crucial for assessing U-mobility and U-retention in aquifers and sediments. Few studies have focused on trapping or release of U during the aging of ferric oxides. In contrast to unaltered Fh that lost all adsorbed U when lowering the pH to 2.5, 20 – 30 % of U remained in the solid after aging (70 °C, pH 7) had partially converted Fh to Hm, and was resistant to leaching by acid oxalate solution [1]. By EXAFS spectroscopy an uranate-like coordination was suggested for U trapped within aged Hm [2]. The aim of our desorption experiments is to show how the kinetics of U-release and the amount of U fixed in the solids are related to the state of Fe oxide crystallization.

EXPERIMENTAL. Suspensions of coprecipitated ferrihydrite and 50 µM UO_2^{2+} were prepared in deionized water as described [3] and equilibrated for 48 h. Aliquots of 40 mL were used by duplicates for desorption experiments run at room temperature both without aging the suspensions and after heating them at 70°C for 32 to 83 d. U(VI) was liberated from the solids by repetitive leaching with 0.5 M $NaHCO_3$ solution (pH 8.3) or with synthetic groundwater (pH 7.0, [3]), each step lasting between 2 h and 7 d. After each step, the supernatant was removed by centrifugation (0.5 h, 26000 *g*, Beckman Avanti J-20XP), replaced by new medium, and the solid was re-dispersed. Raw and 3kD filtered supernatants were analyzed by ICP-MS for U and AAS-GF for Fe. At the end of the experiments the air-dried solids were analyzed by Mössbauer spectroscopy (Fe mineral phase) and ICP-MS (U content).

RESULTS. Using 0.5 M $NaHCO_3$ as extractant, bound U was completely desorbed from unaltered Fh (Fig. 1a). The amount of incorporated U increased with the ratio of Fh that converted to Hm. At an aging stage of 83 % Hm, more than half of the amount of adsorbed U (~15 mg U/g dry solid) was resistant to desorption even after 19 steps of leaching. Applying the same scheme on a mine water related colloid suspension that contained Fh and adsorbed U(VI), heating at 70 °C for 32 d accelerated the liberation of U, but 25 % of the adsorbed amount (5.0 mg U/g) remained bound after 64 d of leaching irrespective of preceded heating (Fig. 1b). On the same time scale, U-leaching by groundwater was negligible (<0.05 mg U/g).

DISCUSSION. Evidence on intraparticle diffusion and incorporation of U within the Hm solid came from another experiment where irrespective of the initially sorbed U-amount on Hm, a constant amount of ~1 mg U/g was found to be resistant to desorption by 1 mM $NaHCO_3$ solution after four leaching steps [4].
The time course of U-desorption generally resembles the U-adsorption kinetics where a fast reaction precedes a slower one [5]. However, at least three phases of U release are obvious (Fig. 2). Phase A with a half-life of 118 h for the linearized part may be explained by rapid UO_2^{2+} complexation and exchange by HCO_3^- at easily accessible binding sites, *e.g.* $\equiv Fe(O_2)\text{-}UO_2 + 3\ HCO_3^- \leftrightarrow \equiv Fe(OH)CO_3^- + UO_2(CO_3)_2^{2-} + H_2O$. Phase B (half-life of 965 h) may relate to U-exchange from stronger binding sites and to intra-particle diffusion, and phase C to slow Hm or Fh dissolution by forming $Fe(CO_3)_2^-{}_{(aq)}$ species [6]. Strong kinetic control with a half-life ranging from 39 to 150 h was reported for the U-release from a contaminated sediment and attributed to diffusion of adsorbed species from lithic fragment or grain coating interiors or the dissolution of a precipitate [7]. We conclude that Fh on its alteration to Hm provides a high potential to irreversibly bind uranium in the solid and thus to act as a sink for UO_2^{2+} provided that the mineral does not dissolve.

ACKNOWLEDGEMENTS. We thank T. Häßner and R. Pötzsch for help and H. Reuther for Mössbauer analysis.

REFERENCES

[1] Payne, T.E. *et al.* (1994) *Radiochim. Acta* **66/67**, 297-303.
[2] Duff, M.C. *et al.* (2002) *Geochim. Cosmochim. Acta* **66**, 3522-3547.
[3] Weiß, S. *et al.* this report, p. 53.
[4] Ho, C.H., Miller, N.H. (1986) *J. Colloid. Interface Sci.* **110**, 165-171.
[5] Bargar, J.R. *et al.* (2000) *Geochim. Cosmochim. Acta* **64**, 2737-2749.
[6] Bruno, J. *et al.* (2000) *Geochim. Cosmochim. Acta* **64**, 2173-2176.
[7] Qafoku, N.P. *et al.* (2005) *Environ. Sci. Technol.* **39**, 3157-3165.

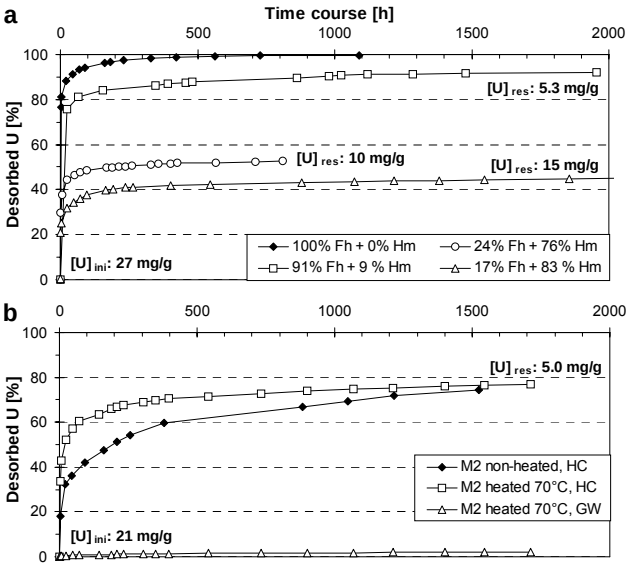

Fig. 1: Percentage of total U desorbed by repetitive leaching with 0.5 M $NaHCO_3$ (HC) from (a) U-loaded Fh at different aging stages, (b) a mine water related colloid sample. Here, leaching by synthetic groundwater (GW) was tested as well. $[U]_{ini}$ and $[U]_{res}$ give initial and residual U-contents of the solid phases.

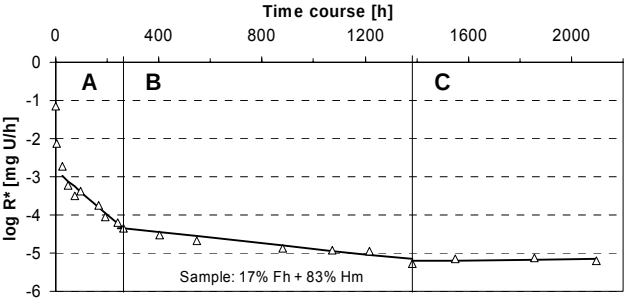

Fig. 2: U desorption rate (R*) of an aged Fh sample as a function of time. Three kinetically different desorption phases are obvious.

Cu(II) sorption onto goethite: The problem of parameter uncertainty in blind prediction

A. Richter, V. Brendler

The effect of protolysis constants scattering in surface complexation modeling (SCM) is illustrated. The uncertainty analysis revealed that the large spreading is actually not critical and did not provide unacceptable distribution coefficients K_D.

PROTOYLYSIS AND COPPER SORPTION MODEL SET-UP. As example the blind prediction of Cu(II) sorption onto goethite is selected, applying the Diffuse Double Layer Model (DDLM). All data collection is fully based on the mineral specific sorption database RES^{3}T [1]. The data compilation strategy is outlined in detail in [2]. The blind prediction of Cu(II) sorption onto goethite [2] has been updated concerning the respective literature data sets and normalized to a surface site density of 2.31 sites/nm^2. The following surface reaction constants log K ± 2σ (values extrapolated to infinite dilution and averaged; 95 % level of significance) were used:

Tab. 1: Selected surface reaction constants (DDLM).

Surface species	log K ± 2σ	
$\equiv FeOH_2^+$	6.97 ± 0.36	16 ref.
$\equiv FeO^-$	-9.51 ± 0.46	16 ref.
$\equiv FeO\text{-}Cu^+$	1.34 ± 0.83	3 ref.
$\equiv FeO\text{-}CuOH$	-6.43	1 ref.

BLIND PREDICTIVE MODELING. The modeling was performed with the FITEQL code, version 3.2 [3]. The experimental data sets by Ali and Dzombak [4] were used to evaluate the prediction (specific surface area 79.4 m^2/g). Fig.1 shows the difference between predicted (result of the FITEQL modeling) and experimental distribution coefficients K_D. The simulation congruence for all data subsets is within one order of magnitude, a spreading which is considered to be reasonable for performance assessment software.

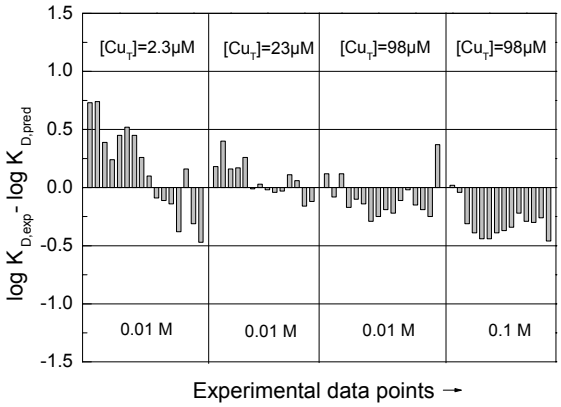

Fig. 1: Differences between experimental [4] and predicted log K_D (varied: pH, Cu(II) content, ionic strength).

As another expression of the prediction quality QP the sum of the absolute difference between experimental and predicted K_D has been computed, here this value is 0.231:

$$QP = \frac{\Sigma\, abs(\Delta \log K_D)}{n} \qquad (n = 64) \qquad (1)$$

UNCERTAINTY ANALYSIS. Protolysis constants in 2pK models cannot be varied independently, they should be distributed symmetrically around the point of zero charge (PZC). Thus the means of all pK value pairs related to the DDLM were transformed into a pair of PZC and ΔpK, calculated according to the following equations:

$$PZC = \frac{-pK_1 + pK_2}{2} \pm 2\sqrt{\frac{\sigma^2_{pK_1} + \sigma^2_{pK_2}}{4}} = 8.24 \pm 0.29 \qquad (2)$$

$$\Delta pK = pK_1 + pK_2 \pm 2\sqrt{\sigma^2_{pK_1} + \sigma^2_{pK_2}} = 2.54 \pm 0.58 \qquad (3)$$

Based on this we generated 20 pK data sets with the aid of normalized Gaussian-distributed random numbers RN:

$$-pK_{1ij} = (PZC + 2\sigma_{PZC} \cdot RN_i) - \frac{1}{2}(\Delta pK + 2\sigma_{\Delta pK} \cdot RN_j) \qquad (4)$$

$$pK_{2ij} = (PZC + 2\sigma_{PZC} \cdot RN_i) + \frac{1}{2}(\Delta pK + 2\sigma_{\Delta pK} \cdot RN_j) \qquad (5)$$

Fig. 2 shows that none of the randomly generated pK parameter sets did deliver unacceptable blind predictions for the K_D values. Thus the formally large spreading of the pK values as extracted from literature is actually not critical. Moreover, the averages for the three different electrostatic approaches Diffuse Double Layer Model (DDLM) ($pK_1 = -6.97 \pm 0.36$, $pK_2 = 9.51 \pm 0.46$), Constant Capacitance Model (CCM) ($pK_1 = -6.61 \pm 0.42$, $pK_2 = 9.28 \pm 0.54$), and Triple Layer Model (TLM) ($pK_1 = -6.77 \pm 0.48$, $pK_2 = 10.15 \pm 0.47$) are comparable within their range of uncertainty. This may imply that a mixing of pK values from different SCM submodels may be tolerable in cases of very sparse data matrices.

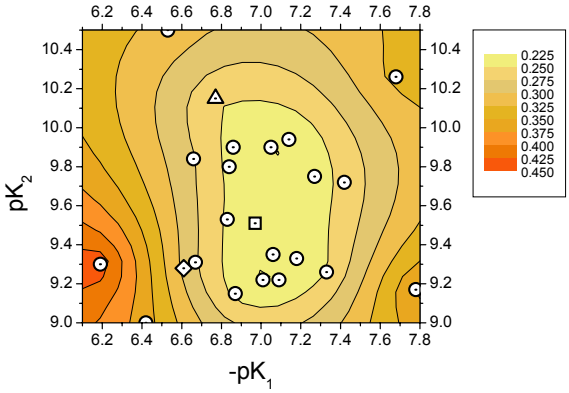

Fig. 2: Randomly distributed pK of goethite (○: varied pK; □, ◇, △: exp. mean pK related to DDLM, CCM, or TLM, resp.) plotted in a surface of the resulting Σabs(Δlog K_D)/n (see legend).

ACKNOWLEDGEMENTS. The development of the database RES^{3}T was funded by the German Federal Ministry of Economics and Labour (BMWA) under contract No. PtWt+E 02E9471, which is gratefully acknowledged.

REFERENCES

[1] Brendler, V. *et al* (2003). *J. Cont. Hydrol.* **61**, 281-291.
[2] Richter, A. *et al.* (2005) *Geochim. Cosmochim. Acta* **69**, 2725-2734.
[3] Herbelin, A.L. *et al.* (1996) *FITEQL -Version 3.2.*, Oregon State University, Corvallis.
[4] Ali, M.A. *et al.* (1996) *Geochim. Cosmochim. Acta* **60**, 291-304.

Search for colloid-borne uranium in mineral waters

H. Zänker, W. Richter, K. Opel, G. Bernhard

Four mineral waters were tested for their colloid contents and the presence of colloid-borne uranium. Only truly dissolved uranium was found in the mineral waters investigated, no colloid-borne U was detectable. The truly dissolved/colloid-borne speciation of U needs to be considered when the health risks of uranium in mineral waters are assessed.

This investigation was aimed at the detection of colloids in four mineral waters relatively rich in uranium (Margon Medium, Margon Classic, Margon Still and San Pellegrino) and at the search for colloid-borne uranium.

EXPERIMENTAL. The mineral water bottles were opened and allowed to degas for 30 min. Then the following analyses were carried out on the raw samples, the supernatants and the subnatants of ultracentrifugations at 40,000 rpm (170,000 x g): Ion chromatography (sulfate, chloride, nitrate), total organic carbon (TOC) analysis, total inorganic carbon (TIC) analysis (carbonate), ICP-MS and/or AAS (cations and Si), photon correlation spectroscopy (colloids, cf. [1]) and laser-induced breakdown detection (colloids, cf. [2]). All experiments (centrifugations and analyses) apart from the measurements by laser-induced breakdown detection were done in 6-fold replicates in order to enable a statistical analysis of the results.

RESULTS AND DISCUSSION. The scattered light intensities of the raw samples and centrifugates exhibited values that are comparable to those of ultrapure laboratory waters such as Milli-Q water, *i.e.* the mineral waters possess very low colloid concentrations. This low particle content is attributable to the de-ironing of mineral waters. The de-ironing is intended for separating iron from the waters but also separates almost all the colloids. The low intensities of scattered light prevented particle sizing by photon correlation spectroscopy due to poor counting statistics. Laser-induced breakdown detection confirmed the low particle content of the mineral waters. It pointed to a particle size of less than 50 nm and for some of the samples to a bimodal particle size distribution with peaks at > 20 nm and at < 10 nm. Ultracentrifugation did not cause noticeable enrichment of the potentially colloid-forming elements Fe, Si and Mn, *i.e.* there was no indication of colloid-borne fractions of these elements. The concentrations of the potentially colloid-forming element Al (not given here) were obviously faked by Al traces originating from the centrifuge tube cover which also seemed to have formed tiny amounts of Al colloids. Based on 6 parallel analyses each, it can be stated for the four mineral waters with considerable statistical reliability that the ultracentrifugation experiments did not result in significant enrichment of uranium (Tab. 1). Thus, colloid-borne uranium could not be detected in any of the mineral waters investigated. Even the unintentional introduction of Al-containing colloids to the waters by the centrifuge tube did not result in the formation of U(VI) pseudocolloids. All the uranium present existed in truly dissolved forms. The non-colloidal behavior of uranium in mineral waters is obviously due to a combination of relatively low uranium concentrations, the lack of significant amounts of potential carrier colloids (in particular iron-rich colloids) and the high carbonate concentrations which shift the solution equilibriums toward the very stable truly dissolved uranyl carbonato [3] and uranyl calcium carbonato [4] complexes. The truly-dissolved/colloid-borne speciation of U needs to be considered when the health risks of uranium in mineral waters are assessed.

Tab. 1: Uranium concentrations (µg/L) of the supernatants and subnatants after 1 h centrifugations at 40,000 rpm (170,000 x g) given as averages of 6 ultracentrifugation experiments and standard deviations (± 1 σ).

Mineral water	Uranium concentration [µg/L]		
	Raw sample	Supernatant	Subnatant
Margon Medium	3.29	3.54 ± 0.29	3.53 ± 0.29
Margon Classic	3.42	3.61 ± 0.26	3.70 ± 0.44
Margon Still	3.24	3.32 ± 0.10	3.36 ± 0.12
San Pellegrino	7.40	7.42 ± 0.12	7.37 ± 0.22

REFERENCES

[1] Ford, N.C. (1985) *Dynamic Light Scattering: Applications of PCS*, p. 7-58, Plenum Press, New York.
[2] Opel, K. *et al.* this report, p. 16.
[3] Clark, D.L. *et al.* (1995) *Chem. Rev.* **95**, 25-48.
[4] Bernhard, G. *et al.* (2001) *Radiochim. Acta* **89**, 511-518.

Part 4:

Reactive transport of actinides

Humic acid diffusion in compacted kaolinite: Influence of porosity

S. Sachs, J. Mibus

The humic acid (HA) diffusion in compacted kaolinite was studied at pH 5 as a function of the bulk density. At higher densities, particle size exclusion effects the HA diffusion, whereas at lower densities, HA sorption becomes more important.

Clay minerals and organic substances are common components of many soils, sediments, and rocks. However, little is known on the migration behavior of humic substances in clay formations, which is governed by diffusion, size exclusion and filtration [1]. In the present study we investigated the HA diffusion in kaolinite at different porosities to elucidate the impact of various processes on the HA diffusion.

EXPERIMENTAL. Kaolinite KGa-1b was compacted in diffusion cells [1] to bulk dry densities of 1.32, 1.56, and 1.67 g/cm^3. The clay plug was equilibrated with 0.01 M $NaClO_4$ solution (1 mM NaN_3) at pH 5. The effective porosities ε and diffusion coefficients D_e were determined with tritiated water (HTO). ^{14}C-labeled synthetic HA type M42 (^{14}C: 17 MBq/g) [2] was used at a concentration of 12 mg/L. A steady-state through-diffusion technique with constant activity gradient, *i.e.*, with constant tracer concentrations at the boundaries, was applied. The HA concentrations in the low and high concentration reservoirs were periodically measured by liquid-scintillation counting. The HA particle size distribution was measured by ultrafiltration (Microsep Centrifugal Devices, Pall, 1 - 1000 kD).

RESULTS. Fig. 1 depicts the amount of HA diffused through the clay and the diffusive flux as a function of time. In the first 20 days the flux steadily increases. Then, it achieves values of about 0.02 to 0.06 µg cm^{-2} d^{-1}. The amount of diffused HA increases with time. The analysis of the particle size distribution of HA in the high and low concentration reservoir showed, that the mean particle size shifts from 50 kD in the high to less than 1 kD in the low concentration reservoir, as also observed in [3]. Only small HA particles pass the kaolinite pore system, which points to a filtration of colloidal particles in the clay.

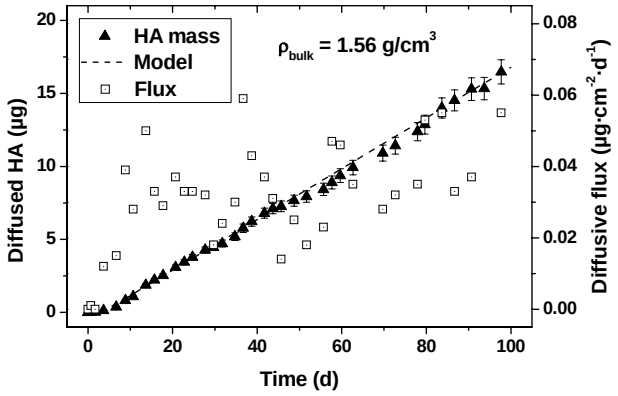

Fig. 1: Cumulative mass and diffusive flux of HA as a function of time.

Based on Fick's second law the amount of diffused HA was modeled resulting in the effective diffusion coefficient D_e and the rock capacity factor α. The relationships between D_e and α are given in Eq. (1) and (2) where D_a represents the apparent diffusion coefficient, ε the effective porosity, ρ the dry bulk density, and K_d the empirical distribution coefficient.

$$D_a = \frac{D_e}{\alpha} \quad (1)$$

$$\alpha = \varepsilon + \rho \cdot K_d \quad (2)$$

The obtained diffusion parameters for HTO and HA are illustrated in Fig. 2a and b. The D_e values of HTO and HA decrease with increasing density (Fig. 2a). HA show smaller D_e values than HTO. This effect intensifies to higher density and indicates an increasing hindrance of the colloidal HA transport in the narrow pore space. This is in agreement with the HA size distribution.

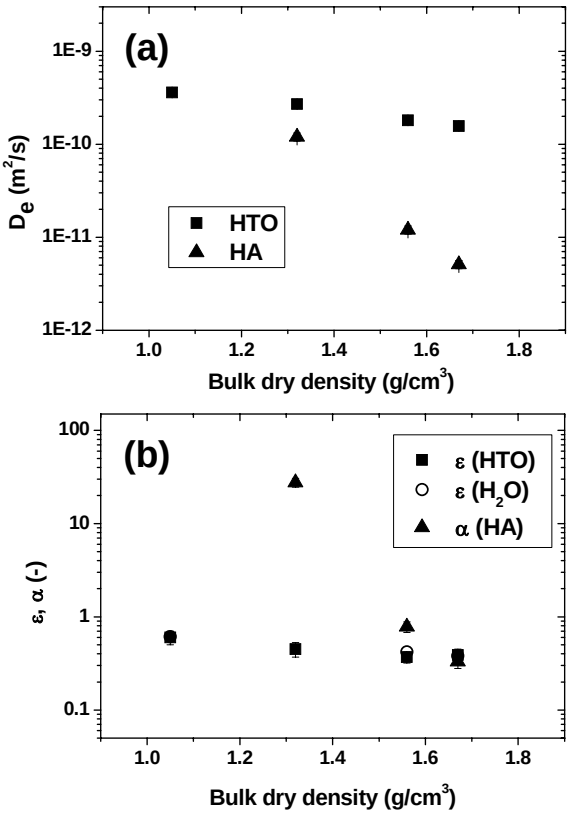

Fig. 2: Diffusion parameters D_e, ε, and α as a function of the bulk dry density (errors smaller than symbol size).

The effective porosity of the system is represented by ε (HTO). It decreases slightly with increasing bulk density (Fig. 2b). In contrast to that, α_{HA} strongly depends on bulk density. It describes the sum of the accessible pore space for the HA diffusion and the sorption (K_d) of the HA in the system. Obviously, sorption processes are less effective at high densities. However, at low densities they become more important, which is concluded from the significantly increased α_{HA} value.

ACKNOWLEDGEMENT. The German Federal Ministry of Economics and Labor funded this work (02E9673).

REFERENCES

[1] Mibus, J. *et al.* (2005) *Report FZR-419*, p. 67.
[2] Sachs, S. *et al.* (2004) *Report FZR-399*.
[3] Mibus, J. *et al.* this report, p. 60.

Impact of humic colloids on uranium(VI) migration in clay

J. Mibus, S. Sachs

The diffusion of humic acid in compacted clay is influenced by its colloidal properties. Particle filtration and the strong uranyl humate complexation give rise to a combined accumulation of both tracers at the boundary between clay and bulk solution.

Organic matter strongly affects the migration of metal ions, in particular of actinides, in natural environments. The transport of humic acid (HA) in argillaceous media is governed by diffusion. Size exclusion and filtration effects are due to its colloidal properties [1]. The influence on uranium(VI) migration is studied here.

EXPERIMENTAL. Kaolinite KGa-1b was compacted to a dry bulk density $\rho = 1.56$ g/cm^3 in a diffusion cell [1] and equilibrated with a sterile 0.01 M $NaClO_4$ solution at pH 5. The diffusion of U(VI) was studied at ambient air in absence and presence of HA. A ^{14}C-labeled HA M42 [2] and ^{234}U or ^{238}U in the HA free system were used as tracer. An identical experimental set-up as in [1] was employed. The tracer concentration C was kept constant at the boundaries ($C(0,t) = C_0$; $C(L,t) = 0$) with $C_{0,HA} = (12.0 \pm 0.06)$ mg/L and $C_{0,U} = (1.0 \pm 0.05)\ 10^{-6}$ mol/L. The low concentration reservoir was analyzed periodically using liquid scintillation counting with α/β separation and ICP-MS. After 70 days the cells were opened and the clay plugs cut into slices of (0.5 ± 0.1) mm. The U and HA were extracted using 1 M HNO_3 or NaOH, respectively, and analyzed as described above.

MODELING. The transient diffusion profiles were interpreted by Eq. (1) according to [3]:

$$\frac{C}{C_B} = erfc\left(\frac{x}{2\sqrt{D_a t}}\right) \qquad (1)$$

where C is the resident concentration in the solid normalized to the concentration at the boundary $C_{B\,(x=0,t)}$ [mg/g], x [m] is the distance, t [s] is the time, and D_a [m^2/s] is the apparent diffusion coefficient. It is related to the effective diffusion coefficient D_e [m^2/s] and the rock capacity factor α [-] by $D_a = D_e/\alpha$ and to the empirical distribution coefficient K_d [mL/g] by $\alpha = \varepsilon + \rho K_d$ with ε [-] being the effective porosity of the clay.

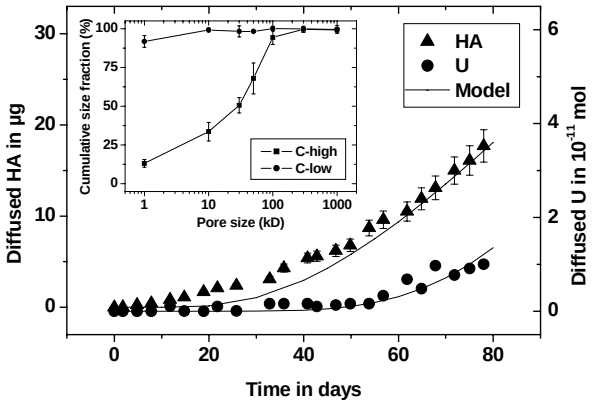

Fig. 1: Tracer breakthrough vs. time in the experiment in presence of HA and size distribution of HA in both solution reservoirs (inset).

RESULTS. In presence of HA, a breakthrough of the low-molecular fraction (≤ 50 kD) of HA to the low concentration side was observed (Fig. 1), whereas only an extremely low fraction of U was detectable. Generally no U breakthrough was measured in the HA-free system.

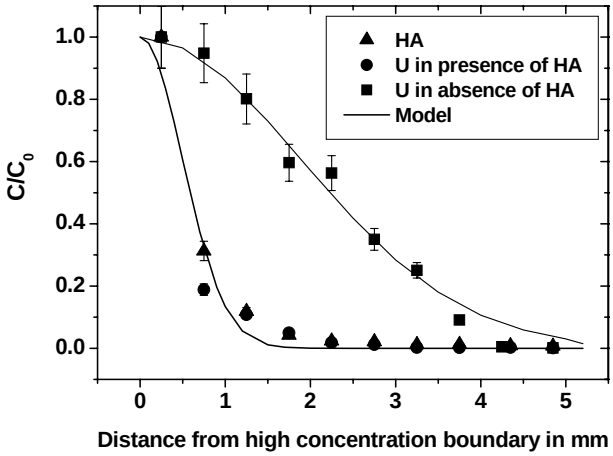

Fig. 2: Tracer concentration in the clay plug after 70 days (absence of HA) and 78 days (presence of HA).

The tracer distribution in the solid is plotted in Fig. 2 and the parameters derived from the curves are given in Tab. 1. Uranium in absence of HA represents a typical in-diffusion profile of a strong sorbing tracer stretching across the clay plug. In presence of HA, the majority of the HA and the U is immobilized near the high concentration boundary.

Tab. 1: Diffusion parameters derived from the concentration profile.

	HA	U + HA	U w/o HA
D_a [m^2/s]	$1 \cdot 10^{-14}$	$1 \cdot 10^{-14}$	$1.5 \cdot 10^{-13}$
K_d [mL/g] [a]	11,200	11,200	800

[a] calculated using $D_e = 1.8 \cdot 10^{-10}$ m^2/s (tritiated water)

In connection with the particle size distribution the immobilization of HA is interpreted as filtration effect. The conjoint immobilization of HA and U points to a strong, largely irreversible humate complexation. Contrariwise, the very low U loading of the HA measured in through-diffusion pointed to a competition of binding sites of clay and HA for U or possibly to a weaker metal complexation by the low molecular fraction of HA.

CONCLUSIONS. HA strongly influences the migration behavior of U in compacted clay. Compared to the HA-free system, U is significantly immobilized.

ACKNOWLEDGEMENT. The German Federal Ministry of Economics and Labor funded this study (02E9673).

REFERENCES

[1] Mibus, J. *et al.* (2005) *Report FZR-419*, p. 67.
[2] Sachs, S. *et al.* (2004) *Report FZR-399*.
[3] Crank, J. (1975) *The mathematics of diffusion, 2nd ed.,* Pergamon Press, Oxford.

Diffusion of cesium in compacted bentonite

S. Brockmann[1], J. Mibus

[1]Faculty of Mechanical and Process Engineering, University of Applied Science, Dresden, Germany

The diffusion of cesium in compacted bentonite was studied. K_D values proved transferable from disperged to compacted systems provided that an adequate pore water is used.

^{137}Cs is a common fission product in nuclear reactors and nuclear weapon tests. Migration parameters of Cs are required for the long-term prognosis of diffusion processes in the near-field of nuclear waste repositories. The transferability of distribution coefficients K_D derived from batch sorption and diffusion experiments and the applicability of the diffusion coefficient of a conservative tracer for modeling the Cs diffusion are tested here.

EXPERIMENTAL. Samples of bentonite MX-80 were compacted in diffusion cells [1] of a cross section $S = 5.2$ cm^2 and a sample thickness $L = 0.53$ cm to bulk dry densities ρ of 1.3, 1.6 and 1.9 g/cm^3. The bentonite plugs were saturated and conditioned for three to four weeks with a synthetic pore water according to [2]. We used through-diffusion experiments with constant boundary conditions ($C(0,t) = C_0$; $C(L,t) = 0$). The effective porosity ε [-] and the effective diffusion coefficient D_e [m^2/s] of the conservative tracer were determined by means of tritiated water (HTO). Cs diffusion was studied using a ^{133}Cs solution of a total concentration $C_0 = 10^{-6}$ mol/L spiked with ^{137}Cs of a specific activity $A = (312 \pm 4)$ Bq/mL. The low concentration reservoir was analyzed periodically by liquid scintillation counting.

MODELING. Data evaluation is based on Fick's second law. Parameter estimation used an analytical solution from [1]. Eq. (1) interprets the diffused amount M [mol] when the diffusive flux J [mol/(m²·s)] becomes constant:

$$M = S \cdot L \cdot C_0 \cdot \left(\frac{D_e \cdot t}{L^2} - \frac{\alpha}{6} \right) \qquad (1)$$

where t [s] is the time and α [-] is the rock capacity factor, which is related to the apparent diffusion coefficient D_a [m^2/s] by $D_a = D_e/\alpha$ and the K_D [mL/g] by $\alpha = \varepsilon + \rho K_D$.

RESULTS. The diffused mass and the diffusive flux of Cs at a density of 1.3 g/cm^3 are shown in Fig. 1. Steady-state is reached after about 40 days. The parameters derived from the experiments are presented in Tab. 1. Additionally, K_D's from batch experiments [3] are given.

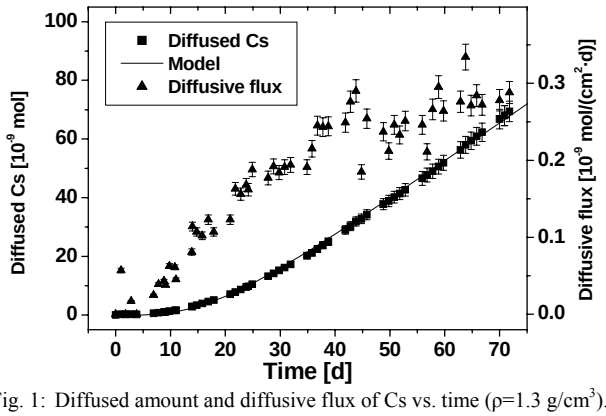

Fig. 1: Diffused amount and diffusive flux of Cs vs. time (ρ=1.3 g/cm^3).

Tab. 1: Migration parameters of HTO and Cs in bentonite at different bulk dry densities.

Density [g/cm^3]	1.3	1.6	1.9
ε [-]	0.65 ± 0.15	0.43 ± 0.04	0.28 ± 0.05
D_e (HTO) [10^{-11} m^2/s]	10.7 ± 0.2	5.8 ±0.05	3.4 ± 0.04
D_e (Cs) [10^{-11} m^2/s]	14.8 ± 0.3	7.8 ±0.1	4.8 ± 0.1
K_D (diffusion) [mL/g]	40.5 ± 7.4	31.0 ± 5.6	45.4 ± 8.2
K_D (batch) [mL/g]	56.4 ± 1.9	49.2 ± 1.6	44.9 ± 1.5

The K_D values derived from batch and diffusion tests differ by approximately 20 to 40 %, which is acceptable. In contrast, the effective diffusion coefficients of Cs in compacted bentonite exceed those of HTO significantly, *i.e.*, Cs migrates faster than water. This is attributed to the "surface diffusion" phenomenon indicating an additional diffusive flux of adsorbed species [4].

Prognosis calculations of Cs diffusion over longer periods were made (Fig. 2). For that, an enhanced diffusion model from [1] accounting for the transient phase was employed and different parameter sets were tested: (i) directly measured D_e and α from the Cs diffusion test, (ii) again, D_e of Cs and α calculated from the batch K_D, and (iii) D_e of HTO and the batch K_D of Cs.

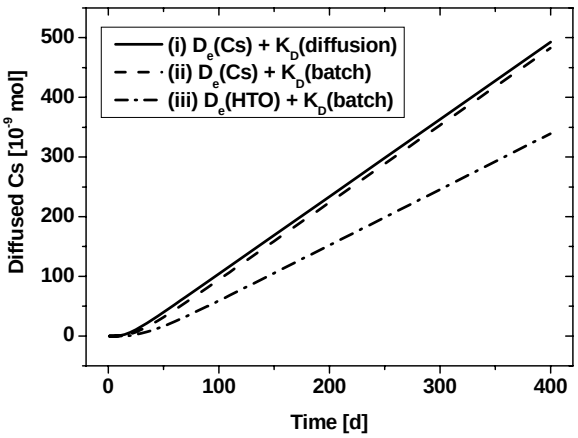

Fig. 2: Calculated diffusion of Cs through the cell at a dry density of 1.3 g/cm^3 using different parameter sets (see text).

The use of directly measured parameters (i) clearly provides the best estimate. Approach (ii) is very close to this indicating a good transferability of the batch derived K_D. In contrast, using the D_e of HTO (iii) fails to model Cs diffusion in the long-term by systematically underestimating the diffusive flux.

CONCLUSIONS. The transfer of K_D values from batch experiments to compacted systems can be recommended, provided that an adequate pore water is used. However, the surface diffusion of Cs deserves further attention in order to provide a profound data base for risk assessment.

ACKNOWLEDGEMENT. This study was partly funded by the European Commission (NF-PRO C2-ST-C-01).

REFERENCES

[1] Van Loon, L.R. *et al.* (2004) *Report PSI 04-03.*
[2] Bradbury, M.H. *et al.* (2002) *Report PSI 02-10.*
[3] Brockmann, S. (2005) *Practical report, FZR.*
[4] Kozaki, T. *et al.* (1999) *Eng. Geol.* **54**, 223-230.

Resaturation behavior of compacted bentonite

P. Trepte[1], J. Mibus, C. Müller
[1]Faculty of Mechanical and Process Engineering, University of Applied Science, Dresden, Germany

A resaturation time of about 30 days is needed to establish constant swelling pressure and pore water conditions in compacted bentonite, thus providing representative samples for laboratory diffusion tests. A minor disturbance of the clay fabric was observed near the filter plates.

When using bentonite as filling material, sorption characteristics and the permeability play a substantial role. For determining these characteristics in the laboratory, reproducible conditions are needed. Therefore, the saturation behavior (water distribution, chloride distribution, pore water chemistry) was examined.

EXPERIMENTAL. MX-80 bentonite samples were compacted in pressure cells [1] of 25.7 mm inner diameter to different dry bulk densities (1.3, 1.6, 1.9 g cm^{-3}) and a final sample thickness of 5.3 mm. The clay plug was sandwiched between stainless steel filters of 1.6 mm thickness and 10 µm pore size.
The samples were saturated with synthetic bentonite pore water [2] related to the dry bulk density, applying a stepwise increased hydraulic pressure, supplied by a HPLC pump, to verify the sealing function. The swelling pressure was measured by Burster pressure sensors. A calibration curve was taken for each sensor. After fluid breakthrough, the percolation was continued over several pore volumes. The effluent was analyzed periodically for major cations and anions. After dropping the hydraulic pressure the cells were conditioned for at least two weeks. One cell was opened. The clay plug was sliced and the water content measured. The other cells were opened after the diffusion experiments and treated as described above.

RESULTS. 1. The swelling pressure depends on the density. For ρ = 1.3 and 1.6 g/cm^3, the swelling pressure establishes at 1.04 and ~3.45 MPa a few days after switching off the hydraulic pressure, and remains constant over several months (Fig. 1). Thus, the clay plug is hydromechanically stable. Due to compaction, the initial load at a density of 1.9 g/cm^3 was too high to measure any additional load with the used equipment.
2. Pore water chemistry: The effluent composition approaches the theoretical composition during the saturation process. This is shown by the comparison of the input solution (synthetic pore water) and effluent during the saturation process (Tab. 1). This effect is best visible from

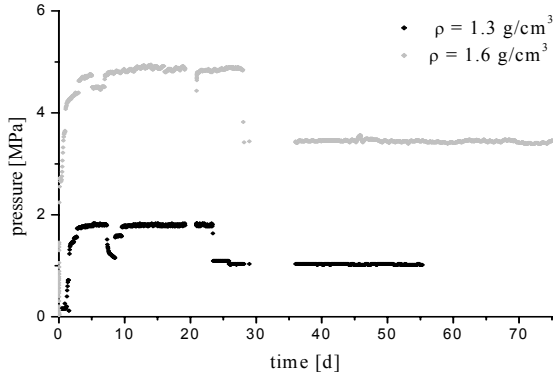

Fig. 1: Swelling pressure during and after the saturation.

Tab. 1: Effluent composition during saturation process (ρ = 1.3 g/cm^3).

Percolated volume [ml]	pH	Na^+ [mol/l]	Mg^+ [mol/l]	K^+ [mol/l]	Cl^- [mol/l]	SO_4^{2-} [mol/l]
1.235	7.42	0.231	$3.41\cdot10^{-3}$	$2.76\cdot10^{-3}$	0.247	$1.10\cdot10^{-1}$
2.348	7.70	0.214	$3.01\cdot10^{-3}$	$2.58\cdot10^{-3}$	0.182	$1.04\cdot10^{-1}$
3.542	8.01	0.206	$3.04\cdot10^{-3}$	$2.66\cdot10^{-3}$	0.151	$1.00\cdot10^{-1}$
4.827	7.76	0.209	$3.53\cdot10^{-3}$	$3.73\cdot10^{-3}$	0.183	$9.49\cdot10^{-2}$
5.889	7.95	0.201	$3.81\cdot10^{-3}$	$3.84\cdot10^{-3}$	0.168	$9.72\cdot10^{-2}$
Input solution	8.00	0.183	$1.00\cdot10^{-2}$	$2.70\cdot10^{-3}$	0.181	$1.02\cdot10^{-1}$

the Na^+ and SO_4^{2-} concentrations. The K^+ concentration is possibly increased by KCl contamination during the pH measurement.
3. Water and chloride distribution: The investigation of the slices of the clay plugs after the saturation and after the long term test showed no changes in the distribution of water and chloride (Fig. 2).

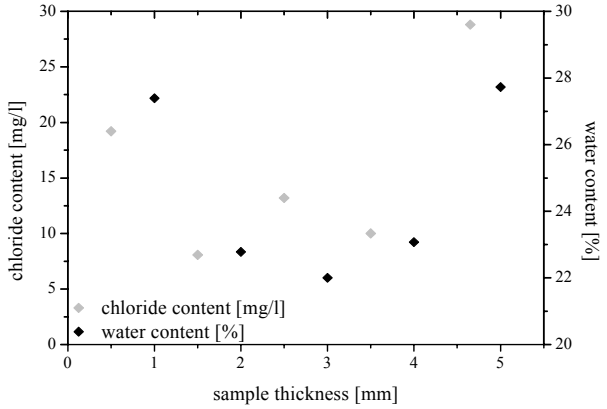

Fig. 2: Water and chloride distribution in a clay plug after saturation (water) and after long-term test (chloride), 8 % error.

The figure shows that the rim of the clay plugs of about 1 mm features a higher porosity, but the distribution of water and chloride remains constant over the duration of the long-term diffusion experiments. Additionally, the water content and chloride concentration within the slices were studied. There no concentration differences were found. This points also to an undisturbed fabric in the inner part of the clay plug.

CONCLUSIONS. The swelling pressure was reached approximately five days after switching off the hydraulic pressure. The saturation time and the used pressure regime supplied representative results. It can be concluded that the clay plugs fulfill the hydraulic sealing function. A sample thickness of at least 5 mm should be used because the edges (each 1 mm) were probably affected by the filter plates.

ACKNOWLEDGEMENT. This study was partly funded by the European Commission (NF-PRO C2-ST-C-01).

REFERENCES

[1] Van Loon, L.R. *et al.* (2004) *Report PSI 04-03*.
[2] Bradbury, M.H. *et al.* (2002) *Report PSI 02-10*.

Sorption of U(VI) on quartz – Experiment and modeling

B. Hollenbach, W. Pfingsten[1], T. Arnold, V. Brendler

[1]Waste Management Laboratory, Paul-Scherrer-Institute, Villigen, Switzerland

The migration of U(VI) in quartz was studied in column experiments under unsaturated conditions. The experimental breakthrough curves of uranium were compared with calculated ones, based on known sorption data. The agreement of calculated and experimental data was excellent. In addition, it was observed that two U(VI) immobilization processes take place within the quartz column: (1) adsorption processes reaching an equilibrium of 5 ppm and (2) for the topmost part additional surface precipitation takes place leading to significant higher uranium concentrations.

EXPERIMENTAL. A solution of $5 \cdot 10^{-6}$ M uranium(VI) was fed into the column inlet at a flow rate of 30 ml/d. The column was 10 cm in length and 3 cm in diameter and filled with quartz (grain size: 200 – 800 µm). A vacuum pump was applied at the bottom of the column to generate a negative pressure of 3 kPa to ensure that the column was operated under unsaturated conditions. Every day a sample of 20 to 30 ml of the eluate was collected at the bottom of the column and analyzed for major cations by ICP-MS. After 19 days the uranium concentration in the eluate reached the same level as in the inlet solution. Then, the experiment was completed and the column was cut into 20 discs of approximately 0.5 cm thickness; and finally, the elemental composition of these disc materials was analyzed by acid digestion and ICP-MS.

MODELING. The breakthrough curve of uranium was calculated by MCOTAC [1] to predict the immobilization and breakthrough behavior of uranium in the quartz column. In advance a separate tracer experiment with lithium was carried out. The computer code CXT-FIT [2] was used to determine the geohydraulic transport parameters porosity, flow velocity and dispersion length from the breakthrough curve of lithium measured for the same column. For the calculation of the breakthrough curve of uranium with MCOTAC these parameters and the following surface complexation reaction describing the adsorption of uranium with its known surface complexation constant, were used [3]:

$\equiv SOH + UO_2^{2+} + H_2O \rightleftharpoons \equiv SOUO_2OH + 2H^+$

$\log K = -4{,}95$

An instantaneous equilibrium between sorbed uranyl species and species in solution was also part of the calculation of MCOTAC.

$\equiv UO_2^{2+} \rightleftharpoons UO_2^{2+}$ $\log k_D = 1.3$; see Ref. [3]

RESULTS. The mass of U(VI) which was retarded in this column amounted to 0.7 mg. The breakthrough curves of U(VI) from the experiment (open squares) and from the calculation with MCOTAC (filled circles) are shown in Fig. 1. In the rising part of the curve there is a good agreement between the experimental data and the calculated ones. The calculation with MCOTAC describes the migration of U(VI) through quartz in this column very well.

The high concentration in the eluate after the breakthrough of uranium is caused by evaporation in the negative pressure environment in which the samples were collected. The distribution of uranium immobilized within the fragmented discs of the column is shown in Fig. 2. U(VI) was not uniformely distributed over the column. Below 3 cm downward from the top, the U(VI) concentration reached an equilibrium of approximately 5 ppm which also holds for all others downstream discs. This uranium content was attributed to adsorption, *i.e.* to surface complexation of aqueous uranium species with surface binding sites on the quartz grains. Significantly higher U(VI) concentrations within the first two centimeters of the column were attributed to surface precipitation of a U(VI) phase in addition to surface complexation reactions between the quartz surface and aqueous uranium.

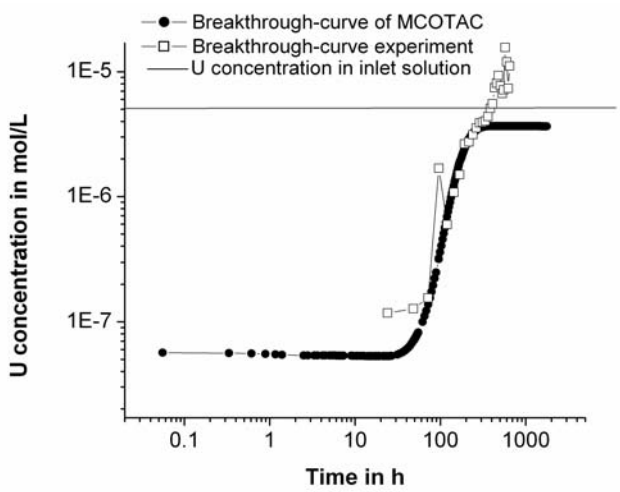

Fig. 1: Comparison of the breakthrough curves.

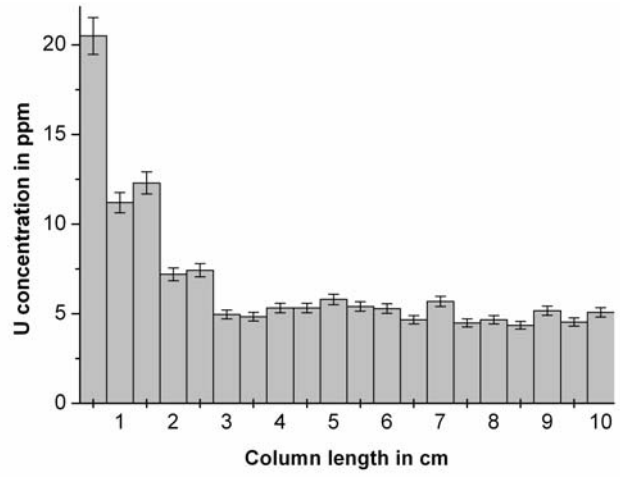

Fig. 2: Uranium distribution in the column.

REFERENCES

[1] Pfingsten, W. (1996) *Nuclear Technology* **16**, 208.

[2] Toride, N. *et al.* (1995) *Research Report 137*, U. S. Department of Agriculture, Riverside, California, U.S.A.

[3] Davis, J.A. *et al.* (2001) *US NRC Report NUREG/CR-6708*, p. 145-150, Washington DC, U.S.A.

- *Articles (peer-reviewed)*
- *Invited review*
- *Proceedings, reports*
- *Lectures, oral presentations*
- *Posters*
- *Habilitation / Venia legendi*
- *Theses*
- *Diploma*
- *Work placements*
- *Awards*

▸ *Articles (peer-reviewed)*

Amayri, S.; Reich, T.; Arnold, Th.; Geipel, G.; Bernhard, G.
Spectroscopic characterization of alkaline earth uranyl carbonates
Journal of Solid State Chemistry, 178, 567-577 (2005).

Baumann, N.; Brendler, V.; Arnold, T.; Geipel, G.; Bernhard, G.
Uranyl sorption onto gibbsite studied by Time-resolved Laser-induced fluorescence spectroscopy (TRLFS)
Journal of Colloid and Interface Science, 290, 318-324 (2005).

Bernhard, G.
Speciation of uranium in environmental relevant compartments
Landbauforschung Volkenrode, 55, 139-148 (2005).

Den Auwer, C.; Llorens, I.; Moisy, P.; Vidaud, C.; Goudard, F.; Barbot, C.; Solari, P.L.; Funke, H.
Actinide uptake by transferrin and ferritin metalloproteins
Radiochimica Acta, 93, 699-703 (2005).

Denecke, M.A.; Rossberg, A.; Panak, P.J.; Weigl, M.; Schimmelpfennig, B.; Geist, A.
Characterisation and comparison of Cm(III) and Eu(III) complexed with 2,6-di(5,6-dipropyl-1,2,4-triazin-3-yl)pyridine using EXAFS, TRFLS, and quantum chemical methods
Inorganic Chemistry, 44, 8418-8425 (2005).

Funke, H.; Chukalina, M.; Rossberg, A.
Wavelet analysis of extended X-ray absorption fine structure data
Physica Scripta, T115, 232-234 (2005).

Funke, H.; Scheinost, A.; Chukalina, M.
Absorption fine structure spectra wavelet analysis of extended X-ray
Physical Review B71, 094110 (2005).

Gaillard, C.; El Azzi, A.; Billard, I.; Bolvin, H.; Hennig, C.
Uranyl complexation in fluorinated acids (HF, HBF4, HPF6, HTf2N): A combined experimental and theoretical study
Inorganic Chemistry, 44, 852-861 (2005).

Großmann, K.; Arnold, T.; Bernhard, G.; Garske, B.; Krawietz, R.
Generation eines Pseudomonas aeruginosa Biofilms auf Biotit und dessen mikroskopische Charakterisierung
GWF-Wasser/Abwasser, 146, 113-118 (2005).

Hennig, C.; Reich, T.; Kraus, W.; Reck, G.; Prokert, K.; Schell, N.
Combining EXAFS and X-ray powder diffraction to solve structures containing heavy atoms
Physica Scripta, T115, 352-355 (2005).

Hennig, C.; Tutschku, J.; Rossberg, A.; Bernhard, G.; Scheinost, A.
Comparative EXAFS investigation of uranium(VI) and -(IV) aquo chloro complexes in solution using a newly developed spectroelectrochemical cell
Inorganic Chemistry, 44, 6655-6661 (2005).

Kopacek, J.; Borovec, J.; Hejzlar, J.; Ulrich, K.-U.; Norton, S.; Amirbahman, A.
Aluminum control of phosphorus sorption by lake sediments
Environmental Science & Technology, 39, 8784-8789 (2005).

Kunicke, M.; Kamensky, I.Y.; Babanov, Y.A.; Funke, H.
Efficient determination of optimal regularization parameter for inverse problem in EXAFS spectroscopy
Physica Scripta, T115, 237-239 (2005).

Le Naour, C.; Trubert, D.; Di Giandomenico, V. Maria; Fillaux, C.; Den Auwer, C.; Moisy, P.; Hennig, C.
First structural characterization of a protactinium(V) single oxo bond in aqueous media
Inorganic Chemistry, 44, 9542-9546 (2005).

Llorens, I.; Den Auwer, C.; Moisy, P.; Ansoborlo, E.; Vidaud, C.; Funke, H.
Neptunium uptake by serum transferring
FEBS Journal, 272, 1739-1744 (2005).

Meißner, T.; Richter, W.; Stephan, H.; Zänker, H.; Kraus, W.
Darstellung und Charakterisierung von Nanopartikeln auf der Basis von $[Ti_2W_{10}PO_{40}]^{7-}$ und Chitosan
Chemie Ingenieur Technik, 77, 1227 (2005).

Merroun, M.; Raff, J.; Rossberg, A.; Hennig, C.; Reich, T.; Selenska-Pobell, S.
Complexation of uranium by cells and S-layer sheets of Bacillus sphaericus JG-A12
Applied and Environmental Microbiology, 71, 5532-5543 (2005).

Mironov, Y.V.; Shestopalov, M.A.; Brylev, K.A.; Yarovoi, S.S.; Romanenko, G.; Fedorov, V.E.; Spies, H.; Pietzsch, H.-J.; Stephan, H.; Geipel, G.; Bernhard, G.; Kraus, W.
$[Re_6Q_7O(3,5\text{-}Me_2PzH)_6]Br_2$*3,5-$Me_2$PzH (Q = S, Se) - new octahedral rhenium cluster complexes with organic ligands: Original synthetic approach and unexpected ligand exchange in cluster core
European Journal of Inorganic Chemistry, 657-661 (2005).

Moll, H.; Geipel, G.; Bernhard, G.
Complexation of curium(III) by adenosine 5'-triphosphate (ATP): A Time-resolved Laser-induced Fluorescence spectroscopy (TRLFS) study.
Inorganica Chimica Acta, 358, 2275-2282 (2005).

Pollmann, K.; Raff, J.; Schnorpfeil, M.; Radeva, G.; Selenska-Pobell, S.
Novel surface layer protein genes in Bacillus sphaericus associated with unusual insertion elements
Microbiology, 151, 2961-2973 (2005).

Radeva, G.; Selenska-Pobell, S.
Bacterial diversity in water samples from uranium wastes as demonstrated by 16S rDNA and RISA retrievals
Canadian Journal of Microbiology, 51, 910-923 (2005).

Richter, A.; Brendler, V.; Nebelung, C.
Blind prediction of Cu(II) sorption onto goethite: Current capabilities of surface complexation modeling
Geochimica et Cosmochimica Acta, 69, 2725-2734 (2005).

Richter, A.; Brendler, V.; Nebelung, C.
The effect of parameter uncertainty on blind prediction of Np(V) sorption onto hematite using the Diffuse Double Layer Model
Radiochimica Acta, 93, 527-532 (2005).

Rossberg, A.; Scheinost, A.
Linking Monte-Carlo simulation and Target Transformation Factor Analysis: A novel tool for the EXAFS analysis of mixtures
Physica Scripta, T115, 912-914 (2005).

Rossberg, A.; Scheinost, A.C.
Three-dimensional modeling of EXAFS spectral mixtures by combining Monte Carlo simulations and Target Transformation Factor Analysis
Analytical and Bioanalytical Chemistry, 383, 56-66 (2005).

Sachs, S.; Bernhard, G.
NIR spectroscopic study of the complexation of neptunium(V) with humic acids: Influence of phenolic OH groups on the complex formation
Radiochimica Acta, 93, 141-145 (2005).

Sachs, S.; Schmeide, K.; Reich, T.; Brendler, V.; Heise, K.-H.; Bernhard, G.
EXAFS study on the neptunium(V) complexation by various humic acids under neutral pH conditions
Radiochimica Acta, 93, 17-25 (2005).

Satchanska, G.; Golovinski, E.; Selenska-Pobell, S.
Bacterial diversity in the uranium mill-tailings Gittersee as estimated via a 16S rDNA approach
Comptes Rendues de l'Académie Bulgare des Sciences, 58, 1105-1112 (2005).

Scheinost, A.; Rossberg, A.; Marcus, M.; Pfister, S.; Kretzschmar, R.
Quantitative zinc speciation in soil with XAFS spectroscopy: Evaluation of iterative transformation factor analysis
Physica Scripta, T115, 1038-1040 (2005).

Schmeide, K.; Reich, T.; Sachs, S.; Brendler, V.; Heise, K.-H.; Bernhard, G.
Neptunium(IV) complexation by humic substances studied by X-ray absorption fine structure spectroscopy
Radiochimica Acta, 93, 187-196 (2005).

Schumacher, M.; Christl, I.; Scheinost, A.; Jacobsen, C.; Kretzschmar, R.
Heterogeneity of water-dispersible soil colloids investigated by Scanning Transmission X-ray microscopy and C-1s XANES micro-spectroscopy
Environmental Science & Technology, 39, 9094-9100 (2005).

Servaes, K.; Hennig, C.; van Deun, R.; Goerller-Walrand, C.
Structure of $[UO_2Cl_4]^{2-}$ in acetonitrile
Inorganic Chemistry, 44, 7705-7707 (2005).

Stephan, H.; Geipel, G.; Bernhard, G.; Appelhans, D.; Tabuani, D.; Komber, H.; Voit, B.
Pegylation of 1,4,8,11-Tetraazacyclotetradecane (Cyclam) and its copper(II) complexation
Tetrahedron Letters, 46, 3209-3212 (2005).

Stephan, H.; Geipel, G.; Bernhard, G.; Comba, P.; Rajaraman, G.; Hahn, U.; Vögtle, F.
Synthesis and binding properties of dendritic oxybathophenanthroline ligands towards copper(II)
European Journal of Inorganic Chemistry, 22, 4501-4508 (2005).

Vantelon, D.; Lanzirotti, A.; Scheinost, A.; Kretzschmar, R.
Spatial distribution and speciation of lead around corroding bullets in a shooting range soil studied by micro-X-ray fluorescence and absorption spectroscopy
Environmental Science & Technology, 39, 4808-4815 (2005).

Voegelin, A.; Pfister, S.; Scheinost, A.; Marcus, M.; Kretzschmar, R.
Changes in zinc speciation in field soil after contamination with zinc oxide
Environmental Science & Technology, 39, 6616-6623 (2005).

Walter, M.; Arnold, T.; Geipel, G.; Scheinost, A.; Bernhard, G.
An EXAFS and TRLFS investigation on uranium (VI) sorption to pristine and leached albite surfaces
Journal of Colloid and Interface Science, 282, 293-305 (2005).

Zorn, T.; Arnold, T.; Bernhard, G.; Nitsche, H.
Sorption von Uran(VI) an Phyllit
Vom Wasser, 103, 20-21 (2005).

▶ *Invited review*

Geipel, G.
Speciation of actinides (environmental, food, clinical, occupational, health)
(The contribution will follow then the arrangement of the actinides in the periodic table.)
Handbook of Elemental Speciation II, 509-563 (R. Cornelis, Ed.), Wiley & Sons Ltd., London (2005).

▶ *Proceedings, reports*

Bryan, N.D.; Bernhard, G.; Geipel, G.; Heise, K.-H.; Schmeide, K.; Benes, P.
Migration case studies and the implications of humic substances for the radiological performance assessment of radioactive waste repositories
Humic Substances in Performance Assessment of Nuclear Waste Disposal: Actinide and Iodine Migration in the Far-Field. Third Technical Progress Report (G. Buckau, ed.), Forschungszentrum Karlsruhe, Wissenschaftliche Berichte, FZKA 7070, Karlsruhe, 81-114 (2005).

Chukalina, M.; Funke, H.; Shabel'nikova, S.
Mathematical aspects of the scattering centers identification problem: mother wavelet choice
Proceedings of the Conference on Mathematical Methods of image recognition (MMRO-12), September 02-09, 2005, Divnomorskoe, Russia, 235-239 (2005).

Geissler, A.; Selenska-Pobell, S.; Scheinost, A.
Changes of bacterial community structure of a uranium mining waste pile sample induced by additon of U(VI)
Uranium Mining and Hydrogeology IV, September 11-16, 2005, Freiberg, Germany, Uranium in the Environment. Mining Impact and Consequences (Merkel, B.J.; Hasche-Berger, A. eds.), Springer, Berlin, 199-205 (2005).

Geissler, A.; Scheinost, A.; Selenska-Pobell, S.
Influence of U(VI) on natural bacterial community of a soil sample from a uranium mining waste
Geochimica et Cosmochimica Acta, 69, A230 (2005).

Krawczyk-Bärsch, E.; Herrmann, S.; Großmann, K.; Vonau, W.; Arnold, T.
Concepts to determine geochemical heterogeneity within a multi component biofilm by microsensors
BioPerspectives 2005 mit 23. DECHEMA-Jahrestagung der Biotechnologen und Jahrestagung der Deutschen Gesellschaft für Proteomforschung (DGPF), May 10-12, 2005, Wiesbaden, Germany (2005).

Meybom, A.; Ulrich, K.-U.
Reservoir ecosystems recover from atmospheric acidification: II. Signs of biological recovery
Acid Rain 2005, 7th International Conference on Acid Deposition, June 12-17, 2005, Prague, Czech Republic, Conference Abstracts (Hůnova, I. et al. eds.), Czech Hydrometeorological Institute, Prague, 558 (2005).

Mibus, J.; Brendler, V.
Interaction of uranium from seepage water with hydroxyapatite
Uranium Mining and Hydrogeology IV, September 11-16, 2005, Freiberg, Germany, Uranium in the Environment. Mining Impact and Consequences (Merkel, B.J.; Hasche-Berger, A. eds.), Springer, Berlin, 359-368 (2005).

Moll, H.; Merroun, M.; Stumpf, Th.; Roßberg, A.; Geipel, G.; Selenska-Pobell, S.; Bernhard, G.
Interaction of actinides with the predominant indigenous bacteria in Äspö aquifer – Interactions of selected actinides U(VI), Cm(III), Np(V) and Pu(VI) with D. äspöensis.
Final Report, BMWA Project No. 02E9491, Wissenschaftlich-Technische Berichte FZR-422 (2005).

Nedelkova, M.; Selenska-Pobell, S.
Bacterial diversity in waters at the Siberian deep-well monitoring site Tomsk-7
Developments in Water Science, Underground Injection Science and Technology (Tsang, C. F.; Apps, J. A., eds.) Elsevier, Amsterdam, 521-536 (2005).

Raff, J.
Biocere mit spezifischer Metallbindungsaktivität
Abschlussbericht zum DFG-Förderprojekt SE 671/7-2: Berichtszeitraum: 01.10.2002-30.09.2004, (2005).

Richter, A.; Brendler, V.; Nebelung, C.
Effects of data scatter and inconsistency in sorption modeling
Geochimica et Cosmochimica Acta, 69, A421 (2005)

Sachs, S.; Geipel, G.; Mibus, J.; Bernhard, G.
Impact of humic acid on the uranium migration in the environment
Uranium Mining and Hydrogeology IV, September 11-16, 2005, Freiberg, Germany, Uranium in the Environment. Mining Impact and Consequences (Merkel, B.J.; Hasche-Berger, A. eds.), Springer, Berlin, 107-116 (2005).

Sachs, S.; Geipel, G.; Bernhard, G.
Study of the redox stability of uranium(VI) in presence of humic substances
Humic Substances in Performance Assessment of Nuclear Waste Disposal: Actinide and Iodine Migration in the Far-Field. Third Technical Progress Report (G. Buckau, ed.), Forschungszentrum Karlsruhe, Wissenschaftliche Berichte, FZKA 7070, Karlsruhe, 9-18 (2005).

Scheinost, A.; Hennig, C.; Somogyi, A.; Martinez-Criado, G.; Knappik, R.
Uranium speciation in two Freital mine tailing samples: EXAFS, micro-XRD, and micro-XRF results
Uranium Mining and Hydrogeology IV, September 11-16, 2005, Freiberg, Germany, Uranium in the Environment. Mining Impact and Consequences (Merkel, B.J.; Hasche-Berger, A. eds.), Springer, Berlin, 117-126 (2005).

Schmeide, K.; Geipel, G.; Bernhard, G.
Study of the neptunium(V) reduction by various natural and synthetic humic substances
Humic Substances in Performance Assessment of Nuclear Waste Disposal: Actinide and Iodine Migration in the Far-Field. Third Technical Progress Report (G. Buckau, ed.), Forschungszentrum Karlsruhe, Wissenschaftliche Berichte, FZKA 7070, Karlsruhe, 19-31 (2005).

Ulrich, K.-U.; Zänker, H.; Roßberg, A.; Furrer, G.
Heavy metals and colloids in streams impaired by acid rain
Acid Rain 2005, 7th International Conference on Acid Deposition, June 12-17, 2005, Prague, Czech Republic, Conference Abstracts (Hůnova, I. et al. eds.), Czech Hydrometeorological Institute, Prague, 613 (2005).

Ulrich, K.-U.; Meybohm, A.
Reservoir ecosystems recover from atmospheric acidification: I. Trends of chemical reversal
Acid Rain 2005, 7th International Conference on Acid Deposition, June 12-17, 2005, Prague, Czech Republic, Conference Abstracts (Hůnova, I. et al. eds.), Czech Hydrometeorological Institute, Prague, 545 (2005).

Ulrich, K.-U.; Rossberg, A.; Scheinost, A.; Foerstendorf, H.; Zaenker, H.; Jenk, U.
Speciation of colloid-born uranium by EXAFS and ATR-FTIR spectroscopy
Uranium Mining and Hydrogeology IV, September 11-16, 2005, Freiberg, Germany, Uranium in the Environment. Mining Impact and Consequences (Merkel, B.J.; Hasche-Berger, A. eds.), Springer, Berlin, 137-148 (2005).

Ulrich, K.-U.; Foerstendorf, H.; Rossberg, A.; Weiß, S.; Zänker, H.
Untersuchungen zur Bindungsstruktur von kolloidgetragenem Uran mit EXAFS und ATR-FTIR
71. Jahrestagung der Wasserchemischen Gesellschaft in der GDCh, May 02-04, 2005, Bad Mergentheim, Germany, 133-137 (2005).

Zänker, H.; Arnold, T.; Hüttig, G.
Bildung von eisenhaltigen Kolloiden bei der Verwitterung von Gesteinsmaterial
71. Jahrestagung der Wasserchemischen Gesellschaft in der GDCh, May 02-04, 2005, Bad Mergentheim, Germany, 421-425 (2005).

▸ *Lectures, oral presentations*

Baraniak, L.; Abraham, A.
Rossendorfer Beiträge zur Flutung von Gruben des Uranbergbaus – Über den Einfluss des Grubenholzes auf das Verhalten von Kontaminanten im Flutungswasser
Veranstaltung, „Steinkohlenbergbauverein Zwickau e.V.“, May 12, 2005, Zwickau, Germany.

Bernhard, G.
Interfacial reactions of uranium related to geology and biology
Pacifichem 2005, The International Chemical Congress of Pacific Basin Societies, December 15-20, 2005, Honolulu, USA.

Bernhard, G.
Speciation of uranium in environmental relevant compartments
APSORC 2005, Asia-Pacific Symposium on Radiochemistry, October 17-21, 2005, Beijing, China.

Bernhard, G.
Urankontamination durch Erzbergbau und Aufarbeitung
Uran-Statusseminar, Bundesinstitut für Risikoforschung, July 21, 2005, Berlin, Germany.

Chukalina, M.; Funke, H.; Shabel'nikova, S.
Mathematical aspects of the scattering centers identification problem: mother wavelet choice
MMRO-12, Conference on Mathematical Methods of image recognition, September 02-09, 2005, Divnomorskoe, Russia.

Funke, H.; Chukalina, M.; Scheinost, A.
Wavelet analysis of EXAFS data
Plenary lecture at ETH Zürich, Institute of Terrestrial Ecology, March 17, 2005, Zürich, Switzerland.

Geipel, G.; Bernhard, G.
Effects of Mg, Ca, Sr and Ba on geochemical uranyl speciation
Pacifichem 2005, The International Chemical Congress of Pacific Basin Societies, December 15-20, 2005, Honolulu, USA.

Geipel, G.
Stability constants evaluated by fluorescence spectroscopy for metal complexes
2nd SUPRAPHONE Meeting (Supramolecularphotonicsnetwork Europe), July 5-7, 2005, Dresden, Germany.

Geipel, G.; Vulpius, D.; Bernhard, G.
TRLFS with fs-Lasers – A tool to study interactions of actinides with organic ligands
APSORC 2005, Asia-Pacific Symposium on Radiochemistry, October 17-21, 2005, Beijing, China.

Geissler, A.; Scheinost, A.; Selenska-Pobell, S.
Fate of U(VI) added to a U mining waste sample and the resulting changes in the indigenous bacterial community
ISSM 05 + ISEB XVII, The Joint International Symposia for Subsurface Microbiology and Environmental Biogeochemistry, August 14-19, 2005, Jackson Hole, Wyoming, USA.

Geissler, A.; Selenska-Pobell, S.; Scheinost, A.
Changes of bacterial community structure of a uranium mining waste pile sample induced by additon of U(VI)
Uranium Mining and Hydrogeology IV, September 11-16, 2005, Freiberg, Germany.

Hennig, C.
Application of a spectro-electrochemical cell for speciation of U(IV) by EXAFS
Royal Institute of Technology, KTH, January 21, 2005, Stockholm, Sweden.

Hennig, C.
A spectro-electrochemical cell for actinide speciation
ACTINET Meeting, Centre for Radiochemistry, August 25, 2005, Manchester, Great Britain.

Hennig, C.
Changing physical parameters to gain more information from EXAFS spectroscopy
CEA Valduc, May 11, 2005, Valduc, France.

Hennig, C.
Die Koordination von Actiniden in wässriger Lösung - Untersuchungen mit EXAFS-Spektroskopie
Wilhelm-Ostwald-Institut für Physikalische und Theoretische Chemie, University of Leipzig, April 19, 2005, Leipzig, Germany.

Hennig, C.; Scheinost, A.; Cannes, C.; Nikitenko, S.; Le Naour, C.; Trubert, D.; Polopov, I.; Sherrand, C.; May, I.
First EXAFS measurements of U(IV)in the room temperature ionic liquid [BuMeIm][Tf_2N]
Mid Term ACTINET Meeting "Ionic Liquids", October 09-10, 2005, Strasbourg, France.

Hennig, C.
Polarization effects at the uranium L_1 and L_3 edges – Theory and applications
Actinides 2005, July 04-08, 2005, Manchester, Great Britain.

Hennig, C.
Spektrochemische Zelle zur Strukturanalyse von Aktinidenspezies in wässriger Lösung – gegenwärtiger Stand und künftige Entwicklungen
Kurt-Schwabe-Institut für Mess- und Sensortechnik e.V., December 09, 2005, Meinsberg, Germany.

Hennig, C.
Structure investigation of actinides in solution by combining EXAFS with electrochemistry
Institute for Transuranium Elements, EU Joint Research Centre, October 21, 2005, Karlsruhe, Germany.

Hennig, C.
X-ray absorption spectroscopy - experimental possibilities and limitations
ACTINET - Theoretical User Lab: Experiment/Theory Workshop, INE Karlsruhe, October 24, 2005, Karlsruhe, Germany.

Hübener, S.
Laser-Induzierte Breakdown Detektion (LIBD) aquatischer Actinidenkolloide
Seminar des Labors für Radio- und Umweltchemie der Universität Bern und des Paul Scherrer Instituts, Labor für Radio- und Umweltchemie der Universität Bern und des Paul Scherrer Instituts, January 14, 2005, Villigen, Switzerland.

Křepelová, A.
EXAFS-Untersuchungen am System U(VI)-Huminsäure-Kaolinit und aktuelle Ergebnisse zur U(VI)-Sorption am Kaolinit
Workshop on research project "Migration von Actiniden im System Ton, Huminstoff, Aquifer", April 04-05, 2005, München, Germany.

Křepelová, A.; Sachs, S.; Reich, T.; Rossberg, A.; Bernhard, G.
Study of the influence of humic acid on the U(VI) sorption onto kaolinite
GDCh-Jahrestagung, September 11-14, 2005, Düsseldorf, Germany.

Merroun, M.

Extreme habitats as reservoir for unusual bacterial strains: Perspectives for bioremediatino and nanotechnology

Civil Engineering Department, University of Sheffield, July 01, 2005, Sheffield, Great Britain.

Merroun, M.; Nedelkova, M.; Heilig, M.; Rossberg, A.; Hennig, C.; Scheinost, A.; Selenska-Pobell, S.

Interaction mechanisms of uranium with bacterial strains isolated from extreme habitats

Actinides 2005, July 04-08, 2005, Manchester, Great Britain.

Merroun, M.

Size and structure of the Au nanoclusters formed on cells and S-layer of Bacillus sphaericus JG-A12

Workshop on research project "Biologische Synthese von Metallclustern an Proteinen und deren technische Nutzung", SMWK 7531.50-03.0370-01, December 16, 2005, Dresden, Germany.

Merroun, M.; Rossberg, A.; Hennig, C.; Romero-Gonzales, M.; Scheinost, A.; Selenska-Pobell, S.

Spectroscopic and microscopic characterization of gold nanoparticles formed by cells and S-layer sheets of Bacillus sphaericus JG-A12

E-MRS 2005, The European Material Conference, May 31 - June 03, 2005, Strasbourg, France.

Mibus, J.

Diffusion of humic acid in clay

Institutsseminar, Paul Scherrer Institut, Labor für Endlagersicherheit, June 21, 2005, Villigen, Switzerland.

Moll, H.; Merroun, M.; Stumpf, Th.; Geipel, G.; Selenska-Pobell, S.; Rossberg, A.; Bernhard, G.

The interaction of actinides with cells of *Desulfovibrio äspöensis*

Project Meeting, Chalmers University of Technology and Göteborg University, May 02-04, 2005, Department of Cell and Molecular Biology, Göteborg, Sweden.

Moll, H.; Merroun, M.; Hennig, C.; Rossberg, A.; Den Auwer, C.; Selenska-Pobell, S.; Bernhard, G.

Interaction of *Desulfovibrio äspöensis* with plutonium

Migration 2005, 10th International Conference on Chemistry and Migration Behaviour of Actinides and Fission Products in the Geosphere, September 18-23, 2005, Avignon, France.

Nedelkova, M.; Merroun, M.; Selenska-Pobell, S.

Microbial diversity and activity in waters of a siberian monitoring well at the deep-bore-hole radioactive waste disposal site TOMSK-7

ISSM 05 + ISEB XVII, The Joint International Symposia for Subsurface Microbiology and Environmental Biogeochemistry, August 14-19, 2005, Jackson Hole, Wyoming, USA.

Pfingsten, W.; Mibus, J.; Küchler, R.

Reactive transport codes applied to gypsum dissolution in a laboratory column experiment with focus on sensitivity of model concepts and data uncertainty

Fifth International Conference on Calibration and Reliability in Groundwater Modelling, Netherlands Institute of Applied Geoscience and International Commision on Groundwater, June 06-09, 2005, Scheveningen, The Netherlands.

Pollmann, K.; Merroun, M.; Selenska-Pobell, S.

Bildung von Goldpartikeln und Molekularbiologie von S-Layern

Workshop on research project "Biologische Synthese von Metallclustern an Proteinen und deren technische Nutzung", SMWK 7531.50-03.0370-01, March 31, 2005, Dresden, Germany.

Pollmann, K.; Raff, J.; Selenska-Pobell, S.

Unusual insertion elements probably involved in the evolution of the S-Layer protein genes of B. sphaericus

BAGECO-8, 8th Symposium on Bacterial Genetics and Ecology, June 26-29, 2005, Lyon, France.

Raff, J.

Die Welt der Bakterien – eine Fundgrube für die Bionik

Open House FZR 2005, September 24, 2005, Dresden, Germany.

Raff, J.

Molekulare Wechselwirkungsmechanismen an der Grenzfläche zwischen Geosphäre und Biosphäre
4. Jenaer Sanierungskolloquium, "Bio-Geo-Interaktionen in der Rhizosphäre", September 29-30, 2005, Jena, Germany.

Raff, J.

S-Layer? Biomolekulare Template zur Erzeugung von Nanostrukturen
Lehrerfortbildungstag Rossendorf 2004/2005, "Nanostrukturen", February 11, 2005, Dresden, Germany.

Raff, J.

Studies on the interaction of actinides with biomolecular and mineral surfaces and their contribution to long-term assessment
GBIZ, Geosphere-Biosphere Interface Zone, September 12-14, 2005, Barcelona, Spain.

Raff, J.

Uranabfallhalden als Reservoir für Bakterien mit hohem Anwendungspotential für die Bio- und Nanotechnologie
Wismut-Kolloquium, Institute of Microbiology, Friedrich-Schiller-Universität Jena, May 17-18, 2005, Jena, Germany.

Richter, A.

Thermodynamics of sorption modeling: Advanced concepts, databases and applicability tests
Chemistry Department, Idaho State University, May 13, 2005, Poccatello, USA.

Richter, A.; Brendler, V.; Nebelung, C.

Effects of data scatter and inconsistency in sorption modeling
15th Annual Goldschmidt Conference 2005, May 20-25, 2005, Moscow, USA.

Roßberg, A.; Ulrich, K.-U.; Scheinost, A.C.

The local structure of U(VI)-ferrihydrite sorption complexes revisited: EXAFS spectroscopy and Monte Carlo simulations
Migration 2005, 10th International Conference on Chemistry and Migration Behaviour of Actinides and Fission Products in the Geosphere, September 18-23, 2005, Avignon, France.

Sachs, S.; Geipel, G.; Mibus, J.; Bernhard, G.

Impact of humic acid on the uranium migration in the environment
Uranium Mining and Hydrogeology IV, September 11-16, 2005, Freiberg, Germany.

Sachs, S.; Mibus, J.

Diffusion von Huminstoffkolloiden im Laborsystem Kaolinit-Wasser
Workshop on research project "Migration von Actiniden im System Ton, Huminstoff, Aquifer", April 04-05, 2005, München, Germany.

Sachs, S.

Spektroskopische Untersuchungen zur Wechselwirkung von U(VI) mit Huminsäure unter neutralen pH-Bedingungen
Workshop on research project "Migration von Actiniden im System Ton, Huminstoff, Aquifer", October 04-05, 2005, Leipzig, Germany.

Scheinost A.C.

The Rossendorf beamline for actinide research
CEA Valduc, May 11, 2005, Valduc, France.

Scheinost, A.; Roßberg, A.; Vantelon, D.; Kretzschmar, R.; Johnson, C. A.

Chemical Forms of Antimony in Shooting Range Soils: An X-Ray Absorption Spectroscopy Study
1st International Workshop on Antimony in the Environment, Institute of Environmental Geochemistry, May 16-19, 2005, Heidelberg, Germany.

Scheinost, A.; Hennig, C.; Somogyi, A.; Martinez-Criado, G.; Knappik, R.
Uranium speciation in 30-year old Freital mine tailings: An EXAFS, µ-XRD, and µ-XRF Study
Migration 2005, 10th International Conference on Chemistry and Migration Behaviour of Actinides and Fission Products in the Geosphere, September 18-23, 2005, Avignon, France.

Scheinost, A.; Hennig, C.; Somogyi, A.; Martinez-Criado, G.; Knappik, R.
Uranium speciation in two Freital mine tailing samples: EXAFS, micro-XRD, and micro-XRF results
Uranium Mining and Hydrogeology IV, September 11-16, 2005, Freiberg, Germany.

Schmeide, K.
Einfluss von Huminsäure auf die Np(V)-Sorption an Kaolinit
Workshop on research project "Migration von Actiniden im System Ton, Huminstoff, Aquifer", October 04-05, 2005, Leipzig, Germany.

Schumann, T.
Entfernung organischer Stoffe aus Wässern durch Ionenaustauscher
University of Applied Sciences, June 29, 2005, Zittau, Germany.

Selenska-Pobell, S.
Addition of U(VI) to uranium mining waste pile soil samples and resulting changes of natural bacterial community structure
Institute of Molecular Biology, Bulgarian Academy of Sciences, October 10, 2005, Sofia, Bulgaria.

Ulrich, K.-U.
Die Erholung der Talsperrenökosysteme von der atmosphärischen Versauerung 1. Trends ausgewählter chemischer Kriterien
Wassergüteberatung des Referats für Wassergütebewirtschaftung, Landestalsperrenverwaltung des Freistaates Sachsen, April 13, 2005, Bad Gottleuba, Germany.

Ulrich, K.-U.; Foerstendorf, H.; Rossberg, A.; Weiß, S.; Zänker, H.
Untersuchungen zur Bindungsstruktur von kolloidgetragenem Uran mit EXAFS und ATR-FTIR
71. Jahrestagung der Wasserchemischen Gesellschaft in der GDCh, May 02-04, 2005, Bad Mergentheim, Germany.

Ulrich, K.-U.; Meybohm, A.; Hoehn, E.
Die Erholung der sächsischen Talsperrenökosysteme von der atmosphärischen Versauerung im Vergleich zu hydrochemischen Trends im Einzugsgebiet der Talsperre Kleine Kinzig (Nordschwarzwald)
15. Limnologisches Gespräch des Zweckverbandes Wasserversorgung Kleine Kinzig (WKK), October 20, 2005, Alpirsbach-Reinerzau, Germany.

Ulrich, K.-U.; Rossberg, A.; Scheinost, A.; Foerstendorf, H.; Zaenker, H.; Jenk, U.
Speciation of colloid-born uranium by EXAFS and ATR-FTIR spectroscopy
Uranium Mining and Hydrogeology IV, September 11-16, 2005, Freiberg, Germany.

▶ *Posters*

Baraniak, L.; Nebelung, C.
Verhalten des Radiums unter den Bedingungen des Endlagers für radioaktive Abfälle Morsleben
GDCh-Jahrestagung, September 11-14, 2005, Düsseldorf, Germany.

Foerstendorf, H.; Seidel, W.; Glotin, F.; Prazeres, R.; Ortega, J.M.
Photothermal beam deflection (PTBD) spectroscopy using an FEL as a pump source
WIRMS 2005, International Workshop on Infrared Microscopy and Spectroscopy with Accelerator Based Sources, June 26-30, 2005, Rathen, Germany.

Foerstendorf, H.; Seidel, W.; Bernhard, G.
FELBE - A new facility providing coherent radiation for infrared spectroscopic investigations in actinide research
Migration 2005, 10th International Conference on Chemistry and Migration Behaviour of Actinides and Fission Products in the Geosphere, September 18-23, 2005, Avignon, France.

Funke, H.; Chukalina, M.; Hennig, C.; Rossberg, A.; Scheinost, A.C.
Wavelet analysis of EXAFS data
15th ESRF Users Meeting, February 08-11, 2005, Grenoble, France.

Geipel, G.; Vulpius, D.; Brendler, V.; Bernhard, G.
Complex formation of small organic ligands with uranium(VI) - Comparison of stability constants with proton dissociation
Migration 2005, 10th International Conference on Chemistry and Migration Behaviour of Actinides and Fission Products in the Geosphere, September 18-23, 2005, Avignon, France.

Geissler, A.; Scheinost, A.; Selenska-Pobell, S.
Fate of U(VI) added to a U mining waste pile sample and the resulting changes in the indigenous microbial community
BAGECO-8, 8th Symposium on Bacterial Genetics and Ecology, June 26-29, 2005, Lyon, France.

Geissler, A.; Scheinost, A.; Selenska-Pobell, S.
Influence of U(VI) on natural bacterial community of a soil sample from a uranium mining waste
15th Annual Goldschmidt Conference 2005, May 20-25, 2005, Moscow, USA.

Gonzalez-Munoz, M; Morcillo, F.; Linares, C.; Martinez-Ruiz, F.; Merroun, M.; Arias, J.
Bioadsorción de Cr, Pb, Co, Mn, La y Ni por biomasa húmeda de una bacteria marina perteneciente a las Pseudomonadaceas
XX. Congress of the Spanish Society of Microbiology, September 19-22, 2005, Cáceres, Spain.

Hennig, C.; Tutschku, J.; Palladino, G.; Poineau, F.; Schmeide, K.; Rossberg, A.; Scheinost, A.C.; Bernhard, G.
EXAFS investigations of U(IV) species in aqueous soultions with a newly developed spectro-electrochemical cell
Migration 2005, 10th International Conference on Chemistry and Migration Behaviour of Actinides and Fission Products in the Geosphere, September 18-23, 2005, Avignon, France.

Hübener, S.; Eichler, B.; Taut, S.
Thermochromatographic adsorption studies of curium and berkelium
Actinides 2005, July 04-08, 2005, Manchester, Great Britain.

Krawczyk-Bärsch, E.; Herrmann, S.; Großmann, K.; Vonau, W.; Arnold, T.
Concepts to determine geochemical heterogeneity within a multi component biofilm by microsensors
BioPerspectives 2005 mit 23. DECHEMA-Jahrestagung der Biotechnologen und Jahrestagung der Deutschen Gesellschaft für Proteomforschung (DGPF), May 10-12, 2005, Wiesbaden, Germany.

Křepelová, A.; Sachs, S.; Reich, T.; Roßberg, A.; Bernhard, G.
Investigation of the influcence of humic acid on the interaction of U(VI) with kaolinite: Sorption and spectroscopic studies
Migration 2005, 10th International Conference on Chemistry and Migration Behaviour of Actinides and Fission Products in the Geosphere, September 18-23, 2005, Avignon, France.

Merroun, M.; Nedelkova, M.; Raff, J.; Roßberg, A.; Hennig, C.; Scheinost, A.; Selenska-Pobell, S.
Characterization of the binding mechanisms of uranium to different isolated bacteria in function of pH
Migration 2005, 10th International Conference on Chemistry and Migration Behaviour of Actinides and Fission Products in the Geosphere, September 18-23, 2005, Avignon, France.

Meybom, A.; Ulrich, K.-U.
Reservoir ecosystems recover from atmospheric acidification: II. Signs of biological recovery
Acid Rain 2005, 7th International Conference on Acid Deposition, June 12-17, 2005, Prague, Czech Republic.

Mibus, J.; Brendler, V.
Interaction of uranium from seepage water with hydroxyapatite
Uranium Mining and Hydrogeology IV, September 11-16, 2005, Freiberg, Germany.

Mibus, J.; Sachs, S.
Diffusion of humic colloids in compacted clay and the influence on uranium migration
Migration 2005, 10th International Conference on Chemistry and Migration Behaviour of Actinides and Fission Products in the Geosphere, September 18-23, 2005, Avignon, France.

Mibus, J.; Trepte, P.; Brendler, V.
Determination of the minimal sample thickness for diffusion experiments with strong sorbing tracers
ANDRA, Natural and Engineered Clay-based Barriers for the Containment of Radioactive Waste, March 14-18, 2005, Tours, France.

Nebelung, C.; Baraniak, L.
Uranium sorption and solubility under conditions relevant for the radioactive waste repository in Morsleben/Germany
Actinides 2005, July 04-08, 2005, Manchester, Great Britain.

Nedelkova, M.; Merroun, M.; Radeva, G.; Selenska-Pobell, S.
Bacterial and archaeal diversity in groundwaters of the Siberian deep-well radioactive disposal site TOMSK-7
BioMicroWorld 2005, 1st International Conference on Environmental, Industrial and Applied Microbiology, March 15-18, 2005, Badajoz, Spain.

Opel, K.; Hübener, S.; Weiß, S.; Zänker, H.; Bernhard, G.
Investigation of environmentally relevant colloids by Laser-Induced Breakdown Detection (LIBD)
Migration 2005, 10th International Conference on Chemistry and Migration Behaviour of Actinides and Fission Products in the Geosphere, September 18-23, 2005, Avignon, France.

Opel, K.; Hübener, S.; Weiß, S.; Zänker, H.; Bernhard, G.
Solubility studies of uranium(IV) by Laser-Induced Breakdown Detection (LIBD)
Actinides 2005, July 04-08, 2005, Manchester, Great Britain.

Opel, K.; Weiß, S.; Hübener, S.; Zänker, H.; Bernhard, G.
Löslichkeitsuntersuchungen an Uran(IV) mittels laserinduzierter Breakdown-Detektion
GDCh-Jahrestagung, September 11-14, 2005, Düsseldorf, Germany.

Pollmann, K.; Raff, J.; Merroun, M.; Fahmy, K.; Mikeehenko, I.; Creamer, N.; Macaskie, L.; Selenska-Pobell, S.
Analysis and engineering of the S-layer protein of Bacillus sphaericus JG-A12 and potential technological applications
2nd Max Bergmann Symposium, February 17-18, 2005, Dresden, Germany.

Raff, J.; Pollmann, K.; Selenska-Pobell, S.
Immobilization of uranium from drinking water by Bacillus sphaericus JG-A12
BioMicroWorld 2005, 1st International Conference on Environmental, Industrial and Applied Microbiology, March 15-18, 2005, Badajoz, Spain.

Reuther, H.; Ulrich, K.-U.
Quantification of iron minerals formed during aging of iron-containing colloids
International Conference on Applications of Mössbauer Effect, Université Montpellier, September 05-09, 2005, Montpellier, France.

Rossberg, A.; A.C. Scheinost, A.C.
Three-dimensional modeling of EXAFS spectral mixtures by combining Monte-Carlo simulations and Target Transformation Factor Analysis
15th ESRF Users Meeting, February 08-11, 2005, Grenoble, France.

Sachs, S.; Geipel, G.; Brendler, V.; Bernhard, G.
Interaction of uranium(VI) and humic acid under neutral pH conditions
Migration 2005, 10th International Conference on Chemistry and Migration Behaviour of Actinides and Fission Products in the Geosphere, September 18-23, 2005, Avignon, France.

Sachs, S.; Schmeide, K.; Geipel, G.; Mibus, J.; Bernhard, G.
Studies of the interaction behavior of humic acids with actinides in the environment
8. German-American Frontiers of Engineering Symposium, May 04-07, 2005, Potsdam, Germany.

Scheinost, A.C.; Hennig, C.; Somogyi, A.; Martinez-Criado, G.; Knappik, R.
Uranium speciation in two Freital mine-tailing samples: SSE, µ-XRD, and µ-XRF results
15th ESRF Users Meeting, February 08-11, 2005, Grenoble, France.

Schmeide, K.; Geipel, G.; Bernhard, G.
Redox stability of neptunium(V) in the presence of humic substances of varying functionality
Migration 2005, 10th International Conference on Chemistry and Migration Behaviour of Actinides and Fission Products in the Geosphere, September 18-23, 2005, Avignon, France.

Shabel'nikova, S.; Funke, H.; Chukalina, M.
EXAFS spectra analysis for nanosystems studying
RSNE-NANO 2005, National Conference on Application the X-rays, Synchrotron Radiation, Neutrons, and Electrons for Studying NANO-Materials, November 14-18, 2005, Moscow, Russia.

Stephan, H.; Röhrich, A.; Steinbach, J.; Geipel, G.; Bernhard, G.
Dendritic encapsulation of radiometals by glcydendrimers having a cyclam-core
BioNanoMaT, Bioinspired Nanomaterials for Medicine and Technologies, November 23-24, 2005, Marl, Germany.

Ulrich, K.-U.; Roßberg, A.; Weiß, S.; Foerstendorf, H.; Brendler, V.; Scheinost, A.; Zänker, H.
Spectroscopic studies on colloid-borne uranium
Migration 2005, 10th International Conference on Chemistry and Migration Behaviour of Actinides and Fission Products in the Geosphere, September 18-23, 2005, Avignon, France.

Ulrich, K.-U.; Weiß, S.; Rossberg, A.; Scheinost, A.; Foerstendorf, H.; Zänker, H.
Surface bond structure of uranium adsorbed onto mine water colloids
15th ESRF Users Meeting, February 08-11, 2005, Grenoble, France.

Ulrich, K.-U.; Zänker, H.; Roßberg, A.; Furrer, G.
Heavy metals and colloids in streams impaired by acid rain
Acid Rain 2005, 7th International Conference on Acid Deposition, June 12-17, 2005, Prague, Czech Republic.

Ulrich, K.-U.; Meybohm, A.
Reservoir ecosystems recover from atmospheric acidification: I. Trends of chemical reversal
Acid Rain 2005, 7th International Conference on Acid Deposition, June 12-17, 2005, Prague, Czech Republic.

Ulrich, K.-U.; Rossberg, A.; Scheinost, A.; Foerstendorf, H.; Zaenker, H.; Jenk, U.
Speciation of colloid-born uranium by EXAFS and ATR-FTIR spectroscopy
Uranium Mining and Hydrogeology IV, September 11-16, 2005, Freiberg, Germany.

Zänker, H.; Arnold, T.; Hüttig, G.; Nitsche, H.; Bernhard, G.
Formation of colloids by the weathering of rock material
Migration 2005, 10th International Conference on Chemistry and Migration Behaviour of Actinides and Fission Products in the Geosphere, September 18-23, 2005, Avignon, France.

Zänker, H.; Arnold, T.; Hüttig, G.
Bildung von eisenhaltigen Kolloiden bei der Verwitterung von Gesteinsmaterial
71. Jahrestagung der Wasserchemischen Gesellschaft in der GDCh, May 02-04, 2005, Bad Mergentheim, Germany.

▶ *Habilitation / Venia legendi*

Scheinost, A.C.
Mechanisms and kinetics of metal sequestration by microcrystalline soil minerals
Université Joseph Fourier, Grenoble, France (2005).

▶ *Theses*

Nedelkova, M.
Mikrobielle Diversität im Grundwasser des radioaktiven Endlagers Tomsk-7, Sibirien, Russland (Microbial diversity in ground water at the deep-well monitoring site SI5 of the radioactive waste depository Tomske-7, Siberia, Russia)
TU Bergakademie Freiberg, Germany (2005).

Vulpius, D.
Zur Komplexbildung von Actiniden (U, Np) mit Hydroxybenzoesäuren (Complex formation of actinides (U, Np) with hydroxybenzoic acids)
Dresden University of Technology, Dresden, Germany (2005).

▶ *Diploma*

Hollenbach, B.
Sorption von Uran an Geomaterialien - Experiment und Modellierung
University of Applied Sciences, Dresden, Germany (2005).

Schumann, T.
Untersuchungen zur Entfernung organischer Wasserinhaltsstoffe mit Ionenaustauschern
University of Applied Sciences, Zittau, Germany (2005).

Steudtner, R.
Untersuchung des Einflusses von Gallussäure auf das Redoxverhalten von Uran(VI)
University of Applied Sciences, Zittau, Germany (2005).

Tschikov, J.
Untersuchung der Verschiebung der bakteriellen Populationen in mit U(VI) inokulierten Bodenproben einer Uranabfallhalde mittels direkter molekularer Analysen
University of Applied Sciences, Köthen, Germany (2005).

▶ *Work placements*

Berger, S.
Untersuchung posttranslationaler Modifikationen bakterieller Hüllproteine (S-Layer) von Uranabfallhaldenisolaten und deren Einfluss auf die Bindung von Uran
University of Applied Sciences, Dresden, Germany (2005).

Brockmann, S.
Migration von Cäsium in Betonit – Einfluss der Porenwasserzusammensetzung
University of Applied Sciences, Dresden, Germany (2005).

Haessner, T.
Untersuchung zur Stabilität der Bindung von Uran an eisenreiche Sekundärmineralkolloide im Verlauf ihrer Alterung durch Desorptionsversuche
University of Applied Sciences, Dresden, Germany (2005).

Jaidane, C.
Schwingungsspektroskopische Untersuchung der molekularen Wechselwirkung von Actiniden und mineralischen Fe-Phasen in wässriger Lösung
University of Applied Sciences, Dresden, Germany (2005).

▶ *Awards*

Amayri, S.; Geipel, G.; Bernhard, G.
Kurt-Schwabe-Preis der Sächsischen Akademie der Wissenschaften, Leipzig, Germany (2005).

- *Seminars (Talks of visitors)*
- *Workshops*
- *Teaching activities*

Seminars

Dr. Marie Urbanová
Department of Physics and Measurements, Institute of Chemical Technology, Prague, Czech Republic
Circular dichroism spectroscopy of biomolecules*
February 21, 2005

Dr. Helena Filipska
Czech Technical University, Prague, Czech Republic
Czech Technical University in Prague
March 15, 2005

Dr. Katrin Cernochova,
Czech Technical University, Prague, Czech Republic
Summary of Scientific Activities
March 15, 2005

Prof. Dr. Erika Kothe
Department of microbial phytopathology, Faculty of Biology and Pharmacy, Friedrich-Schiller-University, Jena, Germany
Mikrobielle Prozesse in der Schwermetallaufnahme und –resistenz
April 07, 2005

Dr. Isabelle Billard
Institut de Recherches Subatomiques, Chimie Nucléaire, Strasbourg, France
F-elements in ionic liquids: spectroscopic studies and extraction processes
May 23, 2005

Prof. Dr. Lothar Dunsch
Electrochemistry and conducting polymers, Institute for Solid State Research (IFF), Dresden, Germany
Spektroelektrochemie an Kohlenstoffnanostrukturen
June 28, 2005

Prof. Maria Teresa González-Munoz
Depertamento de Microbiología, Facultad de Ciencias, University of Granada, Spain
Heavy metal biosorption and biomineralization by Myxococcus xanthus
July 20, 2005

Prof. Dr. Kenji Takeshita
Tokyo Institute of Technology, Tokyo, Japan
Extraction separation of Am(III) and Eu(III) with TPEN (N,N,N',N'-tetrakis(2-pyridylmethyl)ethyl-enediamine) and ist derivatives*
September 26, 2005

Dr. Enrico Marsili
Copernicus Institute for Substainable Development and Innovation, Department of Science, Technology and Society, Faculty of Chemistry at Utrecht University, Utrecht, The Netherlands
Uranium bioremediation using sulfate-reducing biofilms
September 27, 2005

Prof. Dr. Frank-Gerrit Klärner
Institute of Organic Chemistry, University of Duisburg-Essen, Essen, Germany
Neues aus der Chemie der molekularen Pinzetten und Klammern*
October 11, 2005

Prof. Dr. Klaus Lützenkirchen
Institute for Transuranium Elements, Joint Research Center, Karlsruhe, Germany
Aktiniden für die Radio-Immuntherapie*
November 11, 2005

*** Seminars in cooperation with the Institute of Radiopharmacy, FZR.**

▶ *Workshops (organized by the IRC)*

FZR – Friedrich-Schiller-Universität (FSU) Jena Workshop

July 27-28, 2005, FZR, Dresden, Germany.

Ebena, G. (FSU)
Plant establishment in a metal contaminated area

Geißler, A. (FZR)
Untersuchung des Einflusses von U(VI) auf die Struktur der natürlichen bakteriellen Gemeinschaft in einer Bodenprobe einer Uranabfallhalde

Günther, A. (FZR)
Identifizierung und Charakterisierung von U(VI)-Komplexen in höheren Pflanzen

Haferburg, G. (FSU)
Mechanismen der Nickelresistenz eines Haldenisolats aus dem Wismutgebiet

Haferburg, G. (FSU)
Nickelresistenz bei Streptomyceten

Moll, H.; Merroun, M.; Selenska-Pobell, S.; Bernhard, G. (FZR)
Interaction of *Desulfovibrio äspöensis* with selected actinides

Merroun, M. (FZR)
Interaction mechanism of bacterial strains isolated from extreme habitat with uranium

Pollmann, K. (FZR)
Molekulare Analysen von metallbindenden S-Layer-Proteinen

Regenhardt, D. (FZR)
Characterization of the *Bacillus* isolates from the uranium mining waste pile Haberlandhalde

Reinicke, M.(FSU)
Analyse Biodiversität in Bodenproben mittels 16S rDNA Biochips

Zeggel, L. (FSU)
Bioremediation alkalischer Substrate

École Doctorale, Terre Univers Environnement, ROBL-Seminar Minéralogie environnementale: Études à l'échelle nano

Université Joseph Fourier, Grenoble, France, October 06, 2005.

Brown, G. (Stanford University, USA)
Molecular-level studies of chemical and biological interactions at iron and aluminum oxide surfaces

Bertsch P. (University of Georgia, USA)
Natural attenuation of U and co-contaminant metals in aged riparian sediments: Chemical speciation-bioavailability relationships

Guyot, F. (Université Paris VI, France)
Biogeochemical aspects of nanoscale minerals

Rose, J. (CEREGE, CNRS, France)
Ciment and metal immobilization: Confinement of waste materials

Workshop of the Rossendorf-Beamline (ROBL) at the ESRF, Grenoble

FZR, Dresden, Germany, December 07, 2005.

Funke, H.; Hennig, C.; Rossberg, A.; Scheinost, A.
Uranyl Minerals - special features of EXAFS spectra at 10-30 K

Hennig, C.; Schmeide, K.
Strukturanalyse von U(VI), U(IV) und Th(IV) Sulfato-Komplexen in wässriger Lösung

Křepelová, A.; Sachs, S.; Reich, T.; Rossberg, A.; Bernhard, G.
EXAFS-Untersuchungen am System U(VI)-Kaolinit-Huminsäure

Merroun, M.; Pollmann, K.; Raff, J.; Rossberg, A.; Hennig, C.; Scheinost, A.; Selenska-Pobell, S.
XAS Characterization of metallic nanoparticles formed by cells and S-layer of Bacillus sphaericus JG-A12

Moll, H.; Merroun, M.; Hennig, C.; Rossberg, A.; Selenska-Pobell, S.; Bernhard, G.
Interaction of *Desulfovibrio äspöensis* bacteria with plutonium: A solvent extraction and x-ray absorption spectroscopy study

Rossberg, A.; Ulrich, K.-U.; Scheinost, A.
Müssen die Sorptionskomplexe von Uran(VI) an Ferrihydrit revidiert werden? II. Strukturaufklärung und spektroskopischer Nachweis mittels Monte Carlo Simulation und Faktoranalyse von EXAFS-Spektren

Scheinost, A.; Claussner, J.; Dienel, S.; Funke, H.; Hennig, C.; Oehme, W.; Proehl, D.; Rossberg, A.; Strauch, U.
Jahresüberblick: Technische Entwicklungen, Nutzung, Erfolgsbilanz, ACTINET

Ulrich, K.-U.; Brendler, V.; Rossberg, A.; Scheinost, A.C.
Müssen die Sorptionskomplexe von Uran(VI) an Ferrihydrit revidiert werden? I. Modellierung und neue EXAFS-Untersuchungen

Meetings / Visitors

BIOCAT Project Meeting
FZR, April 15, 2005, FZR, Dresden, Germany

Students of Chalmers University of Technology, Göteborg, Sweden within the scope of their "Nuclear chemistry Study Tour 2005",
FZR, April 20, 2005, Dresden, Germany

ACTINET SorptionBoard Project Meeting
FZR, April 18-19, 2005, FZR, Dresden, Germany

▸ *Teaching activities*

Lectures

Bernhard, G.
Radiochemistry – Radiochemical methods
Dresden University of Technology
Summer term 2005

Bernhard, G.
Environmental analysis (Trace analysis)
Dresden University of Technology
Summer term 2005

Bernhard, G.
Environmental chemistry (Environment – Substance – Energy)
Dresden University of Technology
Winter term 2005/2006

Merroun, M.
Lixiviación y Recuperación de Metales: Bioleaching and removal of metals
Centro de Ensenanzas Virtuales de la Universidad de Granada – Fundación Empresa Universidad de Granada & Escuela Superior de Ensenanza Abierta
Study course: Máster de Biotecnología – Master of Biotechnoogy

Courses

The IRC provided two experiments of the laboratory course "Instrumental Analysis" held by the Institute for Analytical Chemistry, Dresden University of Technology, during both summer and winter terms:

- Technetium analysis in environmental samples
- Alpha spectrometric isotope dilution analysis of uranium

Advisers:	*Teaching Assistants:*	
Hübener, S.	Geißler, A.	Lehmann, S.
Krogner, K.	Glorius, M.	Opel, K.
	Großmann, K.	Weiß, S.

Prof. Dr. G. Bernhard (Director)

Administrative Staff
C. Kirmes, G. Kreusel, M. Strauch

Radiation Protection Technics
H. Friedrich, D. Falkenberg, S. Henke, B. Hiller, A. Rumpel, U. Strauch

AQUATIC CHEMISTRY

Dr. G. Geipel

Dr. K.-H. Heise
Dr. S. Hübener
Dr. A. Koban
Dr. W. Richter
Dr. S. Sachs
Dr. K. Schmeide
Dr. J. Tutschku
Dr. K.-U. Ulrich
Dr. H. Zänker

Technical Staff

M. Eilzer
C. Fröhlich
G. Grambole
S. Heller
T. Ludwig
R. Ruske
S. Weiß

BIOGEOCHEMISTRY

Dr. A.C. Scheinost

Dr. H. Funke
Dr. A. Günther
Dr. C. Hennig
Dr. K. Krogner
Dr. M. Merroun
Dr. H. Moll
Dr. K. Pollmann
Dr. J. Raff
Dr. D. Regenhardt
Dr. A. Roßberg
Dr. S. Selenska-Pobell

Technical Staff

M. Dudek
K. Flemming
M. Leckelt
U. Schaefer

MIGRATION

Dr. V. Brendler

Dr. T. Arnold
Dr. N. Baumann
Dr. H.-J. Engelmann
Dr. H. Foerstendorf
Dr. E. Krawczyk-Bärsch
Dr. J. Mibus
C. Nebelung
Dr. A. Richter

Technical Staff

C. Eckhardt
K. Heim
C. Müller
K. Muschter
H. Neubert

PH. D. STUDENTS

A. Geißler
M. Glorius
K. Großmann
A. Křepelová
S. Lehmann
M. Nedelkova
K. Opel
D. Vulpius

DIPLOMA STUDENTS

B. Hollenbach
T. Reitz
T. Schumann
A. Steinborn
R. Steudtner
J. Tschikov

GRADUATE ASSISTANTS, STUDENT ASSISTANTS, TRAINEES

S. Berger
J. Bernhard
S. Brockmann
L. Fuchs
T. Häßner
S. Hedrich
C. Heyn
N. Hofmann
C. Jaidane
R. Pötzsch
K. Salzwedel
C. Schäfer
I. Schwarz
M. Strossova
P. Trepte
O. Vogel

GUEST SCIENTISTS

Dr. K. Cernochova	*Centre for Radiochemistry and Radiation Chemistry, Prague, Czech Republic*
Dr. M. Chukalina	*Institute of Microelectronics Technology, Chernogolovka, Russia*
Prof. R. Colella	*Department of Physics, Purdue University, West Lafayette, USA*
Dr. C. Espiño	*Departamento de Química, Faculty of Sciences and Technology, University Nova de Lisboa, Portugal*
Prof. F. Pina	*Departamento de Química, Faculty of Sciences and Technology, University Nova de Lisboa, Portugal*
Dr. H. Filipska	*Centre for Radiochemistry and Radiation Chemistry, Prague, Czech Republic*
R. Han	*Centre of Environmental Measurements, Province Liaoning, China*
Dr. E. Marsili	*Copernicus Institute, Utrecht University, The Netherlands*
F. Morcillo de Amueda	*Depertamento de Microbiología, Facultad de Ciencias, University of Granada, Spain*
Dr. G. Radeva	*Institute of Molecular Biology, Bulgarian Academy of Sciences, Sofia, Bulgaria*
Prof. J.C. Silvae Pereira de Lima	*Departamento de Química, Faculty of Sciences and Technology, University Nova de Lisboa, Portugal*
V.V. Vilas	*Institute of Nuclear Chemistry, Johannes-Gutenberg-University Mainz, Germany*

Acknowledgements

The Institute of Radiochemistry is part of the Forschungszentrum Rossendorf e. V. which is financed in equal parts by the Federal Republic of Germany and the Free State of Saxony.

The Commission of the European Communities supported the following projects:

- ACTINET Network for Actinide Sciences
  Contract No.: FIR1-CT-2002-20211
  Contract No.: FI6W-CT-2004-508836
- Understanding and Physical and Numerical Modelling of the Key Processes in the Near-Field and their Coupling for Different Host Rocks and Repository Strategies
  Contract No.: FI6W-CT-2003-002389
- Integrated Project FUNMIG: Fundamental Processes of Radionuclide Migration
  Contract No.: 516514

Three projects were supported by the Bundesministerium für Wirtschaft und Arbeit (BMWA) and by the Bundesministerium für Bildung und Forschung (BMBF):

- Mobilisierung von Actiniden durch mikrobiell produzierte Liganden unter Berücksichtigung der Endlagerung von radioaktivem Abfall
  Contract No.: BMWA 02E9985
- Verbundprojekt: Migration von Actiniden im System Ton, Huminstoff, Aquifer – Migrationsverhalten von Actiniden (Uran, Neptunium) in Tonen: Charakterisierung und Quantifizierung des Einflusses von Huminstoffen
  Contract No.: BMWA 02E9673
- Integriertes Sorptionsdatenbanksystem für Wechselwirkungen chemisch-toxischer und radioaktiver Kontaminanten mit mineralischen Systemen in geologischen Formationen (ISDA-FZR)
  Contract No.: BMBF 02C1144

The Sächsisches Staatsministerium für Wissenschaft und Kunst (SMWK) provided support for the following project:

- Biologische Synthese von Metallclustern an Proteinen und deren technische Nutzung
  Contract No.: SMWK 4-7531.50-03-0370-01/5

Two projects were supported by the Deutsche Forschungsgemeinschaft (DFG):

- Fluoreszenzspektroskopie von gelösten Uran(IV)-Komplexen – Aufklärung der Speziation im umweltrelevanten Konzentrationsbereich
  Contract No.: GE 1011/4-1
- Kolloidgetragener Transport von Uran und anderen radiotoxischen Schwermetallen in toxischen Bergwerkswässern
  Contract No.: ZA 238/2-2

One project was supported by Deutscher Akademischer Austauschdienst (DAAD):

- Bakterielle S-Layer als Templat für die Bildung von metallischen Nano-Partikeln für nanotechnologische Anwendungen
  Contract No. D/04/39988

The North Atlantic Treaty Organisation (NATO) supported one project:

- Investigation of the Short-Rage Structure of Layered Double Hydroxides and Phyllosilicates by EXAFS: Development of Wavelet Analysis
  Contract No.: CBP.NR.CLG.981353

One project was supported by AMD Saxony Manufacturing GmbH:

- Alphaspektrometrie an Si-Wafern
  Contract No.: AMD 5200030223

The University of Manchester, Department of Chemistry, Great Britain supported one project:

- Access to Beamtime at Rossendorf Beamline at ESRF in the frame of a scientific collaboration

Index of authors

Forschungszentrum Rossendorf
Institute of Radiochemistry
P.O. Box 51 01 19 - 01324 Dresden/Germany
Tel.: +49 351 260-3210
Fax: +49 351 260-3553
e-mail: contact.radiochemistry@fz-rossendorf.de
www.fz-rossendorf.de

Member of the Leibniz Association